Author responses to referee comments

for

A predictive group-contribution model for the viscosity of aqueous organic aerosol

Natalie R. Gervasi[1], David O. Topping[2], and Andreas Zuend[1]

[1]Department of Atmospheric and Oceanic Sciences, McGill University, Montreal, Quebec, H3A 0B9, Canada
[2]School of Earth, Atmospheric and Environmental Science, University of Manchester, Manchester M13 9PL, U.K.

Additions to the Manuscript and Supplementary Information are shown in blue and removal of information is shown in red. Reviewer comments are shown in purple.

Anonymous Referee #1

We thank the referee for her/his review of our manuscript and for providing thoughtful and constructive comments. The comments are addressed point-by-point in the following.

Comment 1: Arguably, the simple mixing rule of mole fraction-based weighting (eqn 14a) is as good as the proposed AIOMFAC-VISC, and significantly simpler. The authors should also present the results of the mole-fraction based weighed prediction for sucrose, trehalose, as well as the more complex mixtures of Figure 5+, which may demonstrate differences between the simple mixing and AIOMFAC-VISC...It also seems possible/likely that any variations in the predictions between these approaches for treating the mixture may be small compared to the uncertainty caused by the predictions of the pure component viscosities, and this simpler approach would be much more accessible method to users.

Author Response: Based on the reviewer's suggestion, we have added a section to the revised version of the supplement (Section S7) where we compare the mean absolute error (MAE) and mean bias error (MBE) of AIOMFAC-VISC and the mole fraction-weighted simple mixing rule against experimental data for all binary aqueous systems studied in this work. The other simple mixing models, including the use of a mole-fraction-based activity weighting of the pure component viscosities were evaluated as well but are not compared in further detail here as their performance is clearly worse (which is discussed in the new SI Section S7). We also provide additional graphical comparisons of the two mixing models, with a figure showing four binary aqueous systems (different from the glycerol and citric acid systems shown in the main text) and the three SOA systems studied in this work. We have chosen these four binary systems in particular because either their pure-component

viscosities are known or there are experimental mixture viscosity data very close to a mass fraction of water of 0.0, which allows us to assign an experimentally constrained pure-component viscosity estimate. This ensures a direct comparison between AIOMFAC-VISC and the simpler mole fraction-based mixing rule when the pure-component viscosity is measured or well-constrained by measurements, thereby evaluating the skill of the mixture viscosity models distinct from additional uncertainty
5 due to pure component viscosity estimations. For this same reason, we highlight the comparison of the mixing models' MAE and MBE when the highest confidence pure-component viscosity values are used, instead of the more uncertain estimations from the DeRieux et al. (2018) method. The evaluation shows that the cumulative MAE and MBE are slightly smaller for the mole-fraction scaled mixing rule when including all data sets. Notwithstanding, these cumulative metrics are dominated by the model–measurement biases caused by a few data sets, mainly those involving the saccharides raffinose, trehalose and maltose.
10 For those saccharides, the AIOMFAC/UNIFAC models are known to show systematic deviations from measurements in terms of their water activity prediction, which in turn also affects the viscosity prediction with AIOMFAC-VISC, hence relatively large deviations. We also compare the models on a per-data set basis, which is probably more insightful. AIOMFAC-VISC outperforms the mole-fraction weighted mixing rule in approximately 61% of the data sets evaluated according to the MAE and approximately 67% of cases according to the MBE, making AIOMFAC-VISC the less biased model though the model–
15 model deviations in several cases are small compared to the uncertainties of the measurements. Both models substantially outperform the activity-weighted mixing rule (in $\sim 91\%$ of cases in terms of MAE), so that mixing rule is not recommend. Overall, we agree with the reviewer that using a mixing model based on a mole fraction scaling is a viable alternative to AIOMFAC-VISC for aqueous mixtures. This work highlights that the choice of model can be made on a system-by-system basis and suggests that the mole-fraction-based mixing rule is the best among the simple mixing rules. While AIOMFAC-VISC
20 is more complex than the mole fraction-weighted mixing rule, we would like to highlight that AIOMFAC-VISC has been added to the web-based version of AIOMFAC, allowing users to generate AIOMFAC-VISC predictions with relative ease.

Changes to Manuscript: Section S7, Table S5, Figures S8 and S9 have been added to the supplementary information. Reference to this addition is found in the main text on page 15, lines 13–15. *Code and data availability* has been updated to reflect the availability of AIOMFAC-VISC as part of the web version of AIOMFAC.

25 **Comment 2:** Additionally, the authors should consider presenting the results of an activity-based weighing (that is, use the mole-fraction based weighing, but include the mole-fraction activity coefficient for each species based on AIOMFAC calculations, similar to that done by the authors for the combinatoric contributions in eqn. 2).

Author Response: We agree that this would be a valuable addition for the reader, so the activity-based weighting has been added alongside the other simple mixing rules in Figure 4. As mentioned above, an extended evaluation including all suitable
30 binary mixture data sets shows that such a mixing rule is typically (in $\sim 91\%$ of the cases) less accurate than AIOMFAC-VISC or the simple mole-fraction-based mixing rule.

Changes to Manuscript: The results of an activity-based weighting have been added to Fig. 4 of the main text. A discussion of how the activity-based weighting compares to AIOMFAC-VISC and the other simple mixing rules can be found in the revised main text in Section 3.1 and in the SI, Section S7.

Comment 3: The majority of the model uncertainty comes from the pure component viscosity predictions; if these are done correctly, the mixing model is likely correct. The authors should consider ways to improve the predictions of the pure component viscosities, possibility also using their function group contribution methods. This would significantly strengthen the paper.

Author Response: The reviewer is correct in stating that the mixture viscosity approaches differ less than the constraint imposed by the pure-component viscosity prediction. At present, the pure-component viscosity prediction is typically the largest source of error in any of the mixture viscosity models studied here and a better pure-component viscosity prediction tool should be an immediate priority for future work. We would like to highlight that we did detail our attempt to use two different group contribution-based approaches for the prediction of pure component viscosity (manuscript page 8 lines 21–34 and Supplementary Information Section S2). Given the present scarcity of reliable, temperature-dependent experimental data for pure components of interest in the organic aerosol context, both of these attempts proved less reliable and less versatile than the DeRieux et al. (2018) approach. Aside from the DeRieux et al. (2018) approach, we make mention of the attempts of others to develop a pure-component viscosity model (Sastri and Rao, 1992; Nannoolal et al., 2009; Shiraiwa et al., 2017; Rothfuss and Petters, 2017; DeRieux et al., 2018). The difficulty in formulating a universal pure-component viscosity prediction tool for semi-solid and solid compounds at atmospherically relevant temperatures cannot be understated. The work involved to develop such a tool would be significant and would constitute its own publication. Furthermore, our evaluation of available pure component and mixture data, as well as glass transition temperature data, suggests that the scarcity of available pure-component viscosity data for relevant compounds in the atmospheric aerosol context, covering a wide temperature range, is a key limitation. Moreover, our work indicates that the assumption reaching a viscosity of 10^{12} Pa s at the glass transition temperature is only approximate and does not hold for all classes of organics. This highlights a need for careful laboratory experiments. This aside, the development of pure component viscosity estimation models is also an area of active research, so we would like to emphasise that the pure-component viscosity tool used in AIOMFAC-VISC is interchangeable and when a better alternative is developed, it can be adopted with ease.

Changes to Manuscript: Text was added to the figure caption of Fig. 1 to emphasise that the pure-component viscosity estimation tool within AIOMFAC-VISC is an interchangeable part of the model.

Anonymous Referee #2

We thank the referee for her/his review of our manuscript and for providing thoughtful and constructive comments. The comments are addressed point-by-point in the following.

Comment 1: My comments mostly address questions about which part of the multi-step process that AIOMFAC-VISC pre-
scribes leads to the significant improvement in estimating viscosities compared to previous simpler methods. This information might help to guide future research, e.g. tools for conversion of volatility into viscosity, or viscosity into diffusivity coefficients. Fig. S3 shows impressively how big the improvement from GC-UNIMOD to AIOMFAC-VISC is, almost to the extent that it might be worthwhile showing such a plot in the main text and presented alongside the discussion of Fig. 4. My question is, can the authors detail which difference in the calculations leads to the discrepancy in output?

Author Response: The purpose of Fig. S3 is to demonstrate the improvement of the mixture viscosity equations of AIOMFAC-VISC from those of GC-UNIMOD in predicting mixture viscosity. The residual contributions from AIOMFAC-VISC and GC-UNIMOD only differ by a factor of -1; however, the expression for the combinatorial contributions have been modified substantially in AIOMFAC-VISC. We agree with the reviewer that it would be helpful to show the reader what modifications give rise to the AIOMFAC-VISC / GC-UNIMOD discrepancy. To this end, we have modified Fig. S3 to highlight that this discrepancy is largely a result of the modifications made to the combinatorial equation. We have added mixture viscosity pre-
dictions for aqueous glycerol and citric acid using only the combinatorial equations of AIOMFAC-VISC and GC-UNIMOD. Using only the combinatorial contributions in place of the respective full mixing models accounts for almost all of the differ-
ence between AIOMFAC-VISC and GC-UNIMOD.

We appreciate the reviewer's suggestion of moving Fig. S3 to the body of the main text, although we have chosen to keep it in the Supplementary Information. Instead we discuss it alongside Fig. 4 in Section 3.2 of the revised main text. We have done this to avoid crowding Fig. 4 with additional curves and because the GC-UNIMOD results are very similar to those of the volume fraction-weighted mixing rule.

Changes to Manuscript: Fig. S3 has been modified and a discussion comparing GC-UNIMOD and AIOMFAC-VISC has been added to Section 3.2 of the main text.

Comment 2: The authors include a fragile-to-strong crossover (FSC) into their viscosity calculation; however, they do not show how this assumption affects their results. Please indicate the applicability of this model feature. The effect is shown in Fig. 2, but since only glass transition measurements are plotted here, no judgment on the necessity on the FSC is possible. Overall, Fig. 2 strikes me as a figure without much benefit for the reader since, in principal, only the performance of the glass transition estimation tool is evaluated. Can the authors think of any other way to show how temperature-dependence of viscosity is accurately represented by AIOMFAC-VISC?

Author Response: The effect of the FSC is noticeable in the AIOMFAC-VISC results when the temperature of a computation is above or below the glass transition temperature of the organics involved in the mixture. In particular, the effect of the FSC is most noticeable at temperatures much colder than the glass transition temperature. For example, in Fig. 2b we show that regardless of the choice of fragility parameter, the pure-component viscosity of citric acid at ~ 293 K is predicted to be approximately $10^{7.9}$ Pa s. However, at ~ 273 K, the choice of fragility parameter influences the pure-component viscosity of citric acid by several orders of magnitude. At this temperature, a fragility parameter of 30 gives a pure-component viscosity of approximately 10^{15} Pa s and a fragility parameter of 5 gives a pure-component viscosity of approximately 10^{35} Pa s. If we assume the FSC to have occurred for citric acid cooled to ~ 273 K, then we know that a fragility parameter of 5, and by extension, a pure-component viscosity of 10^{35} Pa s, is unreasonable. However, we have no independent data for verifying this for proxy aerosol mixtures comprised of citric acid or similar compounds, because, to our knowledge, there are no viscosity measurements of binary aqueous mixtures at temperatures at or below 273 K.

In practice, for the case of citric acid and compounds which have similar glass transition temperatures, the FSC is a necessary implementation in the model for simulations with temperatures representative of higher altitudes. More generally, the FSC is important for compounds whose glass transition temperature is warmer than the temperature of interest for a prediction. For example, the FSC is relevant for calculations at room temperature involving compounds like sucrose, whose glass transition temperature is above 300 K. For sucrose at ~ 293 K, a fragility parameter of 30 gives a pure-component viscosity of approximately 10^{18} Pa s and a fragility parameter of 10 yields a pure-component viscosity greater than 10^{40} Pa s. Again, we assume the FSC to have occurred for sucrose at room temperature, and indeed, a fragility parameter of 30 produces a pure-component viscosity value that is in better agreement with the viscosity measurements for aqueous sucrose as a function of mass fraction of water when compared to a fragility parameter of 10.

Changes to Manuscript: In order to emphasise the effect of the FSC we have added two panels to Fig. 2, showing the results of AIOMFAC-VISC for citric acid and sucrose at room temperature using different values for the fragility parameter. In Fig. 2e, we show that the choice of fragility parameter does not effect the mixture viscosity because all three parameters produce approximately the same pure component viscosity. This is contrasted with Fig. 2f, where a fragility parameter of 10 causes an overestimation of the pure-component viscosity and by extension, an overestimation of the mixture viscosity by several orders of magnitude, when compared to a fragility parameter of 30. We have also added a summary of the FSC implementation in AIOMFAC-VISC to the end of Section 2.2.2.

Comment 3: A weakness for the applicability of AIOMFAC-VISC (and any group contribution method for that matter) is the need for structure formulas of chemical components. For SOA, these are determined in this study through running the Master Chemical Mechanism (MCM) and hence relies on accuracy of the structures provided from this model calculation. The process is a bit convoluted as it demands running the external model and selection of a subset of chemical compounds based on matching to molecular O/C ratio. It would be beneficial for the reader if the authors could outline which parts of the process

matter a lot and which are not as important. Hence, what is the sensitivity of the final viscosity output to the assumptions that were made?

Author Response: As the reviewer correctly states, the success of AIOMFAC-VISC for accurately predicting SOA mixture viscosity is reliant, in part, on the definition of the SOA mixture by means of selected surrogate structures. In order to demonstrate the sensitivity of the AIOMFAC-VISC results to changes in the molecular O:C ratio, we have added a figure to the supplement, Fig. S7. We show three different AIOMFAC-VISC results when the average molecular O:C ratio of the SOA mixture is varied. Variation of the average O:C ratio is achieved by adjusting the concentrations of mixture components listed in Tables S2–S4. The mixture compositions are adjusted in such a way to represent a reasonable range of O:C (but not necessarily equally likely outcomes from actual gas phase oxidation). Care is taken to ensure the mixture does not become dominated by one or two compounds in the effort to achieve a range of average O:C values. A wider range of average O:C is possible if certain compounds dominate the SOA mixture, but then the AIOMFAC-VISC prediction will mostly be a reflection of the viscosity of the dominant compound.

This new figure demonstrates that changes in the average O:C ratio (in effect, the mixture composition) has an impact with a magnitude similar to the uncertainty in the pure-component viscosity. More precise experimental estimates of the average O:C ratio or chemical composition of the SOA mixtures would help to better inform AIOMFAC-VISC. Furthermore, it is important to note that there may be a tendency to think of the sensitivity of AIOMFAC-VISC to mixture composition as a model uncertainty, but really it is a reflection of the model's ability to represent the mixture viscosity of SOA systems with various compositions. Therefore, while using the MCM and selecting a subset of compounds to represent a given SOA mixture is an added complexity in AIOMFAC-VISC, the benefit of this approach is the precision it offers when comparing the model to data with well-constrained experimental systems. Moreover, the need for structure formulas with a group contribution method for viscosity is not necessarily a weakness, it is merely a reflection of the issues arising from incomplete information about complex organic aerosol systems. It seems obvious that one should not expect a model to provide precise predictions of mixture viscosity when little is known about the actual molecular composition of the system.

Changes to Manuscript: In the Supplementary Information we have added Fig. S7 and accompanying text discussing this figure in Section S6.

Comment 4: Fig. 4 is very helpful for the reader. I wonder however, how well a simpler activity coefficient estimation method than AIOMFAC with a simple mixing scheme would fair in this comparison. Which part is more important: accurate activity coefficients or features such as contribution of the residual viscosity?

Author Response: This comment overlaps with comment 2 from Anonymous Reviewer #1 and comment 1 from Anonymous Reviewer #2. We refer the reader to our responses and changes made to the manuscript under comments 1 and 2 from Reviewer #1 and comment 1 from Reviewer #2.

Technical Comment: p. 22, l.13 – The word "Figure" seems to be missing before (7b).

Manuscript Changes: Added.

References

DeRieux, W. S. W., Li, Y., Lin, P., Laskin, J., Laskin, A., Bertram, A. K., Nizkorodov, S. A., and Shiraiwa, M.: Predicting the glass transition temperature and viscosity of secondary organic material using molecular composition, Atmospheric Chemistry and Physics, 18, 6331–6351, https://doi.org/10.5194/acp-18-6331-2018, 2018.

Nannoolal, Y., Rarey, J., and Ramjugernath, D.: Estimation of pure component properties. Part 4: Estimation of the saturated liquid viscosity of non-electrolyte organic compounds via group contributions and group interactions, Fluid Phase Equilibria, 281, 97–119, https://doi.org/10.1016/j.fluid.2009.02.016, 2009.

Rothfuss, N. E. and Petters, M. D.: Influence of Functional Groups on the Viscosity of Organic Aerosol, Environmental Science and Technology, 51, 271–279, https://doi.org/10.1021/acs.est.6b04478, 2017.

Sastri, S. and Rao, K.: A new group contribution method for predicting viscosity of organic liquids, The Chemical Engineering Journal, 50, 9–25, https://doi.org/10.1016/0300-9467(92)80002-R, 1992.

Shiraiwa, M., Li, Y., Tsimpidi, A. P., Karydis, V. A., Berkemeier, T., Pandis, S. N., Lelieveld, J., Koop, T., and Pöschl, U.: Global distribution of particle phase state in atmospheric secondary organic aerosols, Nature Communications, 8, 1–7, https://doi.org/10.1038/ncomms15002, 2017.

A predictive group-contribution model for the viscosity of aqueous organic aerosol

Natalie R. Gervasi[1], David O. Topping[2], and Andreas Zuend[1]

[1]Department of Atmospheric and Oceanic Sciences, McGill University, Montreal, Quebec, H3A 0B9, Canada
[2]School of Earth, Atmospheric and Environmental Science, University of Manchester, Manchester M13 9PL, U.K.

Correspondence: Andreas Zuend (andreas.zuend@mcgill.ca)

Abstract. The viscosity of primary and secondary organic aerosol (SOA) has important implications for the processing of aqueous organic aerosol phases in the atmosphere, their involvement in climate forcing, and transboundary pollution. Here we introduce a new thermodynamics-based group-contribution model, which is capable of accurately predicting the dynamic viscosity of a mixture over several orders of magnitude ($\sim 10^{-3}$ to $> 10^{12}$ Pa s) as a function of temperature and mixture composition, accounting for the effect of relative humidity on aerosol water content. The mixture viscosity modelling framework builds on the thermodynamic activity coefficient model AIOMFAC (Aerosol Inorganic–Organic Mixtures Functional groups Activity Coefficients) for predictions of liquid mixture non-ideality, including liquid–liquid phase separation, and the calorimetric glass transition temperature model by DeRieux et al. (2018) for pure-component viscosity values of organic components. Comparing this new model with simplified modelling approaches reveals that the group-contribution method is the most accurate in predicting mixture viscosity, although accurate pure-component viscosity predictions (and associated experimental data) are key and one of the main sources of uncertainties in current models, including the model presented here. Nonetheless, we find excellent agreement between the viscosity predictions and measurements for systems in which mixture constituents have a molar mass below $350\,\mathrm{g\,mol^{-1}}$. As such, we demonstrate the validity of the model in quantifying mixture viscosity for aqueous binary mixtures (glycerol, citric acid, sucrose, and trehalose), aqueous multicomponent mixtures (citric acid + sucrose and a mixture of nine dicarboxylic acids), and aqueous SOA surrogate mixtures derived from the oxidation of α-pinene, toluene, or isoprene. We also use the model to assess the expected change in SOA particle viscosity during idealized adiabatic air parcel transport from the surface to higher altitudes within the troposphere. This work demonstrates the capability and flexibility of our model in predicting the viscosity for organic mixtures of varying degrees of complexity and its applicability for modelling SOA viscosity over a wide range of temperatures and relative humidities.

1 Introduction

Viscosity measurements of laboratory-made proxy aerosol particles were the first evidence suggesting that secondary organic aerosol (SOA) particles could exist in a highly viscous state (Zobrist et al., 2008; Murray, 2008). Shortly after, field measurements demonstrated that ambient SOA exhibit semi-solid or glassy behaviour in certain environments (Virtanen et al., 2010).

In the decade since these discoveries, the implications of highly viscous aerosols (or organic-rich phases thereof) have been a focus of intense study. Viscosity can impact the chemical and physical properties of organic aerosol (OA) particles, prolonging their equilibration with the surrounding gas phase. As an example, the gas–particle partitioning of water (Bones et al., 2012; Berkemeier et al., 2014; Price et al., 2015), semivolatile organics (Abramson et al., 2013; Marshall et al., 2016), and oxidizing compounds (Berkemeier et al., 2016) have been shown to be kinetically limited by slow diffusion in highly viscous or glassy particles. The slowed uptake of semivolatile organics from the gas phase can retard SOA formation and growth. Conversely, the slow diffusion of these molecules out of the particle bulk can impede evaporation. Oxidation reactions within a particle or diffusion of reactants to the particle surface are also slowed, leading to the extended preservation of organic species within aerosol phases that would otherwise undergo photodegradation (Zelenyuk et al., 2017). Reduced evaporation and shielding from oxidation may increase the residence time or organic species, giving these particles and their constituents an advantage in undergoing long-range transport (Schum et al., 2018; Zhou et al., 2019) and in turn, contributing to transboundary pollution (Shrivastava et al., 2017).

Oxidation or multiphase reactions in viscous SOA not only have implications for air quality, but for climate as well. Liu et al. (2018) demonstrated that the production of brown carbon aerosol can be viscosity-limited. SOA that would normally undergo browning due to multiphase chemical reactions instead remain translucent due to slowed reaction kinetics. Their translucency causes them to preferentially scatter, rather than absorb, solar radiation. While the prevention of brown carbon by viscous organics has a direct influence on aerosol-radiation-climate effects, in addition, SOA phase state may impact climate and weather indirectly via its potential role in ice nucleation. There is potential for extremely viscous, glassy SOA particles to act as ice nuclei and therefore play a role in ice cloud formation and related optical and lifetime properties of cold clouds (Berkemeier et al., 2014; Lienhard et al., 2015; Knopf et al., 2018; Fowler et al., 2019).

In order to fully understand the implications of viscous SOA we must be able to quantify how frequently SOA precursors and atmospheric conditions, namely relative humidity (RH) and temperature, favour their formation. Semi-solid anhydrous SOA can be formed from biogenic precursors, like monoterpenes (Renbaum-Wolff et al., 2013; Grayson et al., 2016) and isoprene (Song et al., 2015) or from anthropogenic precursors, like polycyclic aromatic hydrocarbons (Zelenyuk et al., 2017). The type of precursor as well as the degree of oxidation governs the degree of functionalization of the resulting SOA species. The pure-component viscosity of an organic species is more sensitive to certain oxygen-bearing functional groups compared to others; although, oxygen-bearing functional group addition is directly proportional to viscosity (Rothfuss and Petters, 2017). Indeed, prolonged oxidation, leading to increased functionalization of precursor and derived hydrocarbons has been shown to increase SOA viscosity at low relative humidity (Saukko et al., 2012).

The hygroscopicity of the SOA mixture also dictates particle viscosity. For a given ambient relative humidity (of typically $> 20\,\%$), less hygroscopic SOA components will tend to form more viscous mixtures as compared to their more hygroscopic counterparts of similar molar mass due to the plasticizing effect of absorbed water under equilibrium conditions (Zobrist et al., 2008). Therefore, closely related to hygroscopicity in effect, relative humidity (or water activity in the particle) is a strong modulator of particle viscosity (Price et al., 2015; Ye et al., 2016). We can expect SOA particles of a given composition to have a higher viscosity under dry conditions and it is possible for organics to undergo a moisture-driven glass transition at typical surface-level temperatures (Dette et al., 2014). More ubiquitous is temperature-driven vitrification, where a compound/mixture is cooled rapidly enough to avoid crystallization and instead, the motions of the molecules are slowed to such an extent that they cannot reach the most stable equilibrium positions (i.e. those at lattice positions of a crystal) on an experimental timescale.

Of course, the effects of temperature and relative humidity cannot be fully decoupled in the atmosphere. Close to the Earth's surface, highly viscous SOA are found in colder, dryer regions (Virtanen et al., 2010), whereas primarily liquid-like SOA dominate in warmer, humid locations (Bateman et al., 2016). The viscosity of SOA at higher tropospheric altitudes remains an open question due to the competing effects of decreasing temperature and increasing relative humidity (Knopf et al., 2018). Recently, a similar ambiguity was observed on a diurnal timescale at the surface in a mixed forest environment, where SOA particles were found to be more viscous during the night as compared to during the day, despite a lower daytime relative humidity. The observed diel cycle of viscosity appears to be dominated by chemical changes in submicron-sized SOA composition (Slade et al., 2019). Therefore, for an advanced assessment of the climate impact of aerosol viscosity, it is imperative that we understand the interplay of chemical composition, ambient temperature, and relative humidity in order to quantify the spatiotemporal range of aerosol viscosity in different geographic regions and vertical levels of the atmosphere.

To this end, several groups have developed novel techniques to measure both laboratory-made, proxy particles and ambient SOA viscosity (see Reid et al. (2018) and references therein). Work has also been carried out for developing predictive tools to model SOA viscosity; although, a lack of experimental data to constrain the models, coupled with an incomplete characterization of SOA chemical composition has made this work challenging. Most of the models developed so far have been trained and tested with simple organic mixtures in the liquid regime (where the dynamic viscosity $\eta_{\mathrm{mix}} < 10^2$ Pa s). These models vary in complexity, for example, Cao et al. (1993a) employ a group-contribution approach adopted from a statistical thermodynamics treatment (Cao et al., 1993b), while the work by Bosse (2005) outlines a simple, mole-fraction-based mixing rule. Song et al. (2016c) demonstrated the validity of the Bosse (2005) mixing rule for binary aqueous mixtures with alcohol, di- or tricarboxylic acids up to a mixture viscosity of 10^4 Pa s. They also showed this simple model overestimated the viscosity of binary aqueous mono-, di- and trisaccharide mixtures. Recently, Rovelli et al. (2019) compared the Bosse (2005) model with their own water-activity-dependent viscosity mixing rule. They show that the water-activity-dependent predictions outperformed the Bosse (2005) for most of their ternary aqueous sucrose–citric acid and aqueous sucrose–$\mathrm{NaNO_3}$ mixtures up to $\eta_{\mathrm{mix}} \sim 10^6 - 10^7$ Pa s. Shiraiwa et al. (2017) were the first to use a semi-empirical modelling approach to constrain the phase state of SOA based on estimations of the (calorimetric) glass transition temperature of SOA species. DeRieux et al. (2018) expanded on that approach, using glass transition temperature estimations to predict the viscosity of α-pinene SOA, toluene SOA, isoprene SOA, and biomass burning particles.

In this study, we introduce our thermodynamics-based group-contribution approach developed to predict the viscosity of aqueous OA phases covering several orders of magnitude in viscosity ($\sim 10^{-3}$ to $> 10^{12}$ Pa s) as a function of organic mixture composition, temperature, and relative humidity. To this end, our mixing model is coupled with pure-component glass transition temperature estimations by the DeRieux et al. (2018) method. This new development aims for extending the predictability and accuracy beyond the range of existing approaches. The rest of this article is structured as follows: we begin by detailing the model framework and discussing model limitations, followed by comparing the performance of the model with simplified mixing rules. We then discuss the training of the model for a dozen binary aqueous organic mixtures followed by presenting the model's predictive ability for well-constrained multicomponent aqueous organic mixtures. Furthermore, model predictions of the RH-dependent mixture viscosities of α-pinene SOA, toluene SOA, and isoprene SOA are compared to viscosity measurements of laboratory generated SOA. Finally, we discuss atmospheric implications of our model's predictions by exploring the mixture viscosity of the aforementioned SOA systems across the atmospherically relevant temperature and relative humidity space.

2 Theory and methods

We have built a method to predict the viscosity of (aqueous) organic mixtures within the Aerosol Inorganic–Organic Mixtures Functional groups Activity Coefficient (AIOMFAC) model framework (Zuend et al., 2008, 2011); this new method is abbreviated as AIOMFAC-VISC. In general terms, our model combines temperature-dependent physicochemical pure-component properties of organic molecules and water with a non-linear mixing model for dynamic viscosity. Hence, the general approach is similar to predictions of the equilibrium vapour pressures of solution components, which also involves pure-component properties and mixing effects.

At the core of AIOMFAC-VISC are a set of equations relating the viscosity of a mixture to the structural features of chemical components, their relative abundance in a phase and to temperature. These equations are based on those from an existing group-contribution thermodynamics-viscosity model called GC-UNIMOD (Cao et al., 1993a), but modified in several important ways. Within AIOMFAC-VISC, AIOMFAC supplies predictions of non-ideal thermodynamic mixing effects in a solution phase in the form of component activity coefficients, while two additional parameterizations are used for pure-component properties. First, the parameterization described by Dehaoui et al. (2015) is used to estimate the viscosity of water as a function of temperature. Second, the method introduced by DeRieux et al. (2018) is used to estimate the pure-component viscosity of individual organic molecules for a given temperature. In the following, we describe the combination of models and parameterizations that comprise the AIOMFAC-VISC method.

2.1 Mixture viscosity predictions

We have modified the semi-empirical viscosity equations of GC-UNIMOD to better represent atmospherically relevant organic mixtures. Following Cao et al. (1993a), the natural logarithm of the dynamic viscosity of a mixture, η_{mix}, is expressed in
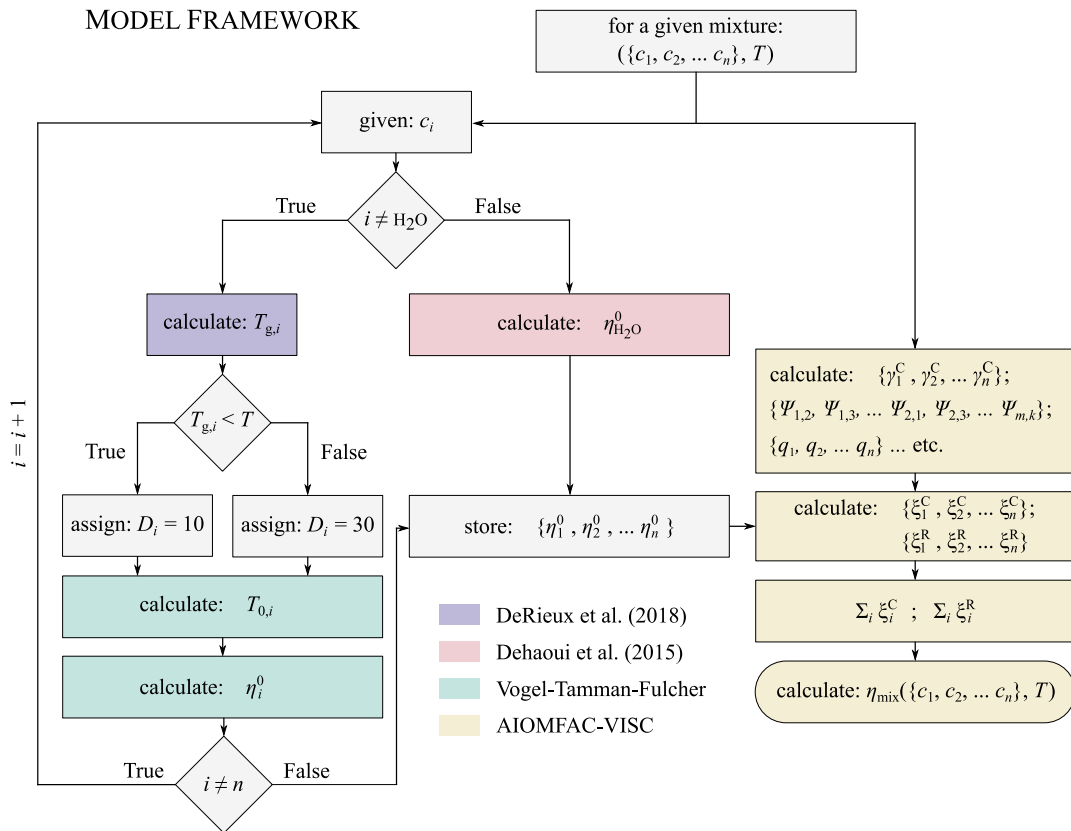
Figure 1. A flow chart showing a simplified schematic of the AIOMFAC-VISC model framework. The colour shadings of the boxes denote the model or parameterization being used at a given point in the framework. Blue indicates the use of the DeRieux et al. (2018) model to predict the pure-component calorimetric glass transition temperature, green indicates the use of the modified Vogel–Tammann–Fulcher equation to predict the pure-component viscosity of the organic components, red indicates the use of the Dehaoui et al. (2015) parameterization to estimate the pure-component viscosity of water, and yellow indicates the use of AIOMFAC-VISC to calculate the mixture viscosity. The model components shown in blue, green, and red are interchangeable with other methods of calculating the pure-component viscosities. Should more accurate methods of predicting pure-component viscosity become available in the future, the AIOMFAC-VISC framework can be updated.

AIOMFAC-VISC as

$$\ln\left(\eta_{\text{mix}}\right) = \sum_{i=1}^{n} \left[\xi_i^C + \xi_i^R\right]. \tag{1}$$

Here, n is the number of individual mixture components (molecules), and ξ_i^C and ξ_i^R are the combinatorial and residual viscosity contributions of the ith molecule, respectively. The combinatorial contributions represent the geometric properties of each molecule in a simplified form, whereas the residual contributions account for the inter-molecular interactions, e.g. due to van der Waals forces. Specifically, and unlike the equation for ξ_i^C in GC-UNIMOD, we introduce the combinatorial contribution of the ith molecule as the product of pure-component viscosity times combinatorial activity,

$$\xi_i^C = \gamma_i^C x_i \ln(\eta_i^0), \tag{2}$$

where γ_i^C is the combinatorial activity coefficient, x_i is the molar fraction (with respect to the mixture of molecules), and η_i^0 is the temperature-dependent pure-component viscosity. The mole-fraction-based combinatorial activity ($a_i^C = \gamma_i^C x_i$) is routinely computed as part of the Universal Quasi-Chemical Functional group Activity Coefficients (UNIFAC) model (Fredenslund et al., 1975) equations within the AIOMFAC model. It can be considered an effective measure of composition – a modification of the mole fraction composition scale to account for differences in shapes and sizes of molecules, which is important when mixtures contain small molecules like water as well as significantly larger molecules like sucrose, raffinose or various oligomers.

The residual contributions are written as

$$\xi_i^R = \Phi_i \left[\sum_k \nu_k^{(i)} \Xi_k^{(i)} - \sum_k \nu_k^{(i)} \Xi_k^{(i),\text{ref}}\right], \tag{3}$$

where $\Xi_k^{(i)}$ is the residual viscosity of (sub)group k for component i (indicated by the superscript) in the mixture of components and with $\nu_k^{(i)}$ being the number of groups k within molecule i. $\Xi_k^{(i),\text{ref}}$ is the group residual viscosity of group k for component i in the pure-component solution of the ith component, representing a reference value for each component. Both terms are expressed as

$$\Xi_k^{(i)} = \frac{Q_k}{R_k} N_{k,i}^{vis} \sum_m \left[\Gamma_{m,k} \ln\left(\Psi_{m,k}\right)\right], \tag{4}$$

where for the ith molecule there exist functional subgroups k, while subgroup-index m covers here all subgroups from all molecules of the mixture (with the definition of a subgroup as in UNIFAC, AIOMFAC). Hence, in the reference value calculation for $\Xi_k^{(i),\text{ref}}$, index m covers all subgroups of that molecule (i). For subgroup k, Q_k and R_k are its relative van der Waals surface area and volume parameters, respectively (Hansen et al., 1991). The parameter $N_{k,i}^{vis}$ is computed as follows (Cao et al., 1993a):

$$N_{k,i}^{vis} = Q_k \left(\frac{q_i - r_i}{2} - \frac{1 - r_i}{z}\right), \tag{5}$$

where,

$$q_i = \sum_k \nu_k^{(i)} Q_k \quad \text{and} \quad r_i = \sum_k \nu_k^{(i)} R_k. \tag{6}$$

Variables q_i and r_i are the molecule-specific relative surface area and volume parameters, respectively. The lattice coordination number, z, is set as a constant of value 10 (Zuend et al., 2008).

Next, we note that the local interaction composition of subgroups, $\Gamma_{m,k}$ (Eq. 4), is described by the following set of expressions involving the fractional relative subgroup surface area Θ_m:

$$\Theta_m = \frac{X_m Q_m}{\sum_k X_k Q_k} \quad \text{and} \quad \Gamma_{m,k} = \frac{\Theta_m \Psi_{m,k}}{\sum_k \Theta_k \Psi_{m,k}}, \tag{7}$$

where

$$\Psi_{m,k} = \exp\left[\frac{-a_{m,k}}{T}\right]. \tag{8}$$

Here $\Psi_{m,k}$ is a function of the AIOMFAC subgroup interaction parameter, $a_{m,k}$ and temperature, T. X_m in Eq. (7) is the molar fraction of subgroup m within the mixture of subgroups. For additional information regarding Θ_m and $\Psi_{m,k}$ we refer the reader to Zuend et al. (2008).

Finally, returning to Eq. (3), the volume fraction, Φ_i, which is here based on the relative van der Waals molecular volumes (Eq. 6), can be expressed as

$$\Phi_i = \frac{x_i r_i}{\sum_{j=1}^{n} x_j r_j}. \tag{9}$$

We note that the residual contribution to viscosity, ξ_i^R is nearly identical to the formulation of GC-UNIMOD, except for the expression for $N_{k,i}^{vis}$; our expression (Eq. 5) differs from its counterpart in GC-UNIMOD by a factor -1 (both are semi-empirical expressions and not fundamentally derived from theory). Doing so allows for significantly better agreement between AIOMFAC-VISC and measurements of dynamic viscosity for binary aqueous mixtures (see Supplementary Information, SI, Section S5).

2.2 Pure-component viscosity predictions

2.2.1 Water

AIOMFAC-VISC requires knowledge of the pure-component dynamic viscosity (η^0) of the individual mixture components. The pure-component viscosity is the viscosity of a given component in its pure liquid, semi-solid or amorphous solid state as a function of temperature. Bulk measurements for a range of pure-component viscosity values ($10^{-3} - 10^8$ Pa s) can be made using conventional equipment, like a viscometer or rheometer at temperatures typically between -40 and $200\,^\circ\text{C}$ (Reid et al., 2018). With a sufficient number of measurements, the pure-component viscosity can be described empirically or semi-empirically for the temperature range over which the measurements were made.

For example, in this work we estimate the pure-component viscosity of water using the semi-empirical power law parameterization given by Dehaoui et al. (2015):

$$\eta_{\text{H}_2\text{O}}(T) = \text{A}\left(\frac{T - T_\text{s}}{T_\text{s}}\right)^{-\text{B}}, \tag{10}$$

where η_{H_2O} is the pure-component viscosity of water, T is the temperature in Kelvin (K), A and B are constants with values of $(1.3788 \pm 0.0026) \times 10^{-4}$ Pa s and 1.6438 ± 0.0052, respectively. T_s is theorized to be the mode-coupling temperature of water with a value of 225.66 ± 0.18 K. The Dehaoui et al. (2015) parameterization is supported by experimental data over the temperature range $\sim 230 - 400$ K (and likely reasonable to lower T), covering most of the atmospherically relevant temperature range (see Fig. S1 in the SI).

2.2.2 Organic compounds

It should be noted that AIOMFAC-VISC typically does not consider the crystallization of organic compounds; rather, the model assumes that all components remain amorphous over the entire temperature and relative humidity space. In practice, this is a reasonable assumption because crystallization in complex SOA mixtures is likely suppressed owing to the variety of compounds that comprise the SOA phase. As a result, this assumption necessitates supplying AIOMFAC-VISC with the pure-component viscosity for all individual components.

Given the abundance of experimental data and the quality of the Dehaoui et al. (2015) power law fit, we have a high degree of confidence in the predicted temperature-dependent pure-component viscosity of water for a range of atmospherically relevant temperatures. However, the estimate of the temperature-dependent pure-component viscosity for organic components is a significantly more nuanced problem. First, for most atmospherically relevant organics there are no measurements of their pure-component viscosity. Often the lack of data is a result of the organics having ultra-high pure-component viscosities ($> 10^8$ Pa s) near room temperature, making their measurement experimentally inaccessible. For those organics whose pure-component viscosities have been measured, the experiments are typically performed at room temperature ($\sim 20 - 25\,^\circ$C), which limits our ability to determine the temperature dependence and to parameterize the functional form to lower temperatures. Therefore, the lack of available data precludes our use of empirically determined pure-component viscosity values.

The scarcity of high-viscosity experimental data motivated us to instead use the group contribution model developed by Nannoolal et al. (2009) for the prediction of the pure-component viscosity values. However, the Nannoolal et al. (2009) model was developed/validated only for predicting liquid-like viscosities $\ll 1$ Pa s and, therefore, it is not reliable for predicting viscosity in the semi-solid and glassy regime for the compounds we are interested in. Sastri and Rao (1992) have developed a group-contribution model for pure-component viscosity based on a relationship of viscosity with pure-component vapour pressure; however, this model was also developed for liquid-state viscosities only.

We also attempted to determine a semi-empirical relationship between pure-component viscosity and pure-component vapour pressure. We compared experimentally-determined and modelled values of pure-component viscosity with modelled pure-component vapour pressures. Modelled viscosity values were calculated using the Nannoolal et al. (2009) group-contribution approach and vapour pressure values were determined using the online tool UManSysProp (http://umansysprop.seaes.manchester. ac.uk) (Topping et al., 2016) with the model by Nannoolal et al. (2008) or by using the EVAPORATION model (Compernolle et al., 2011) without the empirical factor for functionalized dicarboxylic acids. At lower viscosity and vapour pressure, the relationship is linear in double logarithmic space; however, this relationship does not apply sufficiently well at higher viscosity values (see Fig. S2).
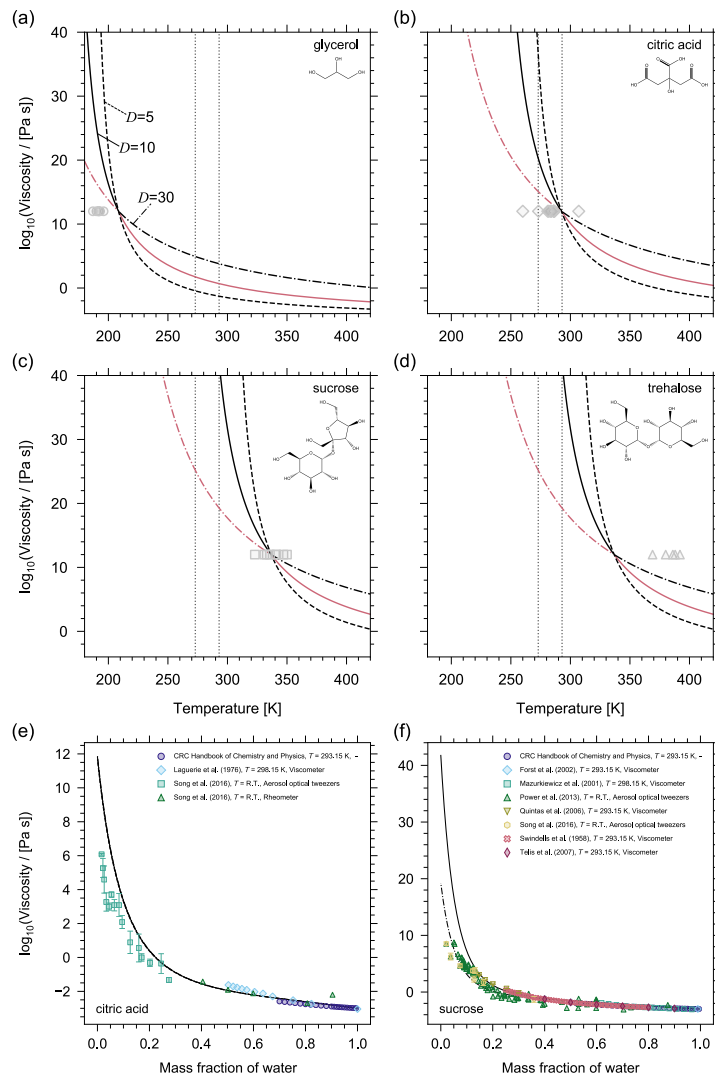
Figure 2. Prediction of the pure-component viscosity (η^0) as a function of temperature using the method by DeRieux et al. (2018) for (**a**) glycerol, (**b**) citric acid, (**c**) sucrose, and (**d**) trehalose. The three curves in each panel show the effect of different fragility parameters on the pure-component viscosity prediction (solid, $D = 10$; dashed, $D = 5$; dash-dotted, $D = 30$). The pink lines illustrates which fragility parameter the model uses as a function of temperature, i.e. when $T > T_g$ then $D = 10$ and when $T < T_g$ then $D = 30$. The grey symbols are reference values of T_g (either measured or parameterized) where horizontal error bars have been omitted for clarity (additional information and the sources of the T_g values can be found in Table S1). The reference values of T_g have been plotted using the convention that $\eta^0(T_g) = 10^{12}$ Pa s. The vertical grey dotted lines denote 0 °C and 22 °C. (**e, f**) Mixture viscosity predictions from AIOMFAC-VISC for (e) citric acid and (f) sucrose are shown for different fragility parameters where the curve line styles follow the same convention as in (a – d). For citric acid, the model results with $D = 5$, $D = 10$, and $D = 30$ are nearly identical, so the curves are indistinguishable. For sucrose, $D = 10$ (solid) and $D = 30$ (dash-dotted) are shown. For a detailed discussion of the AIOMFAC-VISC results see Fig. 5 and Section 3.2.

Ultimately, at present it is not possible to rely on directly measured or predicted pure-component viscosity values of organic compounds over the atmospheric temperature range. As a result, we employ the method developed by DeRieux et al. (2018), which uses the calorimetric glass transition temperature, T_g (herein called the glass transition temperature) to predict the pure-component viscosity of organic compounds. This method is an updated T_g parameterization based on previous work done by Shiraiwa et al. (2017). Compared to the Shiraiwa et al. (2017) method (validated for compounds $M < 450\,\mathrm{g\,mol^{-1}}$), the DeRieux et al. (2018) method was designed to perform better also for higher molar mass compounds. With the DeRieux et al. (2018) method, we first predict T_g of the organic compounds. We then use the glass transition temperature to calculate the pure-component viscosity of the organics via the modified Vogel–Tammann–Fulcher equation (Angell, 1991; DeRieux et al., 2018). A semi-empirical, elemental-contribution model is used by DeRieux et al. (2018) to predict the glass transition temperature for a given organic molecule:

$$T_{\mathrm{g}} = \left(y_{\mathrm{C}}^0 + \ln(y_{\mathrm{C}})\right) b_{\mathrm{C}} + \ln(y_{\mathrm{H}})b_H + \ln(y_{\mathrm{C}})\ln(y_{\mathrm{H}})b_{\mathrm{CH}} + \ln(y_{\mathrm{O}})b_{\mathrm{O}} + \ln(y_{\mathrm{C}})\ln(y_{\mathrm{O}})b_{\mathrm{CO}} \tag{11}$$

where y_{C}, y_{H}, and y_{O} are the number of carbon, hydrogen and oxygen atoms of the molecule. b_{C}, b_{H}, b_{O}, b_{CH}, and b_{CO} are model parameters determined by optimization using T_{g} training data from experiments. For the parameter values and a full description of the model, the reader is referred to the aforementioned work. The estimated glass transition temperature is then used to calculate the Vogel temperature, T_0 and subsequently, the pure-component viscosity (Angell, 1991):

$$T_0 = \frac{39.17 T_{\mathrm{g}}}{D + 39.17}\;; \qquad \log_{10}(\eta^0) = -5 + 0.434\frac{T_0 D}{T - T_0} \tag{12}$$

where Angell (1991) has assumed,

$$\lim_{T \to \infty} \eta = 10^{-5}\ \mathrm{Pa\ s} \quad \text{and} \quad \eta^0(T_{\mathrm{g}}) = 10^{12}\ \mathrm{Pa\ s}. \tag{13}$$

The Vogel temperature, T_0, and the fragility parameter, D, are component-specific properties. T_0 is thought to be related to the Kauzmann temperature (the ideal glass transition temperature) (Angell, 1997). The fragility parameter, D indicates whether the (liquid) compound is a "strong" or "fragile" glass-former. Strong glass-formers show an approximately linear increase in $\log_{10}(\eta^0)$ (Arrhenius behaviour) as they are cooled toward their glass transition (Debenedetti and Stillinger, 2001). In other words, the activation energy for viscous flow in strong liquids is temperature independent (i.e. $T_0 = \mathrm{constant}$ in Eq. 12). Conversely, as a fragile glass-former undergoes cooling it will show very little increase in viscosity until near the glass transition, whereupon it will experience a steep increase in viscosity (so-called super-Arrhenius behaviour). In the case of a fragile glass-former, the activation energy for viscous flow is temperature dependent (i.e. $T_0 = T_0(T)$ in Eq. 12). In practice, D is calculated from a so-called Arrhenius plot. An Arrhenius plot illustrates the curve produced on a graph of $\log_{10}(\eta_i^0)$ vs. $\frac{T_{\mathrm{g}}}{T}$. The slope of the curve at $\frac{T_{\mathrm{g}}}{T} = 1$ produces the fragility index, m, from which the fragility parameter is derived via $D = \frac{665.89}{m-17}$ (DeRieux et al., 2018).

Predictions of pure-component viscosity as a function of temperature using Eqs. (11) and (12) are shown for glycerol, citric acid, sucrose, and trehalose in Fig. 2. Grey symbols indicating reference T_{g} values (either measured or parameterized) are also shown according to the convention that $\eta^0(T_{\mathrm{g}}) = 10^{12}$ Pa s. Although, it is important to note that for fragile glass-formers

$\eta^0(T_\mathrm{g})$ may be up to four orders of magnitude lower than 10^{12} Pa s (Angell, 1995). As such, including the reference T_g values does not provide a clear picture of the performance of the DeRieux et al. (2018) method for individual components; however, it allows us to make relative comparisons among certain components. For example, sucrose and trehalose, both disaccharides, are structural isomers differing in their composition from two monosaccharides, with reference T_g values that reflect this

5   difference; however, both compounds have the same number of carbon, hydrogen and oxygen atoms, so the DeRieux et al. (2018) method produces identical pure-component viscosity predictions. The inherent omission of more detailed structural information illustrates one potential limitation of that pure-component viscosity prediction method. Nonetheless, the fact that the pure-component viscosity prediction can be made for any organic over a large temperature range affords a level of flexibility and predictability that, at present, outweighs the potential inaccuracies. More importantly, the potential inaccuracy of this

10   method may be largely associated with our choice of the fragility parameter. For organic compounds, D values typically range from $\sim 5-30$ (Angell, 1997; DeRieux et al., 2018) and for most organics at or around room temperature, assuming a fragility parameter of 10 has been shown to be appropriate (Shiraiwa et al., 2017; DeRieux et al., 2018). We believe this to be especially true in the context of complex SOA mixtures where individual components may have fragility parameters that deviate from $D = 10$, but with a sufficient number of components in the mixture, these deviations will be offset. Moreover, for some organics

15   whose T_g is close to the temperature of interest in a mixture viscosity calculation, the choice of fragility parameter may only have a small influence on the pure-component viscosity prediction. Figure 2 illustrates that for citric acid near 298 K any value of D between 5 and 30 will produce nearly identical values of pure-component viscosity. However, we highlight this case in particular because it appears to be the exception. For glycerol, sucrose, and trehalose in Fig. 2 the choice of D at room temperature presents a large discrepancy (several orders of magnitude) in the pure-component viscosity. This is true for most

20   organics studied in this work.

    In general, the choice of D becomes most influential in the supercooled regime, specifically beyond the organic's T_g if T_g occurs at the conventionally assigned viscosity of 10^{12} Pa s. For example, $D = 10$ will produce similar values of pure-component viscosity at either room temperature or at 273 K for glycerol, however the opposite is true for citric acid, sucrose, and trehalose (Fig. 2). As such, we must consider our choice of D not only for comparison with laboratory (room temperature)

25   data, but for temperatures representative of where we expect viscous aerosol to be most relevant (around and below 15 °C). The temperature at which we must begin to concern ourselves with the influence of the fragility parameter varies from compound to compound, but for each compound this issue always presents itself above and below its T_g.

    There is also recent evidence to suggest that some liquid glass-formers undergo a fragile-to-strong crossover (FSC) at a temperature $T_\times$, where $T_\mathrm{g} < T_\times < T_\mathrm{M}$, with T_M being the melting temperature. The physical reason behind the FSC is poorly

30   understood at present, but it is thought to be related to a spatially inhomogeneous arrest of molecules in the liquid/amorphous phase during cooling. This phenomenon, known as "spatially heterogeneous dynamics" postulates that correlated domains in a liquid may exhibit different relaxation dynamics than the average over the entire bulk (Ediger, 2000). The FSC has been observed for water (Jagla, 2001) and silicon dioxide (La Nave et al., 2002; Saika-Voivod et al., 2004) and recently for a number of organics (see Novikov and Sokolov (2003) and Mallamace et al. (2010) and references therein). Both of these latter works

35   suggest there is a universal, material-independent FSC pure-component viscosity based on experiments of relaxation dynamics
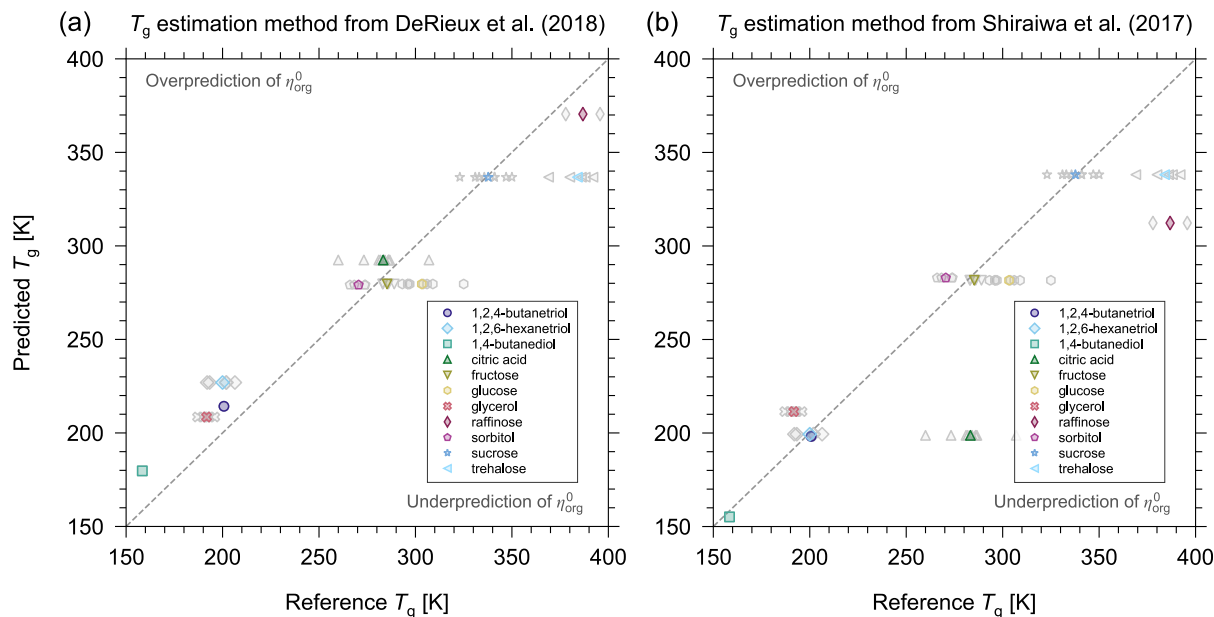
Figure 3. Prediction of T_{g} using the methods presented in (**a**) DeRieux et al. (2018) and (**b**) Shiraiwa et al. (2017) versus measured reference T_{g} values for some of the binary aqueous mixtures considered in this study. The grey markers represent individual reference T_{g} values and the coloured markers represent the average T_{g}. Error bars for reference values have been omitted for clarity. For a list of the reference values and their uncertainties see Table S1. The grey dashed 1:1 lines represent perfect agreement between predicted and reference values.

for glass-forming liquids. Novikov and Sokolov (2003) suggest that $\eta^{\times}$ is on the order of 10^{6} Pa s. However Mallamace et al. (2010) find that $\eta^{\times}$ is on the order of 10^{3} Pa s. Notwithstanding this discrepancy, the presence of the FSC motivates our choice to change the assignment of D from 10 to 30 on a per-component basis if the temperature of a simulation case is below the component's T_{g}. We note that the results of the aforementioned studies would suggest that for at least some organics the

5 FSC occurs at temperatures warmer than T_{g}. This is also supported by recent measurements of a super-Arrhenius to Arrhenius transition observed in citric acid, having occured at $302 - 312$ K, which is approximately $20 - 30$ K warmer than average values of the citric acid glass transition reported in the literature. While it would be more appropriate to change the D assignment at the FSC viscosity, we do not have a clear scientific basis to assign universal pure-component FSC. At least for temperatures below T_{g} it is reasonable to assume that the FSC has occurred.

10 To summarise, we choose to assign a fragility parameter of $D = 10$ for all organic compounds, with the exception of those whose T_{g} is warmer than the simulation temperature. For compounds with a T_{g} warmer than the simulation temperature, a fragility parameter of $D = 10$ drastically overestimates the pure-component viscosity, and by extension, the mixture viscosity (see Fig. 2f). The FSC provides us with the theoretical basis to assign a fragility parameter of $D = 30$ in these cases, which provides much better agreement between the model and experiment.

2.3 Estimation of pure-component viscosity uncertainty

The uncertainty in the pure-component viscosity as predicted by the DeRieux et al. (2018) method arises from the uncertainty in the prediction of T_g and the uncertainty in D. Given that the T_g model is parameterized using a collection of measured T_g values, any uncertainty in T_g measurements will be propagated into the fitted DeRieux et al. (2018) model parameters. In addition, the fragility parameter is derived from measurements of T_g, so any uncertainty in T_g will also propagate into the value of D. Therefore, we assess the uncertainty in the pure-component viscosity prediction by prescribing an uncertainty for T_g. T_g measurements are made by cooling a compound until a liquid-to-glass phase transition occurs. For example, differential scanning calorimetry reveals a change in heat capacity of the single-component substance when T_g is reached (e.g. Angell et al., 2002; Lienhard et al., 2012). However, in some ways the glass transition temperature is a misnomer; the measured vitrification temperature of a liquid is dependent on the cooling rate from liquid (or the heating rate starting from the glassy state). In reality, the calorimetric glass transition temperature is not a discrete value; rather, it describes a range of temperatures (or a retrieved average temperature) corresponding to appropriate cooling rates that induce vitrification. Faster cooling rates will result in a slightly warmer T_g value than if the same substance were cooled at a slower rate (Debenedetti and Stillinger, 2001; Angell et al., 2002). For cooling rates that differ by an order of magnitude the resulting T_g range is approximately $3-5$ K (Debenedetti and Stillinger, 2001). Another, more consequential factor that contributes to experimental T_g measurement uncertainty is the purity of the substance being measured. In essence, depending on laboratory conditions and sample preparation procedure, it is possible that the substance being measured is not entirely anhydrous – and trace amounts of water, being an excellent plasticizer, may cause a lower measured T_g value than what is true for the anhydrous compound.

Factoring in the effects of cooling rate and the substance purity on T_g, we choose to assign a 5 % uncertainty. For a compound whose glass transition is within the range of atmospherically relevant temperatures, an uncertainty of $\sim 10-20$ K is produced. This is also in good agreement with findings from DeRieux et al. (2018), who state that for the compounds they investigated, their model can estimate T_g within ± 21 K based on a 68 % prediction interval. We also note that this appears to be a reasonable uncertainty based on the spread in reference T_g values for the components we have studied, where glass transition temperature data are available (see Table S1). The reference values of T_g are either values measured experimentally or extrapolated from parameterizations of measurements of pure-component viscosity. Independent reference values of T_g for the same pure-component can differ by as little as one or two Kelvin, but in the most extreme case (citric acid) considered here, values span almost 50 K.

Figure 3 shows a comparison of the T_g values predicted by the DeRieux et al. (2018) and Shiraiwa et al. (2017) models with the reference values listed in Table S1. The average relative difference between the predicted values and the mean of the reference values are 6.76 % and 8.71 % for the DeRieux et al. (2018) and Shiraiwa et al. (2017) models, respectively. This demonstrates that, for the compounds studied here, the DeRieux et al. (2018) model is more appropriate. In addition, we note that a 5 % uncertainty in T_g is in good agreement with the difference between the predicted and reference T_g values.

2.4 Estimation of AIOMFAC-VISC sensitivity

We calculated the sensitivity of AIOMFAC-VISC as a proxy for the uncertainty in the mixture viscosity prediction. We chose to prescribe the AIOMFAC-VISC sensitivity as the response of the mixture viscosity prediction to a small change in mixture composition. The mixture composition adjustment was done by adjusting the mixture water content by a small amount. This is meant to represent the uncertainty in the composition measurement in a laboratory setting, which would be typical of all experiments. The calculation of AIOMFAC-VISC sensitivity is described in Section S3 of the SI.

2.5 Treatment of Secondary Organic Aerosol Systems

For SOA mixtures we used the AIOMFAC-VISC method within the MCM–EVAPORATION–AIOMFAC equilibrium gas–particle partitioning framework (Zuend and Seinfeld, 2012) to account for complex aerosol composition and the potential for liquid–liquid phase separation (LLPS). The Master Chemical Mechanism (MCM; Jenkin et al., 1997; Saunders et al., 2003; Jenkin et al., 2015) simulates the oxidation of parent hydrocarbons in the gas phase and provides a set of reaction products and stoichiometric yields for prescribed environmental conditions. We select a subset of the MCM reaction products, using those to generate surrogates mixtures of $14 - 21$ components as a representation of the SOA composition formed from a specific precursor, as is done frequently when molecular-structure input information is required by models (e.g. Zuend and Seinfeld, 2012; Rastak et al., 2017; Gorkowski et al., 2019). The procedures used to determine the molar concentrations of SOA components along with the lists of MCM products used for the three SOA systems studied are provided in Section S6 of the SI.

3 Results and Discussion

3.1 Comparison with simplified models

A group-contribution model like AIOMFAC-VISC has the potential to offer a high degree of fidelity, owing to its relatively detailed description of a given mixture of organics plus water. However, it is important to question whether the estimation of mixture viscosity actually requires the complexity offered by a group-contribution model – or if a simpler mixing rule would suffice. To this end, we have compared the performance of AIOMFAC-VISC with ~~three~~four different expressions:

$$\ln(\eta_{\text{mix}}) = \sum_i^n x_i \ln(\eta_i^0) \quad ; \quad \ln(\eta_{\text{mix}}) = \sum_i^n \phi_i \ln(\eta_i^0) \quad ; \quad \ln(\eta_{\text{mix}}) = \sum_i^n \sigma_i \ln(\eta_i^0) \quad ; \quad \ln(\eta_{\text{mix}}) = \sum_i^n \gamma_i x_i \ln(\eta_i^0). \quad (14)$$

Here, x_i is the mole fraction, ϕ_i is the volume fraction, ~~and~~ σ_i is the surface area fraction, and $\gamma_i x_i$ is the mole-fraction-based activity of the ith mixture component. Implicit in these expressions is the assumption that mixture viscosity can be described simply as a weighted mean of the pure-component viscosities of the mixture components. The weighting is representative of the fractional amount of each component present in the mixture, either by their number of moles, their occupied volume, ~~or~~ their surface area, or their activity.

Figure 4 shows a comparison of these different mixture viscosity models at $T = 293.15$ K for two binary systems: water + glycerol and water + citric acid. To remove the influence of a potential inaccuracy in the pure-component viscosity prediction on the model intercomparison, the panels on the left in Fig. 4 show the systems with the pure-component viscosities taken from measurements or a case-specific model estimation. For glycerol, the pure-component viscosity has been determined experimentally while for citric acid experimental data exists at very low mass fractions of water, allowing an extrapolation to the pure-component viscosity by leaving the pure-component viscosity of citric acid at the system temperature as a single fit parameter of our AIOMFAC-VISC model. With assigned pure-component viscosities, it becomes clear that the mixing rules based on molecular volume fraction or surface area fraction in the mixture are unsuitable predictors of mixture viscosity. The mole-fraction-weighted mixing and the activity-weighted mixing rules performs reasonably for glycerol, but AIOMFAC-VISC remains the most accurate mixing model. For the aqueous citric acid system, the mole-fraction-weighted mixing rule, the activity-weighted mixing rule, and the AIOMFAC-VISC predictions are similar and both all three are in good agreement with the available experimental data. At least for binary aqueous systems, the mole-fraction-weighting appears to be the best among the simple mixing rules. A more detailed, quantitative comparison of AIOMFAC-VISC with the expressions in Eq. 14 demonstrates that when the pure-component viscosities are well constrained, AIOMFAC-VISC predictions are an improvement over the simple mixing rules (see Sect. S7 of the Supplementary Information). Additionally, it is confirmed that the mole-fraction-weighted mixing rule is the best choice among the simple mixing rules.

The combinatorial contribution of AIOMFAC-VISC (Eq. 2) is similar in formulation to the mole-fraction- and activity-weighted mixing rules, which suggests that the residual contribution of viscosity in AIOMFAC-VISC is less important, but not negligible in the mixture viscosity prediction. This is further demonstrated when comparing the mixture viscosity results of AIOMFAC-VISC with those of GC-UNIMOD. The GC-UNIMOD prediction of mixture viscosity is not shown in Fig. 4 although it provides a nearly identical result to that of the volume-fraction-weighted mixture viscosity. As detailed in Section 2, the most significant changes made to GC-UNIMOD were in the modification of the combinatorial contributions to viscosity, which account for most of the improvement from GC-UNIMOD to AIOMFAC-VISC (see Section S4 and Fig. S3).

Comparing the panels from the left column with the right column in Fig. 4 highlights the effect of uncertainty in the pure-component viscosity prediction on the mixture viscosity and the variability in the quality of this prediction depending on the component. For glycerol, the DeRieux et al. (2018) method only slightly overpredicts the pure-component viscosity. For citric acid, the overprediction of η^0_{org} spans almost four orders of magnitude. It should also be noted that while the pure-component viscosity is overpredicted for both citric acid and glycerol, this is not the case for every organic. For eleven single-organic component systems studied for which we have reference values of T_{g}, η^0_{org} was overpredicted for six of the components and underpredicted for five of the components, related to over-/under-predictions of the corresponding T_{g} values (Fig. 3).

Figure 4 demonstrates that the AIOMFAC-VISC prediction of mixture viscosity is highly sensitive to the pure-component viscosity value. With the appropriate pure-component viscosity value (either from experiment or a model fit) we have the ability to make the mixture viscosity prediction highly accurate (in these specific cases, but not generally). In using the DeRieux et al. (2018) method we sacrifice some accuracy in predicting mixture viscosity in order to have the flexibility of predicting the

mixture viscosity for systems containing organics for which we have no information about their pure-component viscosity from experimental data. This is especially important in the context of SOA systems.

3.2 Binary aqueous organic mixtures

Before running AIOMFAC-VISC for multicomponent mixtures, including a selection of SOA systems, the model was first tested with a dozen binary aqueous mixtures, which were chosen based on the availability of experimental data covering the low-viscosity and semi-solid regimes. The binary aqueous mixtures were used to test and validate the model, i.e., we tested potential adjustments to the AIOMFAC-based viscosity equations (Eqs. $2 - 3$) to optimally predict the viscosity of as many binary aqueous mixtures as possible. Figure 5 shows the results for four of these systems. For aqueous glycerol and aqueous citric acid mixtures, the AIOMFAC-VISC model (solid line) slightly overpredicts the mixture viscosity at lower mass fractions of water due to the overestimation in η^0. The experimental data at low mass fractions of water lie within the η^0 uncertainty (grey shaded region) for glycerol, although not for citric acid. At higher mass fractions of water, the experimental data for both systems agree very well with the model prediction. For sucrose we observe a similar pattern; the model shows higher predictive power at higher mass fractions of water. The agreement of the model with experimental data where $\eta_{\mathrm{mix}} > 10^8$ Pa s is especially encouraging for modelling ultra-high viscosities. However, we note that the logarithmic scale leads to seemingly good agreement at higher viscosities and seemingly higher scatter among experimental data at lower viscosity, while in absolute (non-logarithmic) terms, the agreement at lower viscosity is typically far better.

For compounds with a small molar mass (< 200 g mol^{-1}) the AIOMFAC-VISC mixture viscosity prediction works well. Assessing the validity of the AIOMFAC-VISC viscosity prediction for compounds with larger molar masses (> 200 g mol^{-1}) is challenging, because experimental data are available only for a select few binary aqueous mixtures with large molecules (sucrose, trehalose, maltose, and raffinose). Moreover, these data sets are all for cyclic sugars, so it is questionable whether they serve as a widely-applicable assessment for AIOMFAC-VISC validity at higher molar mass or just AIOMFAC-VISC validity for mono, di, and tri-saccharides. Nonetheless, it appears as molar mass increases, the AIOMFAC-VISC prediction starts to deviate from experimental data for the binary mixtures tested that contain larger, highly-functionalized organic molecules. For example, this is evident for binary aqueous mixtures with trehalose. This reduction in predictability may be occurring for two reasons. First, the η^0 prediction becomes less accurate for larger molecules, particularly those with a molar mass above > 350 g mol^{-1}. Second, AIOMFAC-VISC may not be able to capture certain structural characteristics of the mixture components with the group-contribution approach. Namely, as the mass fraction of water decreases, the movement of trehalose molecules in the mixture may become restricted due to an increase in the so-called free volume of each molecule. The free volume of trehalose molecules would be greater than the volume predicted based on the sum of contributing group volumes.

3.3 Multicomponent aqueous organic mixtures

A direct way to assess the accuracy of AIOMFAC-VISC mixture viscosity predictions is by evaluating model predictions against available experimental data for aqueous multicomponent mixtures for which we know the mass or mole fractions of components in the mixture. An example of an aqueous multicomponent system is shown in Fig. 6, where AIOMFAC-VISC
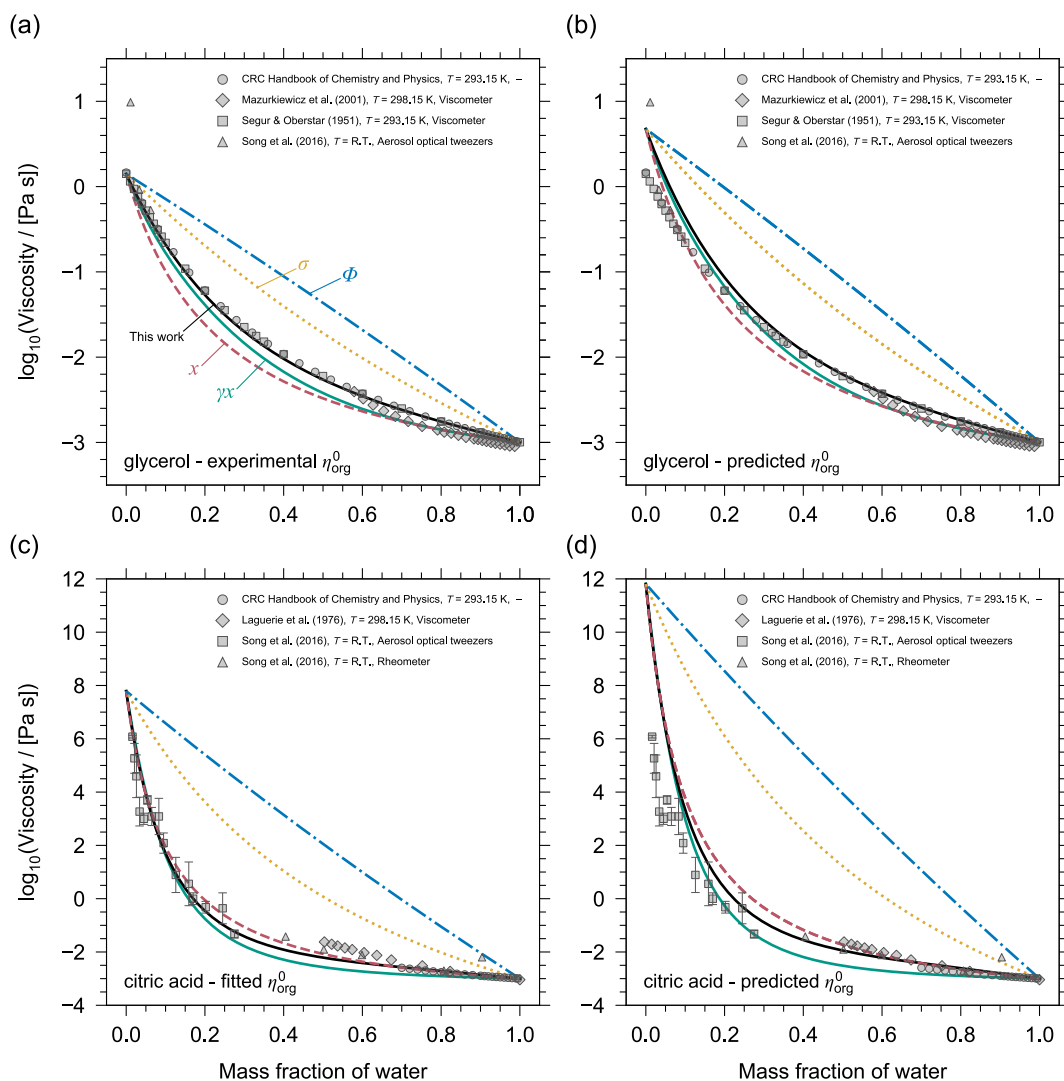
Figure 4. Model intercomparison of mixture viscosity predictions as a function of mass fraction of water at $T = 293.15$ K. The mixing models shown are AIOMFAC-VISC (black solid lines) and ~~three~~four simple viscosity mixing rules (Eq. 14): molecular mole-fraction-weighted (pink dashed lines), volume-fraction-weighted (blue dash-dotted lines), ~~and~~ surface-area-fraction-weighted (yellow dotted lines), and mole-fraction-based activity-weighted (green solid lines) means of pure-component viscosities. Top row: the binary mixture of glycerol and water, with the pure-component viscosity of glycerol assigned from (**a**) the measured value or (**b**) predicted by the DeRieux et al. (2018) method. Bottom row: the binary mixture of citric acid and water, with the pure-component viscosity of citric acid assigned (**c**) based on an AIOMFAC-VISC fit of η_{org}^0 using the shown experimental data or (**d**) predicted by the DeRieux et al. (2018) method. Grey markers show experimental data from different methods (see key).
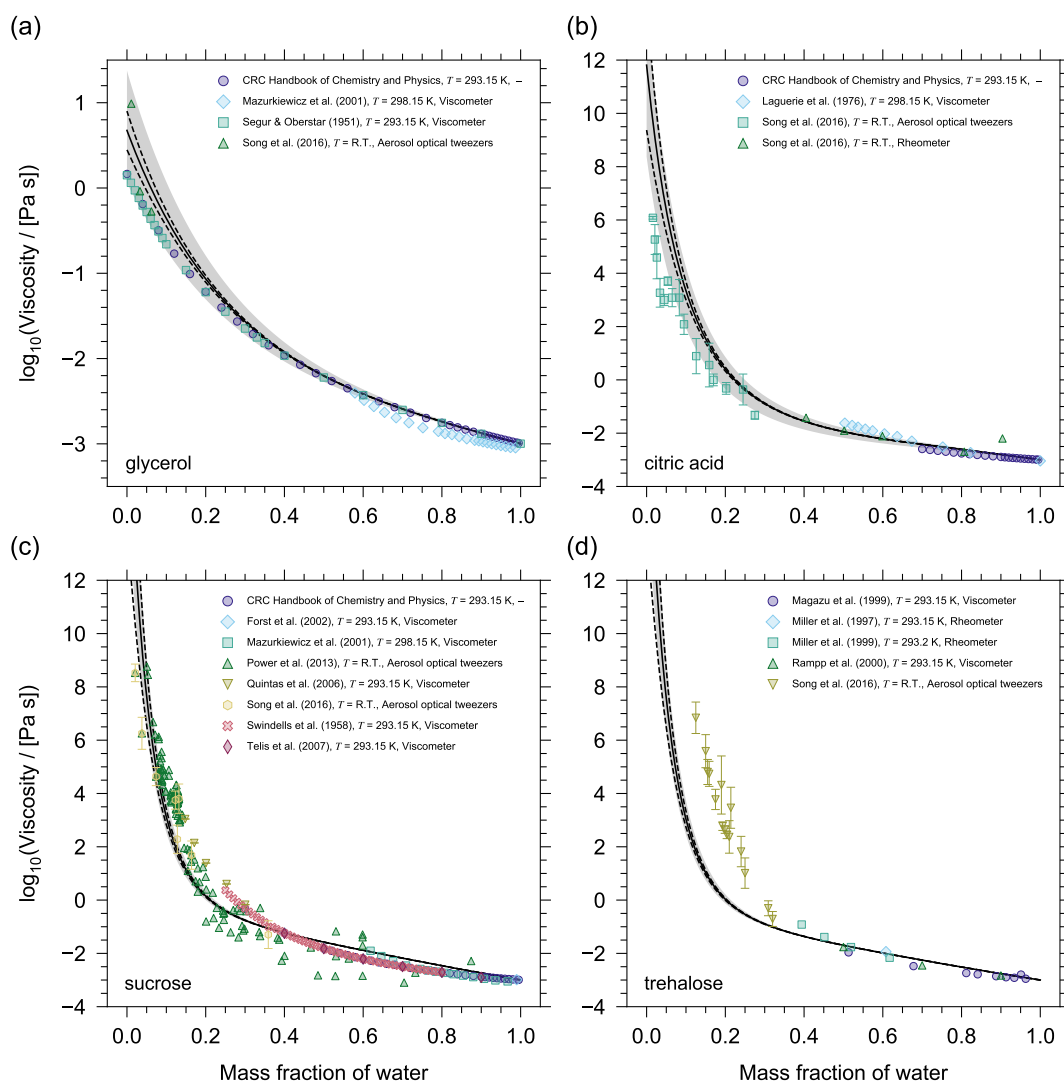
Figure 5. AIOMFAC-VISC mixture viscosity predictions as a function of mass fraction of water at 293.15 K for: (**a**) glycerol, (**b**) citric acid, (**c**) sucrose, and (**d**) trehalose. The solid black line is the AIOMFAC-VISC mixture viscosity prediction. The dashed black lines show the AIOMFAC-VISC sensitivity. The model sensitivity is assessed by calculating the response of the model to a small change in mixture composition (see Sect. 2.4). The grey shaded area denotes a 5 % uncertainty in the prediction of T_g. Markers show experimental data. Error bars have been omitted when the length of the error bar does not exceed the width of the marker.
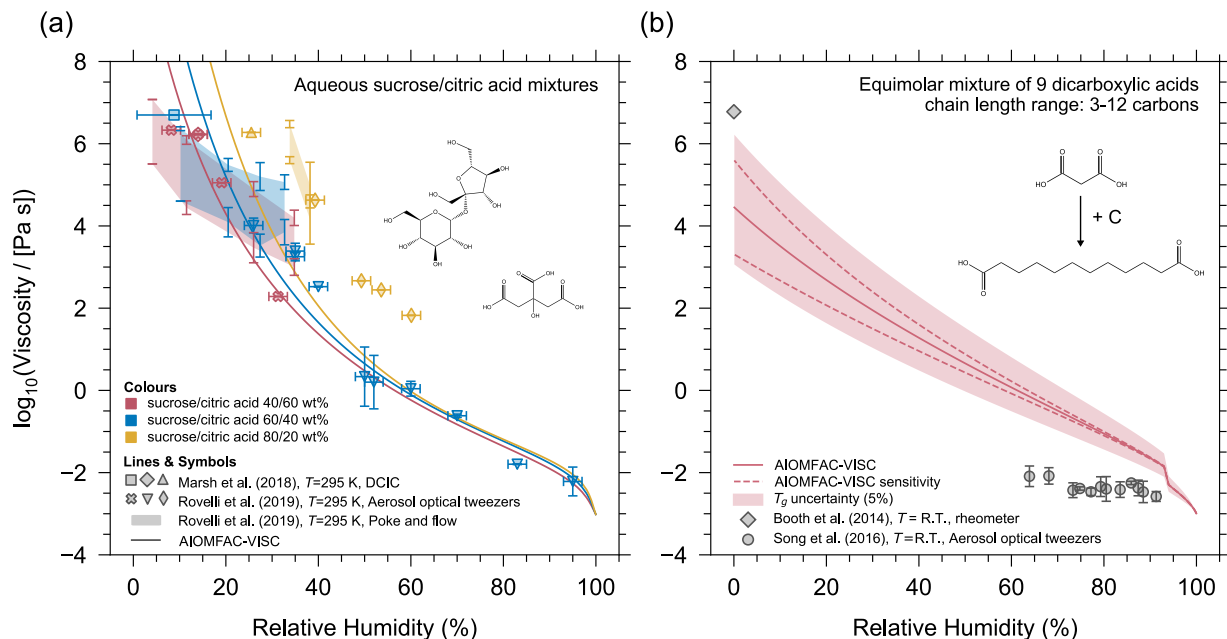
Figure 6. (**a**) AIOMFAC-VISC-AIOFMAC mixture viscosity predictions as a function of relative humidity (lines) for a aqueous mixtures of sucrose and citric acid compared with aerosol optical tweezer experimental data (symbols) and poke-and-flow experimental data (shaded regions). The colours of the markers and curves correspond to mixtures with different concentrations of sucrose and citric acid. The three mixtures are composed of dry compositions of 40:60 (pink), 60:40 (blue), and 80:20 (yellow) percent mass fraction of sucrose:citric acid. (**b**) AIOMFAC-VISC mixture viscosity for the equimolar dicarboxylic acid mixture presented in Cappa et al. (2008). The solid line shows the AIOMFAC-VISC predicted mixture viscosity, dashed lines represent model sensitivity, and the shaded region represents a 5 % uncertainty in T_g. Grey markers show the viscosity measurements in a limited RH range.

is tested for aqueous sucrose and citric acid systems of different organic mixing ratios (40:60, 60:40, and 80:20 percent mass fraction of sucrose : citric acid). The model is run at the same temperature of 295 K as the mixture viscosity measurements conducted by Marsh et al. (2018) and Rovelli et al. (2019). We have omitted the model sensitivity envelope in Fig. 6 for clarity. Fitted pure-component viscosity values were used for this simulation for citric acid and sucrose in order to assess the

5   AIOMFAC-VISC mixture viscosity prediction without introducing uncertainty from the DeRieux et al. (2018) pure-component viscosity prediction method. The model shows good agreement with the aerosol optical tweezers data for the 40:60 and 60:40 aqueous sucrose : citric acid mixtures. The model is less accurate for the 80:20 mixture, in which case the model consistently underestimates the measured viscosities. Based on Fig. 5, it appears the model is more accurate for predicting the mixture viscosity of binary, aqueous citric acid than for binary, aqueous sucrose. This may explain the better model performance in

10   case of the 40:60 and 60:40 sucrose : citric acid mixtures as compared to the 80:20 mixture. Furthermore, we note that these optical tweezers measurements do not provide an independent estimation of the water contents at given RH; hence, a part of
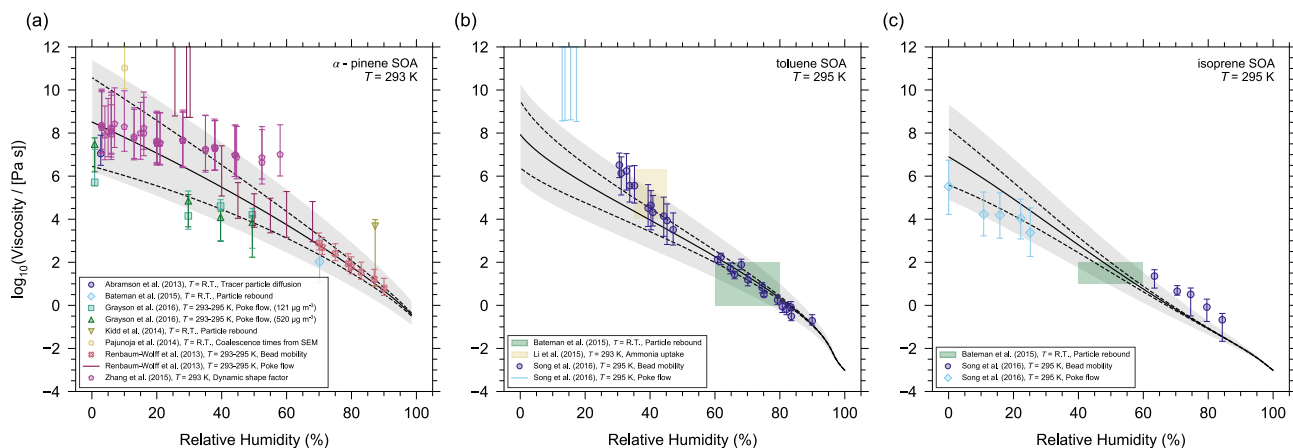
Figure 7. AIOMFAC-VISC mixture viscosity predictions (solid line) for (**a**) α-pinene SOA at $T = 293$ K, (**b**) toluene SOA at $T = 295$ K, and (**c**) isoprene SOA at $T = 295$ K. The dashed lines represent the model sensitivity and the grey shaded regions represent a 5% uncertainty in estimated T_g values. The markers and colour shaded regions represent experimental data obtained by different methods (see legend). $T = $ R.T. indicates the measurements were taken at room temperature ($\sim 293 \pm 4$ K).

the model–measurement deviations may also be attributed to over-/underestimations of the actual mixture water content by AIOMFAC.

Well-characterized mixtures of known molecular compositions for viscosity purposes are scarce. The only other multicomponent mixture data to which we can compare our model to is shown in Fig. 6b. This multicomponent mixture (herein termed

5 the "Cappa mixture") was first presented in Cappa et al. (2008). The Cappa mixture is comprised of equimolar amounts of nine dicarboxylic acids ($C_3 - C_{12}$). As before, the solid line in Fig. 6b indicates the AIOMFAC-VISC prediction, the dashed lines indicate the model sensitivity and the shaded region represents the 5% uncertainty in T_g. Both the anhydrous and aqueous viscosity was measured experimentally by Booth et al. (2014) (diamond marker) and Song et al. (2016a) (~~degree le~~circle markers) for the Cappa mixture. Booth et al. (2014) measured the water-free viscosity to be approximately 6×10^6 Pa s and they also

10 reported that the aqueous mixture viscosity remained semi-solid $> 10^5$ Pa s above ~ 0.8 mole fraction of water. This appears to differ from experimental data on the same system by Song et al. (2016a), which suggests that the viscosity of the Cappa mixture is in the liquid regime ($\sim 10^{-2}$ Pa s) even between 60 and 70 % RH. The AIOMFAC-VISC prediction does not agree well with either set of experimental data, although it falls in between the measured range and it does exhibit the same trend of moderate viscosity at low relative humidity, which steeply declines with increasing relative humidity.

15 **3.4 Secondary organic aerosol systems**

Finally, we test the AIOMFAC-VISC predictions against experimental data for three secondary organic aerosol systems, SOA derived from the oxidation of α-pinene, toluene, or isoprene (Fig. 7). In the case of α-pinene SOA, there are several distinct

experimental data sets from the literature, which we used to compare to the AIOMFAC-VISC prediction. Most of the measurements were carried out at/near room temperature ($T = $ R.T.), without a clearly quantified temperature range. A few sets of measurements are specified to have been taken between 293 – 295 K. Here we assume room temperature to be approximately 20 °C and so we have chosen to run the AIOMFAC-based gas–particle partitioning computations as well as AIOMFAC-VISC

5   at 293 K. In the case of toluene- and isoprene-derived SOA, there are fewer experimental data sets and most measurements have been made at $\sim$ 295 K, so for these two systems we matched our simulation temperature accordingly. For further details about the surrogate mixtures and compositions for all SOA defined in AIOMFAC-VISC see Section S6 of the SI.

3.4.1 SOA formed from α-pinene oxidation

In the case of laboratory measurements, α-pinene SOA is the most studied SOA system in the viscosity literature. Despite this,

10   its viscosity remains poorly constrained in relative humidity space, i.e. there are large discrepancies in viscosity measurements taken at approximately the same relative humidity. Some of these discrepancies span several orders of magnitude. For example, at $\sim$ 30 % RH, measurements of viscosity range from $\sim$ 10^4 – 10^9 Pa s (Fig. 7a). The differences between those data sets occur likely for two reasons. First, a range of novel experimental techniques are used to measure the aerosol viscosity. The novelty of these techniques is owing to the non-trivial challenge of measuring ultra-high viscosities in situ. As a result, these

15   techniques have a high degree of uncertainty and often only a range of possible viscosities can be provided, rather than a precise viscosity measurement. With large experimental uncertainties it is unsurprising that we also see a disparity between data sets. Second, the laboratory-made α-pinene SOA mixtures may vary greatly in composition from data set to data set depending on the method of SOA generation and sample extraction/preparation for viscosity measurements. For example, an SOA particle that experiences a longer oxidation time (or higher exposure to ozone and/or OH radicals) may contain a mixture with a higher

20   average O : C ratio when compared to a particle that experienced a shorter oxidation time. A higher average O : C ratio for the particle mixture suggests it may contain a larger fraction of molecules with oxygen-bearing functional groups and potentially more diversity in the branching characteristics of molecular structures from the parent hydrocarbon. The molecules may also be larger and of higher molar mass on average (barring substantial fragmentation). As a result, the SOA particle that was given more time to oxidize may have a higher mixture viscosity (particularly at low RH). Grayson et al. (2016) also provide evidence

25   that production aerosol mass concentrations are inversely proportional to the SOA viscosity. From gas–particle partitioning theory and experimental evidence, a higher abundance of less-oxidized components in the SOA is expected for high aerosol loading chamber experiments. This provides further evidence that the production method of α-pinene SOA can have a non-trivial influence on the measured viscosity. It also suggests that the viscosity of laboratory-generated SOA may underestimate ambient SOA viscosity, because laboratory-generated SOA mass concentrations (for viscosity measurement purposes) have

30   often been several orders of magnitude higher than the concentrations typical in ambient air.

Ultimately, the spread in experimental data makes it difficult to assess AIOMFAC-VISC's viscosity prediction capabilities in great detail. Of course, AIOMFAC-VISC cannot simultaneously agree with all experimental data sets. However, we can compare the AIOMFAC-VISC prediction with specific measurements by adjusting our representative α-pinene SOA mixture in the model. Specifically, we adjust the molar ratios of products in our representative α-pinene SOA mixture, such that its av-

erage O : C ratio is similar to the average O : C of the SOA reported for the experimental data set in question. For the viscosity simulations, we further turn off partitioning of organics between the particle and the gas phase in order to ensure that the O : C remains constant and the particle composition remains fixed (except for water content) regardless of relative humidity. This approach mimics the conditions under which viscosity measurements at different RH levels are typically done with a specific

5 SOA sample extracted during a laboratory experiment. We have chosen to "target" the data set of bead mobility measurements from Renbaum-Wolff et al. (2013) because they report an expected O : C for the mixtures used in their bead mobility experiments and this is the data set with the smallest experimental uncertainty across all measurements (for RH > 70 %). The small uncertainties are likely a result of the higher relative humidity and therefore lower mixture viscosity. Consequently, if we have a high degree of confidence in this data set then we can assume AIOMFAC-VISC's prediction to be an extrapolation of the

10 SOA properties from these measurements over the whole RH range.

Renbaum-Wolff et al. (2013) report that the expected O : C of their SOA mixtures is approximately 0.3 to 0.4, which they justify from previous measurements of O : C for α-pinene generated via ozonolysis in an environmental chamber (see the Supporting Information from Renbaum-Wolff et al. (2013)). In Fig. 7a we have adjusted the composition of the representative α-pinene SOA mixture such that AIOMFAC-VISC is in excellent agreement with bead mobility viscosity measurements from

15 Renbaum-Wolff et al. (2013). Although, the adjustments made to achieve this agreement results in an average O : C of 0.51. If SOA constituent concentrations are modified to produce an average mixture O : C of ~ 0.4, then the model is in agreement with the measurements from Grayson et al. (2016), but not with those of Renbaum-Wolff et al. (2013). By choosing to fit the model to the data of Renbaum-Wolff et al. (2013), the general shape of the AIOMFAC-VISC prediction curve appears reasonable and ensures most of the experimental data fall within the uncertainty in T_g values. Furthermore, the T_g value predictions produce

20 a water-free mixture viscosity for the SOA mixture that agrees well with the data by Zhang et al. (2015) for RH < 1 %. Although, we acknowledge that this approach removes an element of predictability from AIOMFAC-VISC.

We also note that AIOMFAC-VISC is capable of predicting the mixture viscosity of multiple aerosol phases should liquid–liquid phase separation (LLPS) occur. For example, in α-pinene SOA free of ammonium sulfate, LLPS is still expected to occur at high RH, although it is not resolved in Fig. 7 because LLPS occurs in this case at very high water activity only.

25 ### 3.4.2 SOA formed from toluene and isoprene oxidation

Similarly, for comparison with the toluene SOA experimental data we also adjusted the representative toluene SOA mixture (see Supplementary Information). Song et al. (2016b) determined an average O : C ratio of 1.08 for SOA particles they generated with a mass concentration of $60 - 100\ \mu g\,m^{-3}$ during production. They also note that this is in agreement with previous measurements of toluene SOA O : C of $0.9 - 1.3$ generated under similar conditions. The toluene SOA particles investigated

30 by Li et al. (2015) also have an O : C in the range of $1.0 - 1.2$. Therefore, we adjusted our representative mixture in terms of relative surrogate compound composition, such that an O : C of 1.2 resulted. The AIOMFAC-VISC viscosity predictions for the adjusted toluene SOA system can be found in Fig. (7b). Accounting for error and model sensitivity, the predictions agree very well with the data for RH > 40 %, while the agreement decreases below 40 % RH. It seems the model lacks the curvature necessary to fully capture the experimental data at low relative humidity; however, both the experimental uncertainty
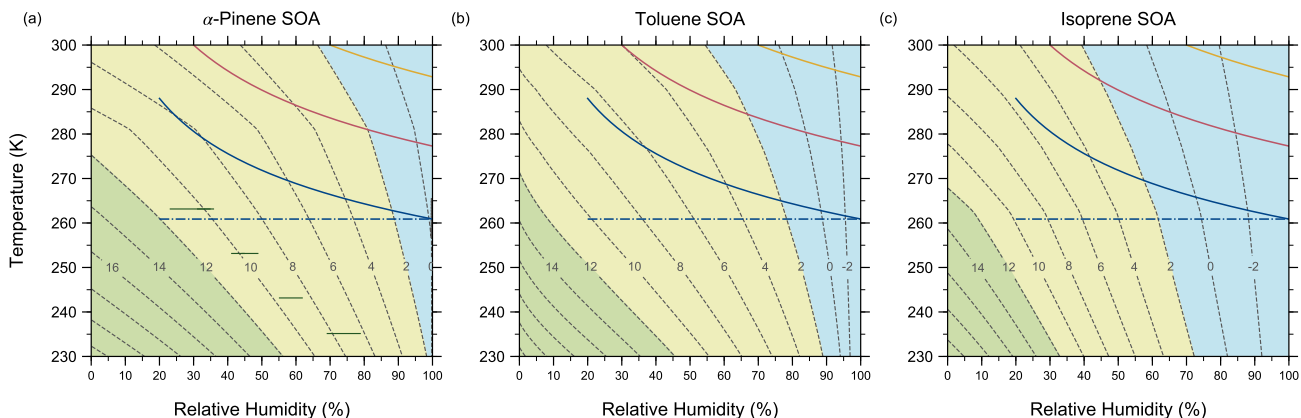
Figure 8. Mixture viscosity predicted by AIOMFAC-VISC as a function of temperature and relative humidity for simulated (**a**) α-pinene SOA, (**b**) toluene SOA, and (**c**) isoprene SOA. Dashed contour lines denote the values of $\log_{10}(\eta_{\mathrm{mix}}\ \mathrm{Pa}\ \mathrm{s})$. Coloured regions indicate conventional, viscosity-based classifications of liquid (blue), semi-solid (yellow), and amorphous solid (green) physical states. The green horizontal lines in (a) denote ranges of RH and T for which Järvinen et al. (2016) measured a viscosity "phase" transition from solid or semi-solid to liquid in α-pinene SOA. They determined this viscosity transition to occur at $\eta_{\mathrm{mix}} = 10^7\ \mathrm{Pa}\ \mathrm{s}$. The solid coloured lines indicate three trajectories in temperature versus RH space for an idealized adiabatic air parcel uplift containing SOA particles for different initial conditions. The assigned initial conditions are $T = 288$ K, RH $= 20\ \%$ (blue); $T = 300$ K, RH $= 30\ \%$ (pink); and $T = 300$ K, RH $= 70\ \%$ (yellow). The dash-dotted blue line depicts the possible range of relative humidity experienced by SOA particles should they survive cloud processing and remain at their saturation altitude.

and model sensitivity span orders of magnitude in mixture viscosity for RH $< 30\ \%$. In addition, as mentioned above, the chemical makeup of toluene SOA was likely different in different experiments, with the specific $\mathrm{O} : \mathrm{C}$ having an influence on the water uptake and thereby viscosity, which may lead to a lower viscosity of higher-$\mathrm{O} : \mathrm{C}$ SOA samples, especially for RH $> 10\ \%$, where water uptake is non-negligible in these systems of relatively high average $\mathrm{O} : \mathrm{C}$.

5   Neither Song et al. (2016a) nor Bateman et al. (2015) have provided $\mathrm{O} : \mathrm{C}$ values for their isoprene SOA; however, Li et al. (2015) produced isoprene SOA under similar conditions and they measure an $\mathrm{O} : \mathrm{C}$ of $0.8 - 1.0$. After adjustment, the $\mathrm{O} : \mathrm{C}$ of our representative isoprene SOA mixture is 1.1 (see SI for details) and the AIOMFAC-VISC viscosity prediction for this mixture is shown in (7c). Here, the model slightly underpredicts the viscosity of isoprene SOA at high relative humidity and slightly overpredicts at low relative humidity. However, considering the combination of experimental error and model

10   uncertainty, there is reasonable agreement between the AIOMFAC-VISC predictions and most data points. Overall, the model does a reasonable job of representing isoprene SOA in comparison to these experimental data sets.

4 Atmospheric Implications

While SOA reside largely in the planetary boundary layer (PBL) (Tsigaridis and Kanakidou, 2003), there are aircraft (Heald et al., 2006) and ground-based measurements (Schum et al., 2018) of significant SOA concentrations in the free troposphere (FT). As such, we can expect SOA to be exposed to a wide range of temperature and relative humidity conditions. Shiraiwa et al. (2017) investigated the phase state of SOA for ambient temperature and relative humidity conditions for the PBL and the FT. Using a global chemistry climate model and estimating SOA phase state based on a glass transition temperature approach, they conclude that SOA phase state is largely dependent on relative humidity in the PBL. Their results showed SOA exist mostly in the liquid state in the tropics and polar regions while SOA are in semi-solid phase state in arid, continental regions. Shiraiwa et al. (2017) also predict that SOA would be almost entirely semi-solid and/or glassy in the FT.

The aforementioned work is also consistent with the results from Maclean et al. (2017) for the PBL. Maclean et al. (2017) used a parameterization of viscosity as a function of temperature and relative humidity based on experimental data for laboratory-generated α-pinene SOA. They found that the mixing times within α-pinene SOA particles were less than one hour in the PBL, where SOA concentrations were most spatially and temporally significant, suggesting SOA would be mostly liquid or somewhat semi-solid.

Both Shiraiwa et al. (2017) and Maclean et al. (2017) consider the phase state of SOA strictly based on averaged ambient temperature and relative humidity conditions. In effect, this approach provides a snapshot of SOA phase state for a given location in the atmosphere, but it ignores the temperature and relative humidity changes the SOA particles are exposed to during transport. The snapshot approach may overestimate the significance of semi-solid and glassy SOA at higher tropospheric altitudes. Indeed, SOA transported from the PBL to the FT may be lifted in convective updrafts, in which they will experience a decrease in temperature, but simultaneously an increase in relative humidity. Due to the plasticising effect of water, initially viscous SOA carried in an updraft may transition from semi-solid to liquid and go on to activate as cloud condensation nuclei or experience in-cloud scavenging. Alternatively, SOA may undergo some plasticising in an updraft, but remain viscous enough to avoid substantial cloud processing, depending on their CCN ability and whether cloud formation conditions are reached during transport. SOA may avoid such drastic temperature and relative humidity changes altogether if they meander to higher altitudes in slowly moving air masses. Of course, these scenarios are all contingent on the initial SOA viscosity and hygroscopicity and the extent of relative humidity increase the SOA experiences, which is linked to the the type and duration of upward/downward transport. Ultimately, the history of the SOA is important for understanding the potential of viscous aerosol particles to act as ice nuclei or to be involved in long-range transport of pollutants.

To this end, we have used the AIOMFAC-VISC model to simulate the change in viscosity during an idealized adiabatic uplift of an air parcel containing α-pinene, toluene, or isoprene SOA. In Fig. 8, we first compute the relationship between SOA viscosity, temperature, and relative humidity as predicted by the model. We note that the simulated SOA mixtures used to generate Fig. 8 are the same as those shown in Fig. 7. Comparing the three SOA cases investigated, α-pinene SOA is highly viscous for a larger area of the tropospherically-relevant temperature–relative humidity space than toluene or isoprene SOA. With the enhanced hygroscopicities of the latter contributing to their lower viscosity at higher temperatures and RH > 60 %.

Overlaid on the contour plots of Fig. 8 are three idealized adiabatic air parcel updrafts represented by their temperature and relative humidity relationship prior to cloud formation (i.e. for RH < 100 %). Each updraft has a temperature lapse rate of $10\,\mathrm{K\,km^{-1}}$ and is assumed to start near $0\,\mathrm{m}$ above sea level, where the mean air pressure is $1000\,\mathrm{hPa}$.

The three convective updrafts have different initial temperature and RH conditions, meant to represent different surface climates. Colder and rather dry surface conditions are represented by the blue curves, which have an initial temperature of 288 K and relative humidity of 20 %, where the lifting condensation level (RH = 100 %) of the SOA-containing air parcel is $\sim 2712\,\mathrm{m}$ above sea level. These initial conditions are meant to mirror the ambient conditions of the field experiments done by Virtanen et al. (2010). By considering the conventional viscosity-based phase state classifications, the viscosity for all three SOA in this simulation are initially semi-solid, but all transition to liquid at higher altitudes. If we consider that fragile organic compounds may transition to a glassy state at viscosities up to four orders of magnitude lower than $10^{12}\,\mathrm{Pa\,s}$, then the α-pinene SOA may be glassy just above the surface. In this case, the final altitude of the SOA before saturation, suggests it can reach the free troposphere if we assume the PBL does not extend beyond $1\,\mathrm{km}$ altitude, which may be a reasonable assumption for cold and dry regions during day time.

The pink curves in Fig. 8 show relatively warm (300 K) and dry (30 % RH) surface conditions, meant to represent arid climates. Here the lifting condensation level of the parcel is reached at $\sim 2272\,\mathrm{m}$ altitude. Again, all three SOA types are semi-solid near the surface where the intermediate relative humidity level dominates over the warmer temperature concerning mixture viscosity. At higher altitudes, the transition from semi-solid to liquid occurs. In subtropical arid regions, we expect the PBL to extend to higher altitudes, so it is possible for SOA-containing updrafts to reach water saturation prior to entering the free troposphere. Finally, warm and wet climates are represented by the yellow curves with an initial temperature of 300 K and RH of 70 %, where the parcel altitude reached at 100 % RH is $717\,\mathrm{m}$. In this case, none of the three SOA mixtures will have viscosities greater than that of a liquid and they will experience water saturation within the PBL.

The initial conditions of the updrafts were chosen to demonstrate examples of mixture viscosity values we can expect for ambient SOA at equilibrium with their environment. This is to say that we do not expect to frequently see drier conditions at the surface than what is represented with the blue curves in Fig. 8. As a result, we can expect that SOA carried adiabatically to higher altitudes have the potential to become highly viscous, but not necessarily glassy before they experience their first cloud-processing event. After spending time in a cloud along their parcel trajectory, in the absence of wet removal via precipitation, such SOA particles (potentially cloud-processed) may remain at similar altitude in the upper PBL or the FT and experience there conditions of lower RH (moving horizontally in the diagrams of Fig. 8), leading to evaporative loss of aerosol water accompanied by an increase in viscosity. Hence, while the aerosols may end up remaining for hours to days in the FT in a semi-solid or glassy viscosity range at lower temperatures, these particles may have experienced conditions of liquid-like viscosity and associated fast internal mixing and gas–aerosol exchange during certain times of their journey to the free troposphere.

5   Conclusions

The main product of this work is a new model, AIOMFAC-VISC, which predicts the viscosity of atmospherically relevant mixtures as a function of temperature, relative humidity, and mixture composition over a wide range of phase states. The model uses a thermodynamic group-contribution approach to predict mixture viscosity. The mixture viscosity prediction is constrained by parameterizations of the pure-component viscosity values of the individual mixture components. For water we use a parameterization by Dehaoui et al. (2015). For the organic components we use the method of DeRieux et al. (2018). Over the course of developing the model we found that the parameterization of the pure-component viscosity of the organic constituents is likely the largest source of uncertainty in the AIOMFAC-VISC predictions. This uncertainty arises from an underlying uncertainty in the prediction of pure-component glass transition temperatures and the choice of the fragility parameter.

We have assessed the validity of the AIOMFAC-VISC mixture viscosity predictions for binary as well as multicomponent aqueous mixtures where the pure-component viscosities of the organics are well constrained by experimental data. In those cases we did not use the DeRieux et al. (2018) pure-component viscosity prediction method; instead we supplied the mixing model with known pure-component viscosity values. By doing so, we demonstrate that AIOMFAC-VISC can predict mixture viscosity over a range of > 12 orders of magnitude (validated by data from $\sim 10^{-3} - 10^{9}$ Pa s). To further motivate the use of a complex mixing model, we compared the predictions of AIOMFAC-VISC to the predictions of several simple mixing rules. Of all simple mixing rules evaluated in this work, a mole-fraction-weighted scaling of the logarithms of pure-component viscosity values was shown to perform best and to be nearly as robust as AIOMFAC-VISC, particularly when the mixture viscosity varies of several orders of magnitude with composition. The mole-fraction-scaled mixing model is therefore a viable alternative when the application of a simple model is more practical. A quantitative comparison of both models revealed that, for the binary aqueous systems here, AIOMFAC-VISC outperforms the mole-fraction-scaled mixing model when the mixing models are supplied with pure-component viscosity values known from experiment or when well constrained by measurements at mixture compositions near the pure organic viscosity.

Using the DeRieux et al. (2018) pure-component viscosity prediction method ~~for the same cases~~ can introduce a notable error in the predicted mixture viscosity. However, at present, the DeRieux et al. (2018) method is the most widely-applicable and reliable way for the prediction of pure-component viscosities of multifunctional organics of atmospheric relevance. Ultimately, in order to fully realize the predictive power of AIOMFAC-VISC, or any mixture viscosity prediction tool discussed here, the pure-component viscosity prediction will need to be improved.

At present, the improvement and new development of accurate, predictive pure-component viscosity models, targeting multifunctional compounds and the temperature range of interest in the context of atmospheric aerosols, suffers from a scarce amount of experimental data for model training and validation. This necessitates reliable measurements of pure-component viscosities and binary mixture viscosities across a wide temperature range for a variety of compounds. Such a comprehensive data set will be integral to developing more sophisticated pure-component viscosity models. While the use of models to estimate the glass transition temperatures of pure components offers predictive capabilities, this study, alongside with previous work, shows that relatively large uncertainties are involved. The limitations appear both in the accuracy of the T_g estimates

based on bulk elemental composition as well as the assumptions involved in the estimation of pure-component viscosity values derived from T_g-based models. Our evaluation of (i) pure-component viscosities derived from glass transition temperatures in comparison to (ii) direct viscosity measurements or estimates based on model extrapolation of fitted mixture viscosities to the pure-component limit, suggests strongly that the commonly assumed viscosity of $\sim 10^{12}\,\mathrm{Pa\,s}$ at the glass transition temperature remains a rough estimate of the glass transition viscosity of organic compounds. Pure component viscosity values at a component's T_g of one or two orders of magnitude higher or lower than $10^{12}\,\mathrm{Pa\,s}$ are indicated in certain cases.

Notwithstanding, the AIOMFAC-VISC mixture viscosity prediction alongside the DeRieux et al. (2018) pure-component viscosity prediction method is shown to be valid for SOA mixtures where the model can be compared to room temperature experimental data (α-pinene, toluene, and isoprene SOA) and where adequate SOA surrogate mixtures can be established. Mixture viscosity was also simulated for relevant ranges in temperature (230 – 300 K) and relative humidity (0 – 100 %) to determine expected viscosity regimes for ambient SOA. The validity of the AIOMFAC-VISC prediction for SOA mixtures provides insight into the viscosity of SOA formed near the Earth's surface that are then transported to higher altitudes. By simulating an idealized adiabatic updraft, we determine that under most conditions α-pinene, toluene, and isoprene SOA will either be semi-solid or liquid close to the surface, but that an increase in relative humidity with upward transport will result in a transition to the liquid state. Only in the coldest and driest conditions can we expect SOA to approach a glassy state and remain semi-solid during transport into the free troposphere. In the lower troposphere at temperatures above $0\,^{\circ}$C, given the slight to moderate hygroscopicity of SOA phases, our model predicts that such particles are typically semi-solid or liquid-like. Associated diffusion times for water are fast; however, the gas–particle equilibration time of organic compounds is on the order of seconds to minutes (Koop et al., 2011). While relatively fast, such viscosities may impact the interpretation of ground-based or aircraft aerosol measurements with instruments within which the aerosol sample experiences a residence time of order ten seconds or less (Shingler et al., 2016).

The ability of AIOMFAC-VISC to provide mixture viscosity predictions for complex multicomponent mixtures is owing to the flexibility afforded by the group-contribution approach and the DeRieux et al. (2018) pure-component viscosity prediction method. While further investigation will be needed to refine the pure-component viscosity prediction, at present AIOMFAC-VISC is suitably robust to make predictions of SOA mixture viscosity from the liquid to the amorphous glassy regime. Future work will involve extending AIOMFAC-VISC to account for the effect of dissolved inorganic electrolyte components present in aerosol phases.

Code and data availability. The source code of AIOMFAC-VISC will be made available as part of the AIOMFAC model code repository on GitHub (https://github.com/andizuend/AIOMFAC). Data shown in the figures are provided in the SI. AIOMFAC-VISC is also available as part of the AIOMFAC web model at https://aiomfac.lab.mcgill.ca.

Author contributions. AZ conceptualized the project and developed the methodology. NG and AZ wrote the software. NG established a database, analysed the data, and created the visualizations. DT provided original data. NG, AZ and DT co-wrote the manuscript.

Competing interests. The authors declare no competing interests.

Acknowledgements. We thank Jonathan Reid, Manabu Shiraiwa, and Wing-Sy DeRieux for providing us with access to their data. We
5 acknowledge support by the Fonds de recherche du Québec – Nature et technologies (FRQNT), grant 2015-NC-181620, and by the Natural Sciences and Engineering Research Council of Canada (NSERC), through grant RGPIN/04315- 2014.

References

Abramson, E., Imre, D., Beránek, J., Wilson, J., and Zelenyuk, A.: Experimental determination of chemical diffusion within secondary organic aerosol particles, Physical Chemistry Chemical Physics, 15, 2983, https://doi.org/10.1039/c2cp44013j, 2013.

Angell, C.: Relaxation in liquids, polymers and plastic crystals - strong/fragile patterns and problems, Journal of Non-Crystalline Solids, 131, 13–31, https://doi.org/10.1016/0022-3093(91)90266-9, 1991.

Angell, C.: Entropy and Fragility in Supercooling Liquids, vol. 102, https://doi.org/10.6028/jres.102.013, 1997.

Angell, C. A.: Formation of Glasses from Liquids and Biolymers, Advancement Of Science, 267, 1924–1935, https://doi.org/10.1126/science.267.5206.1924, 1995.

Angell, C. A., Bressel, R. D., Green, J. L., Kanno, H., Oguni, M., and Sare, E. J.: Liquid Fragility and the Glass Transition in Water and Aqueous Solutions, Journal of Food Engineering, 102, 2627–2650, https://doi.org/10.1016/0260-8774(94)90028-0, 2002.

Bateman, A. P., Bertram, A. K., and Martin, S. T.: Hygroscopic influence on the semisolid-to-liquid transition of secondary organic materials, Journal of Physical Chemistry A, 119, 4386–4395, https://doi.org/10.1021/jp508521c, 2015.

Bateman, A. P., Gong, Z., Liu, P., Sato, B., Cirino, G., Zhang, Y., Artaxo, P., Bertram, A. K., Manzi, A. O., Rizzo, L. V., Souza, R. A., Zaveri, R. A., and Martin, S. T.: Sub-micrometre particulate matter is primarily in liquid form over Amazon rainforest, Nature Geoscience, 9, 34–37, https://doi.org/10.1038/ngeo2599, 2016.

Berkemeier, T., Shiraiwa, M., Pöschl, U., and Koop, T.: Competition between water uptake and ice nucleation by glassy organic aerosol particles, Atmospheric Chemistry and Physics, 14, 12 513–12 531, https://doi.org/10.5194/acp-14-12513-2014, 2014.

Berkemeier, T., Steimer, S. S., Krieger, U. K., Peter, T., Pöschl, U., Ammann, M., and Shiraiwa, M.: Ozone uptake on glassy, semi-solid and liquid organic matter and the role of reactive oxygen intermediates in atmospheric aerosol chemistry, Physical Chemistry Chemical Physics, 18, 12 662–12 674, https://doi.org/10.1039/c6cp00634e, 2016.

Bones, D. L., Reid, J. P., Lienhard, D. M., and Krieger, U. K.: Comparing the mechanism of water condensation and evaporation in glassy aerosol, Proceedings of the National Academy of Sciences, 109, 11 613–11 618, https://doi.org/10.1073/pnas.1200691109, 2012.

Booth, A. M., Murphy, B., Riipinen, I., Percival, C. J., and Topping, D. O.: Connecting bulk viscosity measurements to kinetic limitations on attaining equilibrium for a model aerosol composition, Environmental Science and Technology, 48, 9298–9305, https://doi.org/10.1021/es501705c, 2014.

Bosse, D.: Diffusion, Viscosity, and Thermodynamics in Liquid Systems, Ph.D. thesis, https://kluedo.ub.uni-kl.de/frontdoor/deliver/index/docId/1691/file/PhD-Bosse-published.pdf, 2005.

Cao, W., Knudsen, K., Fredenslund, A., and Rasmussen, P.: Group-Contribution Viscosity Predictions of Liquid Mixtures Using UNIFAC-VLE Parameters, Ind. Eng. Chem. Res., 32, 2088–2092, https://doi.org/10.1021/ie00021a034, 1993a.

Cao, W., Knudsen, K., Fredenslund, A., and Rasmussen, P.: Simultaneous correlation of viscosity and vapor–liquid equilibrium data, Ind. Eng. Chem. Res., 32, 2077–2087, https://doi.org/10.1021/ie00021a033, https://doi.org/10.1021/ie00021a033, 1993b.

Cappa, C. D., Lovejoy, E. R., and Ravishankara, A. R.: Evidence for liquid-like and nonideal behavior of a SCIENCES, Proceedings of the National Academy of Sciences of the United States of America, 105, 18 687–18 691, https://doi.org/10.1073pnas.0802144105, 2008.

Compernolle, S., Ceulemans, K., and Muller, J. F.: EVAPORATION: a new vapour pressure estimation methodfor organic molecules including non-additivity and intramolecular interactions, Atmos. Chem. Phys., 11, 9431–9450, https://doi.org/10.5194/acp-11-9431-2011, <GotoISI>://WOS:000295368700001, 2011.

Debenedetti, P. G. and Stillinger, F. H.: Review article Supercooled liquids and the glass transition, Nature, 410, 259, 2001.

Dehaoui, A., Issenmann, B., and Caupin, F.: Viscosity of deeply supercooled water and its coupling to molecular diffusion, Proceedings of the National Academy of Sciences, 112, 12 020–12 025, https://doi.org/10.1073/pnas.1508996112, 2015.

DeRieux, W. S. W., Li, Y., Lin, P., Laskin, J., Laskin, A., Bertram, A. K., Nizkorodov, S. A., and Shiraiwa, M.: Predicting the glass transition temperature and viscosity of secondary organic material using molecular composition, Atmospheric Chemistry and Physics, 18, 6331–6351, https://doi.org/10.5194/acp-18-6331-2018, 2018.

Dette, H. P., Qi, M., Schröder, D. C., Godt, A., and Koop, T.: Glass-forming properties of 3-methylbutane-1,2,3-tricarboxylic acid and its mixtures with water and pinonic acid, Journal of Physical Chemistry A, 118, 7024–7033, https://doi.org/10.1021/jp505910w, 2014.

Ediger, M. D.: Spatially heterogeneous dynamics in supercooled liquids., Annual Review of Physical Chemistry, 51, 99–128, https://doi.org/10.1146/annurev.physchem.51.1.99, 2000.

Fowler, K., Connolly, P., and Topping, D.: Modelling the effect of condensed-phase diffusion on the homogeneous nucleation of ice in supercooled water, Atmospheric Chemistry and Physics Discussions, 2019, 1–26, https://doi.org/10.5194/acp-2019-401, https://www.atmos-chem-phys-discuss.net/acp-2019-401/, 2019.

Fredenslund, A., Jones, R. L., and Prausnitz, J. M.: Group-Contribution Estimation of Activity Coefficients in Nonideal Liquid Mixtures, AICHE J., 21, 1086–1099, 1975.

Gorkowski, K., Preston, T. C., and Zuend, A.: RH-dependent organic aerosol thermodynamics via an efficient reduced-complexity model, Atmos. Chem. Phys. Discussions, 2019, 1–37, https://doi.org/10.5194/acp-2019-495, https://www.atmos-chem-phys-discuss.net/acp-2019-495/, 2019.

Grayson, J. W., Zhang, Y., Mutzel, A., Renbaum-Wolff, L., Böge, O., Kamal, S., Herrmann, H., Martin, S. T., and Bertram, A. K.: Effect of varying experimental conditions on the viscosity of α-pinene derived secondary organic material, Atmospheric Chemistry and Physics, 16, 6027–6040, https://doi.org/10.5194/acp-16-6027-2016, 2016.

Hansen, H. K., Rasmussen, P., Fredenslund, A., Schiller, M., and Gmehling, J.: Vapor–liquid-equilibria by UNIFAC group contribution. 5. Revision and extension, Ind. Eng. Chem. Res., 30, 2352–2355, 1991.

Heald, C. L., Jacob, D. J., Turquety, S., Hudman, R. C., Weber, R. J., Sullivan, A. P., Peltier, R. E., Atlas, E. L., de Gouw, J. A., Warneke, C., Holloway, J. S., Neuman, A., Flocke, F. M., and Seinfeld, J. H.: Concentrations and sources of organic carbon aerosols in the free troposphere over North America, Journal of Geophysical Research Atmospheres, 111, 23–47, https://doi.org/10.1029/2005JD007705, 2006.

Jagla, E. A.: Fragile-strong transitions and polyamorphism in glass forming fluids, Molecular Physics, 99, 753–757, https://doi.org/10.1080/00268970010030031, 2001.

Järvinen, E., Ignatius, K., Nichman, L., Kristensen, T. B., Fuchs, C., Hoyle, C. R., Höppel, N., Corbin, J. C., Craven, J., Duplissy, J., Ehrhart, S., El Haddad, I., Frege, C., Gordon, H., Jokinen, T., Kallinger, P., Kirkby, J., Kiselev, A., Naumann, K. H., Petäjä, T., Pinterich, T., Prevot, A. S., Saathoff, H., Schiebel, T., Sengupta, K., Simon, M., Slowik, J. G., Tröstl, J., Virtanen, A., Vochezer, P., Vogt, S., Wagner, A. C., Wagner, R., Williamson, C., Winkler, P. M., Yan, C., Baltensperger, U., Donahue, N. M., Flagan, R. C., Gallagher, M., Hansel, A., Kulmala, M., Stratmann, F., Worsnop, D. R., Möhler, O., Leisner, T., and Schnaiter, M.: Observation of viscosity transition in α-pinene secondary organic aerosol, Atmospheric Chemistry and Physics, 16, 4423–4438, https://doi.org/10.5194/acp-16-4423-2016, 2016.

Jenkin, M. E., Saunders, S. M., and Pilling, M. J.: The tropospheric degradation of volatile organic compounds: A protocol for mechanism development, Atmos. Environ., 31, https://doi.org/10.1016/S1352-2310(96)00105-7, http://dx.doi.org/10.1016/S1352-2310(96)00105-7, 1997.

Jenkin, M. E., Young, J. C., and Rickard, A. R.: The MCM v3.3.1 degradation scheme for isoprene, Atmos. Chem. Phys., 15, 11 433–11 459, https://doi.org/10.5194/acp-15-11433-2015, http://www.atmos-chem-phys.net/15/11433/2015/, 2015.

Knopf, D. A., Alpert, P. A., and Wang, B.: The Role of Organic Aerosol in Atmospheric Ice Nucleation: A Review, ACS Earth and Space Chemistry, 2, 168–202, https://doi.org/10.1021/acsearthspacechem.7b00120, 2018.

Koop, T., Bookhold, J., Shiraiwa, M., and Pöschl, U.: Glass transition and phase state of organic compounds: Dependency on molecular properties and implications for secondary organic aerosols in the atmosphere, https://doi.org/10.1039/c1cp22617g, 2011.

La Nave, E., Stanley, H. E., and Sciortino, F.: Configuration Space Connectivity across the Fragile-to-Strong Transition in Silica, Physical Review Letters, 88, 4, https://doi.org/10.1103/PhysRevLett.88.035501, 2002.

Li, Y. J., Liu, P., Gong, Z., Wang, Y., Bateman, A. P., Bergoend, C., Bertram, A. K., and Martin, S. T.: Chemical Reactivity and Liquid/Nonliquid States of Secondary Organic Material, Environmental Science and Technology, 49, 13 264–13 274, https://doi.org/10.1021/acs.est.5b03392, 2015.

Lienhard, D. M., Zobrist, B., Zuend, A., Krieger, U. K., and Peter, T.: Experimental evidence for excess entropy discontinuities in glass-forming solutions, Journal of Chemical Physics, 136, 74 515, https://doi.org/10.1063/1.3685902, 2012.

Lienhard, D. M., Huisman, A. J., Krieger, U. K., Rudich, Y., Marcolli, C., Luo, B. P., Bones, D. L., Reid, J. P., Lambe, A. T., Canagaratna, M. R., Davidovits, P., Onasch, T. B., Worsnop, D. R., Steimer, S. S., Koop, T., and Peter, T.: Viscous organic aerosol particles in the upper troposphere: Diffusivity-controlled water uptake and ice nucleation?, Atmospheric Chemistry and Physics, 15, 13 599–13 613, https://doi.org/10.5194/acp-15-13599-2015, 2015.

Liu, P., Li, Y. J., Wang, Y., Bateman, A. P., Zhang, Y., Gong, Z., Bertram, A. K., and Martin, S. T.: Highly Viscous States Affect the Browning of Atmospheric Organic Particulate Matter, ACS Central Science, 4, 207–215, https://doi.org/10.1021/acscentsci.7b00452, 2018.

Maclean, A. M., Butenhoff, C. L., Grayson, J. W., Barsanti, K., Jimenez, J. L., and Bertram, A. K.: Mixing times of organic molecules within secondary organic aerosol particles: A global planetary boundary layer perspective, Atmospheric Chemistry and Physics, 17, 13 037–13 048, https://doi.org/10.5194/acp-17-13037-2017, 2017.

Mallamace, F., Branca, C., Corsaro, C., Leone, N., Spooren, J., Chen, S.-H., and Stanley, H. E.: Transport properties of glass-forming liquids suggest that dynamic crossover temperature is as important as the glass transition temperature, Proceedings of the National Academy of Sciences, 107, 22 457–22 462, https://doi.org/10.1073/pnas.1015340107, 2010.

Marsh, A., Petters, S. S., Rothfuss, N. E., Rovelli, G., Song, Y. C., Reid, J. P., and Petters, M. D.: Amorphous phase state diagrams and viscosity of ternary aqueous organic/organic and inorganic/organic mixtures, Physical Chemistry Chemical Physics, 20, 15 086–15 097, https://doi.org/10.1039/c8cp00760h, 2018.

Marshall, F. H., Miles, R. E., Song, Y. C., Ohm, P. B., Power, R. M., Reid, J. P., and Dutcher, C. S.: Diffusion and reactivity in ultraviscous aerosol and the correlation with particle viscosity, Chemical Science, 7, 1298–1308, https://doi.org/10.1039/c5sc03223g, 2016.

Murray, B. J.: Inhibition of ice crystallisation in highly viscous aqueous organic acid droplets, Atmospheric Chemistry and Physics, 8, 5423–5433, https://doi.org/10.5194/acp-8-5423-2008, 2008.

Nannoolal, Y., Rarey, J., and Ramjugernath, D.: Estimation of pure component properties - Part 3. Estimation of the vapor pressure of non-electrolyte organic compounds via group contributions and group interactions, Fluid Phase Equilib., 269, http://dx.doi.org/10.1016/j.fluid.2008.04.020, 2008.

Nannoolal, Y., Rarey, J., and Ramjugernath, D.: Estimation of pure component properties. Part 4: Estimation of the saturated liquid viscosity of non-electrolyte organic compounds via group contributions and group interactions, Fluid Phase Equilibria, 281, 97–119, https://doi.org/10.1016/j.fluid.2009.02.016, 2009.

Novikov, V. N. and Sokolov, A. P.: Universality of the dynamic crossover in glass-forming liquids: A "magic" relaxation time, Physical Review E - Statistical Physics, Plasmas, Fluids, and Related Interdisciplinary Topics, 67, 6, https://doi.org/10.1103/PhysRevE.67.031507, 2003.

Price, H. C., Mattsson, J., Zhang, Y., Bertram, A. K., Davies, J. F., Grayson, J. W., Martin, S. T., O'Sullivan, D., Reid, J. P., Rickards, A. M., and Murray, B. J.: Water diffusion in atmospherically relevant α-pinene secondary organic material, Chemical Science, 6, 4876–4883, https://doi.org/10.1039/c5sc00685f, 2015.

Rastak, N., Pajunoja, A., Acosta Navarro, J. C., Ma, J., Song, M., Partridge, D. G., Kirkevåg, A., Leong, Y., Hu, W. W., Taylor, N. F., Lambe, A., Cerully, K., Bougiatioti, A., Liu, P., Krejci, R., Petäjä, T., Percival, C., Davidovits, P., Worsnop, D. R., Ekman, A. M. L., Nenes, A., Martin, S., Jimenez, J. L., Collins, D. R., Topping, D. O., Bertram, A. K., Zuend, A., Virtanen, A., and Riipinen, I.: Microphysical explanation of the RH-dependent water affinity of biogenic organic aerosol and its importance for climate, Geophys. Res. Lett., 44, 5167–5177, https://doi.org/10.1002/2017GL073056, https://doi.org/10.1002/2017GL073056, 2017.

Reid, J. P., Bertram, A. K., Topping, D. O., Laskin, A., Martin, S. T., Petters, M. D., Pope, F. D., and Rovelli, G.: The viscosity of atmospherically relevant organic particles, https://doi.org/10.1038/s41467-018-03027-z, 2018.

Renbaum-Wolff, L., Grayson, J. W., Bateman, A. P., Kuwata, M., Sellier, M., Murray, B. J., Shilling, J. E., Martin, S. T., and Bertram, A. K.: Viscosity of -pinene secondary organic material and implications for particle growth and reactivity, Proceedings of the National Academy of Sciences, 110, 8014–8019, https://doi.org/10.1073/pnas.1219548110, 2013.

Rothfuss, N. E. and Petters, M. D.: Influence of Functional Groups on the Viscosity of Organic Aerosol, Environmental Science and Technology, 51, 271–279, https://doi.org/10.1021/acs.est.6b04478, 2017.

Rovelli, G., Song, Y. C., Maclean, A. M., Topping, D. O., Bertram, A. K., and Reid, J. P.: Comparison of Approaches for Measuring and Predicting the Viscosity of Ternary Component Aerosol Particles, Analytical Chemistry, 91, 5074–5082, https://doi.org/10.1021/acs.analchem.8b05353, 2019.

Saika-Voivod, I., Sciortino, F., and Poole, P. H.: Free energy and configurational entropy of liquid silica: Fragile-to-strong crossover and polyamorphism, Physical Review E - Statistical Physics, Plasmas, Fluids, and Related Interdisciplinary Topics, 69, 13, https://doi.org/10.1103/PhysRevE.69.041503, 2004.

Sastri, S. and Rao, K.: A new group contribution method for predicting viscosity of organic liquids, The Chemical Engineering Journal, 50, 9–25, https://doi.org/10.1016/0300-9467(92)80002-R, 1992.

Saukko, E., Lambe, A. T., Massoli, P., Koop, T., Wright, J. P., Croasdale, D. R., Pedernera, D. A., Onasch, T. B., Laaksonen, A., Davidovits, P., Worsnop, D. R., and Virtanen, A.: Humidity-dependent phase state of SOA particles from biogenic and anthropogenic precursors, Atmospheric Chemistry and Physics, 12, 7517–7529, https://doi.org/10.5194/acp-12-7517-2012, 2012.

Saunders, S. M., Jenkin, M. E., Derwent, R. G., and Pilling, M. J.: Protocol for the development of the Master Chemical Mechanism, MCM v3 (Part A): tropospheric degradation of non-aromatic volatile organic compounds, Atmos. Chem. Phys., 3, 161 – 180, https://doi.org/10.5194/acp-3-161-2003, http://dx.doi.org/10.5194/acp-3-161-2003, 2003.

Schum, S. K., Zhang, B., Dzepina, K., Fialho, P., Mazzoleni, C., and Mazzoleni, L. R.: Molecular and physical characteristics of aerosol at a remote free troposphere site: Implications for atmospheric aging, Atmospheric Chemistry and Physics, 18, 14 017–14 036, https://doi.org/10.5194/acp-18-14017-2018, 2018.

Shingler, T., Crosbie, E., Ortega, A., Shiraiwa, M., Zuend, A., Beyersdorf, A., Ziemba, L., Anderson, B., Thornhill, L., Perring, A. E., Schwarz, J. P., Campazano-Jost, P., Day, D. A., Jimenez, J. L., Hair, J. W., Mikoviny, T., Wisthaler, A., and Sorooshian, A.: Airborne

characterization of subsaturated aerosol hygroscopicity and dry refractive index from the surface to 6.5 km during the SEAC4RS campaign, J. Geophys. Res. Atmos., 121, 4188–4210, https://doi.org/10.1002/2015JD024498, 2016.

Shiraiwa, M., Li, Y., Tsimpidi, A. P., Karydis, V. A., Berkemeier, T., Pandis, S. N., Lelieveld, J., Koop, T., and Pöschl, U.: Global distribution of particle phase state in atmospheric secondary organic aerosols, Nature Communications, 8, 1–7, https://doi.org/10.1038/ncomms15002, 2017.

Shrivastava, M., Cappa, C. D., Fan, J., Goldstein, A. H., Guenther, A. B., Jimenez, J. L., Kuang, C., Laskin, A., Martin, S. T., Ng, N. L., Petaja, T., Pierce, J. R., Rasch, P. J., Roldin, P., Seinfeld, J. H., Shilling, J., Smith, J. N., Thornton, J. A., Volkamer, R., Wang, J., Worsnop, D. R., Zaveri, R. A., Zelenyuk, A., and Zhang, Q.: Recent advances in understanding secondary organic aerosol: Implications for global climate forcing, Reviews of Geophysics, 55, 509–559, https://doi.org/10.1002/2016RG000540, 2017.

Slade, J. H., Ault, A. P., Bui, A. T., Ditto, J. C., Lei, Z., Bondy, A. L., Olson, N. E., Cook, R. D., Desrochers, S. J., Harvey, R. M., Erickson, M. H., Wallace, H. W., Alvarez, S. L., Flynn, J. H., Boor, B. E., Petrucci, G. A., Gentner, D. R., Griffin, R. J., and Shepson, P. B.: Bouncier Particles at Night: Biogenic Secondary Organic Aerosol Chemistry and Sulfate Drive Diel Variations in the Aerosol Phase in a Mixed Forest, Environmental Science and Technology, 53, 4977–4987, https://doi.org/10.1021/acs.est.8b07319, 2019.

Song, M., Liu, P. F., Hanna, S. J., Li, Y. J., Martin, S. T., and Bertram, A. K.: Relative humidity-dependent viscosities of isoprene-derived secondary organic material and atmospheric implications for isoprene-dominant forests, Atmospheric Chemistry and Physics, 15, 5145–5159, https://doi.org/10.5194/acp-15-5145-2015, 2015.

Song, M., Liu, P. F., Hanna, S. J., Zaveri, R. A., Potter, K., You, Y., Martin, S. T., and Bertram, A. K.: Relative humidity-dependent viscosity of secondary organic material from toluene photo-oxidation and possible implications for organic particulate matter over megacities, Atmospheric Chemistry and Physics, 16, 8817–8830, https://doi.org/10.5194/acp-16-8817-2016, 2016a.

Song, Y. C., Haddrell, A. E., Bzdek, B. R., Reid, J. P., Bannan, T., Topping, D. O., Percival, C., and Cai, C.: Supplement: Measurements and Predictions of Binary Component Aerosol Particle Viscosity, Tech. Rep. 41, https://doi.org/10.1021/acs.jpca.6b07835, 2016b.

Song, Y. C., Haddrell, A. E., Bzdek, B. R., Reid, J. P., Bannan, T., Topping, D. O., Percival, C., and Cai, C.: Measurements and Predictions of Binary Component Aerosol Particle Viscosity, The Journal of Physical Chemistry A, 120, 8123–8137, https://doi.org/10.1021/acs.jpca.6b07835, 2016c.

Topping, D., Barley, M., Bane, M. K., Higham, N., Aumont, B., Dingle, N., and McFiggans, G.: UManSysProp v1.0: an online and open-source facility for molecular property prediction and atmospheric aerosol calculations, Geosci. Model Dev., 9, 899–914, https://doi.org/10.5194/gmd-9-899-2016, http://www.geosci-model-dev.net/9/899/2016/, 2016.

Tsigaridis, K. and Kanakidou, M.: Global modelling of secondary organic aerosol in the troposphere: A sensitivity analysis, Atmospheric Chemistry and Physics, 3, 1849–1869, https://doi.org/10.5194/acp-3-1849-2003, 2003.

Virtanen, A., Joutsensaari, J., Koop, T., Kannosto, J., Yli-Pirilä, P., Leskinen, J., Mäkelä, J. M., Holopainen, J. K., Pöschl, U., Kulmala, M., Worsnop, D. R., and Laaksonen, A.: An amorphous solid state of biogenic secondary organic aerosol particles, Nature, 467, 824–827, https://doi.org/10.1038/nature09455, 2010.

Ye, Q., Robinson, E. S., Ding, X., Ye, P., Sullivan, R. C., and Donahue, N. M.: Mixing of secondary organic aerosols versus relative humidity, Proceedings of the National Academy of Sciences, 113, 12 649–12 654, https://doi.org/10.1073/pnas.1604536113, 2016.

Zelenyuk, A., Imre, D. G., Wilson, J., Bell, D. M., Suski, K. J., Shrivastava, M., Beránek, J., Alexander, M. L., Kramer, A. L., and Massey Simonich, S. L.: The effect of gas-phase polycyclic aromatic hydrocarbons on the formation and properties of biogenic secondary organic aerosol particles, Faraday Discussions, 200, 143–164, https://doi.org/10.1039/c7fd00032d, 2017.

Zhang, Y., Sanchez, M. S., Douet, C., Wang, Y., Bateman, A. P., Gong, Z., Kuwata, M., Renbaum-Wolff, L., Sato, B. B., Liu, P. F., Bertram, A. K., Geiger, F. M., and Martin, S. T.: Changing shapes and implied viscosities of suspended submicron particles, Atmospheric Chemistry and Physics, 15, 7819–7829, https://doi.org/10.5194/acp-15-7819-2015, 2015.

Zhou, S., Hwang, B. C. H., Lakey, P. S. J., Zuend, A., Abbatt, J. P. D., and Shiraiwa, M.: Multiphase reactivity of polycyclic aromatic hydrocarbons is driven by phase separation and diffusion limitations, PNAS, 116, 11 658, https://doi.org/10.1073/pnas.1902517116, 2019.

Zobrist, B., Marcolli, C., Pedernera, D. A., and Koop, T.: Do atmospheric aerosols form glasses?, Atmospheric Chemistry and Physics, 8, 5221–5244, https://doi.org/10.5194/acp-8-5221-2008, 2008.

Zuend, A. and Seinfeld, J. H.: Modeling the gas-particle partitioning of secondary organic aerosol: The importance of liquid-liquid phase separation, Atmospheric Chemistry and Physics, 12, 3857–3882, https://doi.org/10.5194/acp-12-3857-2012, 2012.

Zuend, A., Marcolli, C., Luo, B. P., and Peter, T.: A thermodynamic model of mixed organic-inorganic aerosols to predict activity coefficients, Atmospheric Chemistry and Physics, 8, 4559–4593, https://doi.org/10.5194/acp-8-4559-2008, 2008.

Zuend, A., Marcolli, C., Booth, A. M., Lienhard, D. M., Soonsin, V., Krieger, U. K., Topping, D. O., McFiggans, G., Peter, T., and Seinfeld, J. H.: New and extended parameterization of the thermodynamic model AIOMFAC: Calculation of activity coefficients for organic-inorganic mixtures containing carboxyl, hydroxyl, carbonyl, ether, ester, alkenyl, alkyl, and aromatic functional groups, Atmospheric Chemistry and Physics, 11, 9155–9206, https://doi.org/10.5194/acp-11-9155-2011, 2011.

Supplementary Information

for

A predictive group-contribution model for the viscosity of aqueous organic aerosol

Natalie R. Gervasi[1], David O. Topping[2], and Andreas Zuend[1]

[1]Department of Atmospheric and Oceanic Sciences, McGill University, Montreal, Quebec, H3A 0B9, Canada
[2]School of Earth, Atmospheric and Environmental Science, University of Manchester, Manchester M13 9PL, U.K.

S1 Estimation of the pure component viscosity of water

The pure component viscosity of water was estimated using the parameterization developed by Dehaoui et al. (2015) for all model simulations in this work; see Eq. (10) of main text. The experimental data used for developing the Dehaoui et al. (2015) parameterization extends from 239.15 K to 491.95 K. The parameterization is in excellent agreement with the data when temperatures are below $\sim$ 400 K. In Fig. S1, we compare the Dehaoui et al. (2015) parameterization with a parameterization by Viswanath et al. (2007) and with experimental data. The parameterization by Viswanath et al. (2007) is in better agreement with experimental data above $\sim$ 400 K when compared to the Dehaoui et al. (2015) parameterization. The Viswanath et al. (2007) parameterization is also in excellent agreement with the experimental data down to $\sim$ 270 K, below which it begins to deviate substantially from the available experimental data. Between 270 K and $\sim$ 380 K the two parameterizations are almost indistinguishable. Here we choose to use the Dehaoui et al. (2015) parameterization given that it is the more robust parameterization at lower temperatures of relevance in the troposphere.

S2 Exploration of the relationship between pure component vapour pressure and viscosity

In this study, initially an attempt was made to estimate the pure component viscosity of organic compounds from their pure component vapour pressures. The pure component viscosity is shown as a function of pure component vapour pressure in double logarithm space in Fig. S2. There is only a weak linear relationship between viscosity and vapour pressure when considering the range of viscosity from liquid to glassy for both the Nannoolal et al. (2008) and EVAPORATION model vapour pressure predictions. A stronger linear relationship exists in the liquid range, but below a vapour pressure of 10^{-5} Pa, the relationship between viscosity and vapour pressure becomes less clear and reliable data are scarce. We still hypothesize a relationship to exist between the two pure-component properties even in the semi-solid and glassy regimes. Although, it is likely
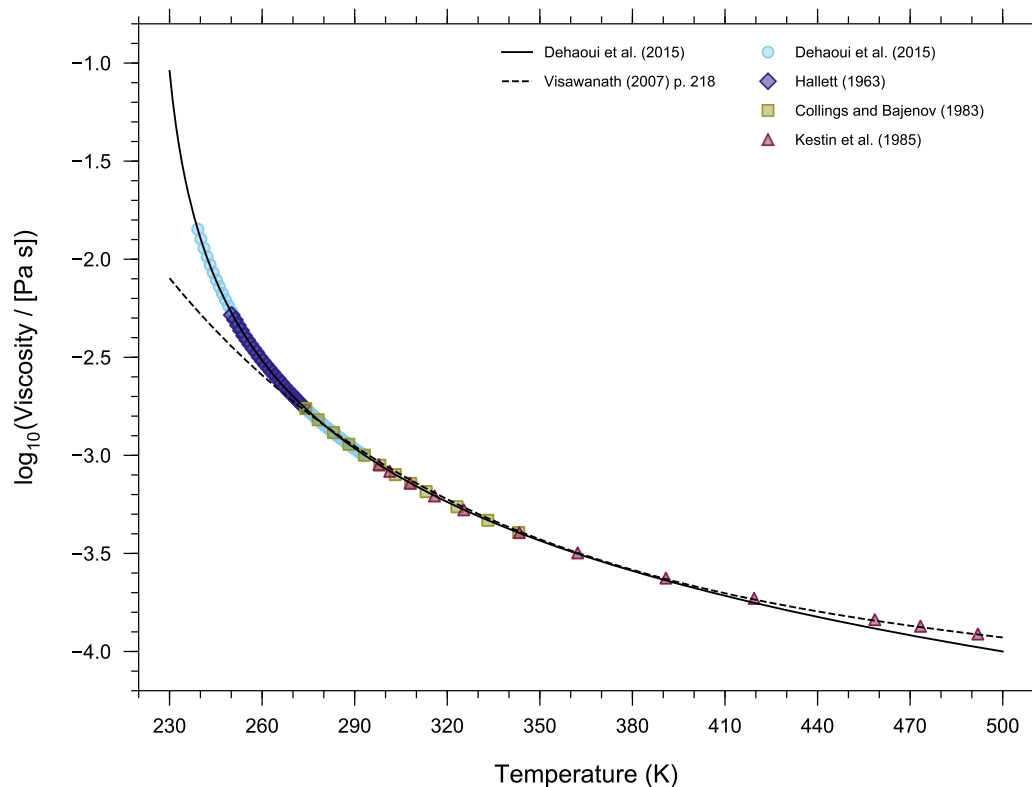
Figure S1. Parameterizations of the pure-component viscosity of water from Dehaoui et al. (2015) (solid line) and Viswanath et al. (2007) (dashed line). Markers represent experimental data where error bars have been omitted for clarity. The Dehaoui et al. (2015) parameterization is supported by measurements from $\sim$ 230 to 400 K and the Viswanath et al. (2007) parameterization is supported by measurements from $\sim$ 270 to 500 K.

this relationship is not resolved with the vapour pressure and viscosity estimation tools used here, given these tools have been trained with compounds that have higher vapour pressure and liquid viscosity only. Just as direct measurements of ultra-high pure-component viscosities are challenging to make, so too are measurements of ultra-low pure component vapour pressures. In order to fully elucidate the relationship between the two material properties, more precise experimental measurements are needed to better constrain pure-component property estimation tools.
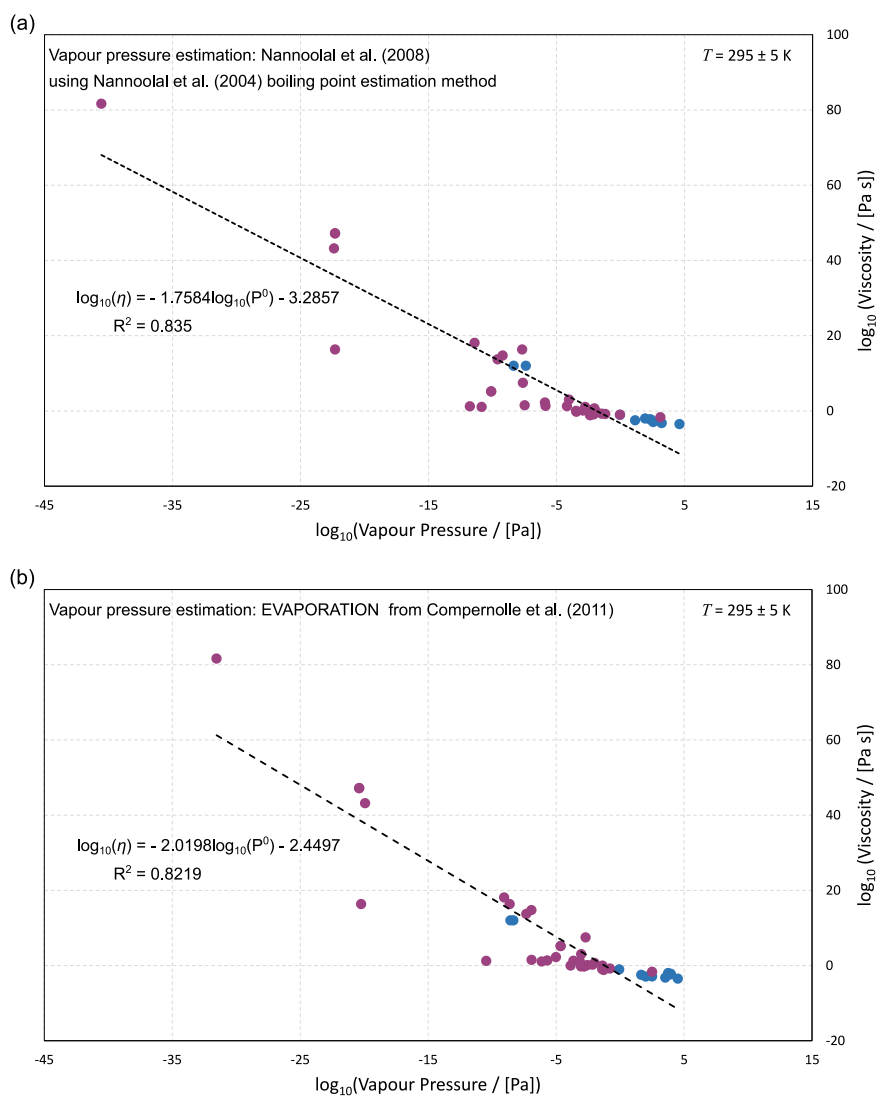
Figure S2. Reference or modelled pure component viscosity as a function of modelled pure component vapour pressure. Vapour pressures have been estimated using (**a**) the online tool UManSysProp (http://umansysprop.seaes.manchester.ac.uk) with the Nannoolal et al. (2008) vapour pressure model and the Nannoolal et al. (2004) boiling point estimation method and (**b**) the EVAPORATION model (Compernolle et al., 2011). Purple markers indicate values where the viscosity has been modelled using the method by Nannoolal et al. (2009). Blue markers indicate reference viscosity values either from direct experimental measurements or from an extrapolation with the Vogel–Tamman–Fulcher equation to $T = 293.15$ K using pure-component viscosity values measured at higher temperatures. All model values have been calculated at 293.15 K. Reference viscosity values are taken at a range of temperatures (295 ± 5 K). Dashed black lines indicate linear regressions (in logarithm space) to the combined reference and model data.

Table S1. Measured, parameterized, or modelled values of the glass transition temperature (T_g) from the literature. Uncertainty values are listed when they are provided from their source.

Compound	T_g (K)	Reference
1,2,4-Butanetriol	200.7	Nakanishi and Nozaki (2011)
1,2,6-Hexanetriol	202	Böhmer et al. (1993)
	206.4 ± 0.5	Dorfmüller et al. (1979)
	201.9	Nakanishi and Nozaki (2011)
	192 ± 2	Zhang et al. (2018)
	193.3 ± 1.3	Zobrist et al. (2008)
1,4-Butanediol	158.4 ± 1.1	Zobrist et al. (2008)
Citric Acid	281 ± 5	Bodsworth et al. (2010)
	286 ± 1.5	Dette et al. (2014)
	273.25 ± 3.4	Hoppu et al. (2009)
	281.9 ± 0.9	Lienhard et al. (2012)
	284.15 ± 0.2	Lu and Zografi (1997)
	286 ± 10	Marsh et al. (2018)
	260 ± 10	Murray (2008)
	283.35[in situ]	Timko and Lordi (1979)
	286.65[bulk]	Timko and Lordi (1979)
	307 ± 5	Zhang et al. (2018)
Fructose	283.15	Ablett et al. (1993)
	286	Angell (1997)
	283	Ollet and Parker (1990)
	289[mid]	Simatos et al. (1996)
Glucose	306	Angell (1997)
	297 ± 2	Dette et al. (2014)
	309	Kawai et al. (2005)
	293.2 ± 0.9	Lienhard et al. (2012)
	304	Ollet and Parker (1990)
	296[mid]	Simperler et al. (2006)
	325[calculated]	Simperler et al. (2006)
	296.1 ± 3.1	Zobrist et al. (2008)

Compound	T_g (K)	Reference
Glycerol	187	Angell (1997)
	193	Angell (1997)
	190	Böhmer et al. (1993)
	191 ± 0.9	Lienhard et al. (2012)
	191.7	Nakanishi and Nozaki (2011)
	196	Seidl et al. (2013)
	192 ± 2	Zhang et al. (2018)
Raffinose	377.9 ± 0.9	Lienhard et al. (2012)
	395.7 ± 21.6	Zobrist et al. (2008)
Sorbitol	266	Angell (1997)
	274	Böhmer et al. (1993)
	268.3	Nakanishi and Nozaki (2011)
	276[mid]	Simatos et al. (1996)
Sucrose	323	Angell (1997)
	331 ± 2	Dette et al. (2014)
	350 ± 3.5	Hancock et al. (1995)
	341	Kawai et al. (2005)
	341	Rothfuss and Petters (2017)
	333[mid]	Simperler et al. (2006)
	347[calculated]	Simperler et al. (2006)
	335.7 ± 3.6	Zobrist et al. (2008)
Trehalose	388	Angell (1997)
	369 ± 1.5	Dette et al. (2014)
	386	Kawai et al. (2005)
	380[mid]	Simperler et al. (2006)
	392[calculated]	Simperler et al. (2006)

S3 Estimation of AIOMFAC-VISC sensitivity

We calculated the sensitivity of AIOMFAC-VISC as a proxy for the uncertainty in the mixture viscosity prediction. We chose to prescribe the AIOMFAC-VISC sensitivity as the response of the mixture viscosity prediction to a small change in mixture composition. A small change in mixture composition is meant to represent the uncertainty in the composition measurement in a laboratory setting, which would be typical of all experiments. Therefore, the AIOMFAC-VISC sensitivity of mixture viscosity, s_η, is calculated using a molar partial derivative:

$$s_\eta = x^{\text{tol}} \left[\frac{\partial \ln(\eta_{\text{mix}})}{\partial n_{\text{H}_2\text{O}}} \right] \tag{S1}$$

where x^{tol} is the molar tolerance (the prescribed uncertainty) in the mixture composition. To retrieve x^{tol} we first perturb the mass of water by $\delta_m = 2\,\%$ of the mass of the total system,

$$m_{\text{H}_2\text{O}} = m_{\text{H}_2\text{O,init}} + \delta_m, \tag{S2}$$

where $m_{\text{H}_2\text{O,init}}$ is the initial mass of water in the mixture (e.g. $m_{\text{H}_2\text{O,init}} = w_{\text{H}_2\text{O,init}}$ for 1 kg of total mass of the mixture) and $m_{\text{H}_2\text{O}}$ is the perturbed mass. Next, the mass fractions of all components are normalized to account for the mass addition via

$$w_i = \frac{w_{i,\text{init}}}{1 + \delta_m}, \tag{S3}$$

where w_i represents the normalized mass fraction of a given component i given the initial mass fraction $w_{i,init}$. By doing this, we prescribe the model sensitivity as strictly a change in water content of the mixture, where the mixing ratio of organic constituents remains fixed. The normalized mass fractions are then converted to mole fractions (x_i) and finally, x^{tol} is calculated as the difference between the mole fractions of the perturbed system and the unperturbed system.

$$x^{\text{tol}} = x_{\text{H}_2\text{O}} - x_{\text{H}_2\text{O,init}}. \tag{S4}$$

S4 Comparison of AIOMFAC-VISC and GC-UNIMOD

Here we compare the performance of the mixture viscosity prediction of AIOMFAC-VISC with the original Cao et al. (1993), GC-UNIMOD model. To compare the mixture viscosity prediction absent of uncertainty introduced by the pure-component viscosity prediction, we have fixed the pure-component viscosity of citric acid to a fitted value at the temperature of interest here (as described in the main text) and we have used the experimental pure-component viscosity of glycerol. As seen in Fig. S3 the AIOMFAC-VISC mixture viscosity prediction is greatly improved from that by the GC-UNIMOD model. The same behaviour was observed for the other binary aqueous mixtures investigated in this work.
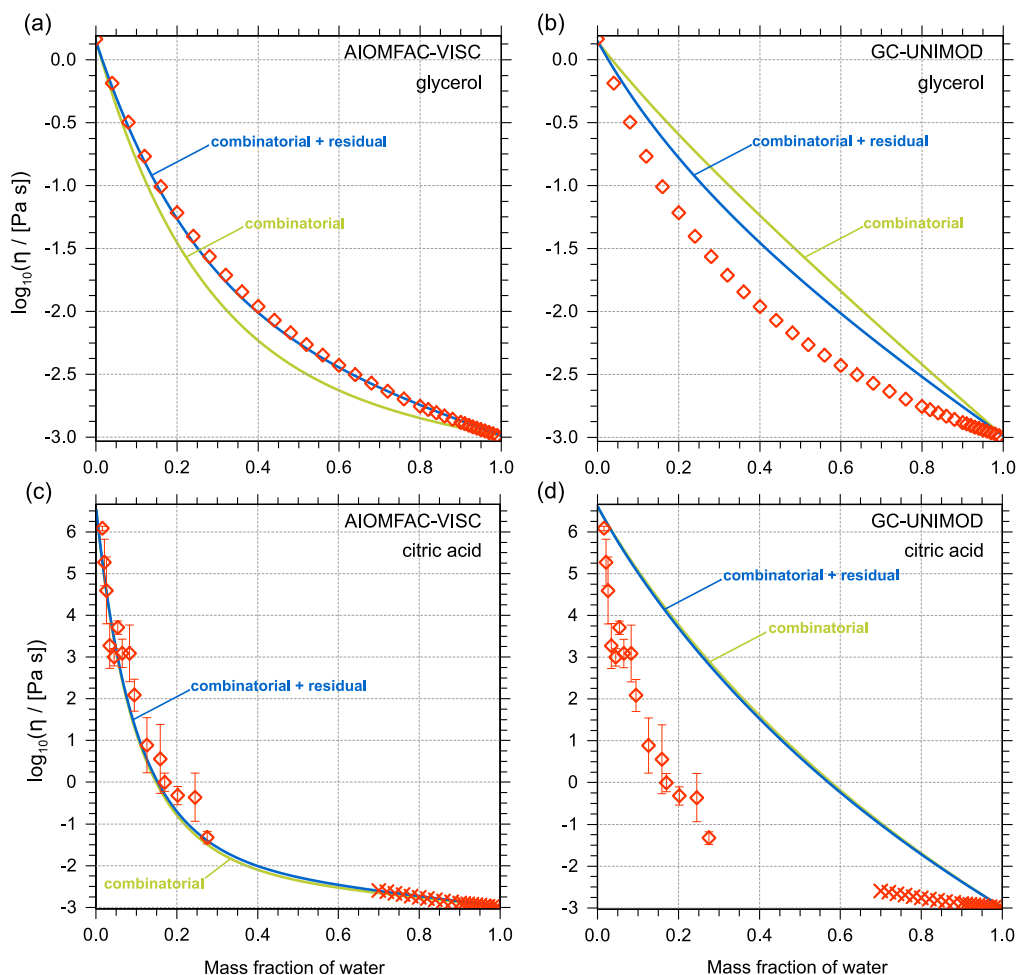
Figure S3. A comparison of predicted mixture viscosity as a function of mass fraction of water (blue curves) shown for glycerol (top two panels) and citric acid (bottom two panels). The blue curves represent mixture viscosity computed with both combinatorial and residual contributions. The yellow curves represent computations using combinatorial mixture viscosity only. The AIOMFAC-VISC mixture viscosity prediction for glycerol (**a**) and citric acid (**c**) is in significantly better agreement with the experimental data (red markers) as compared to the GC-UNIMOD mixture viscosity prediction for both glycerol (**b**) and citric acid (**d**). The changes made to the combinatorial viscosity contribution from GC-UNIMOD to AIOMFAC-VISC account for most of the improvement.

S5 Binary aqueous mixture viscosity predictions for all training data

To optimize the mixing model of AIOMFAC-VISC, we attempted to simultaneously fit the mixing model prediction to experimental viscosity data for the binary aqueous mixtures shown in Figs. S4, S5, and S6. The fit is captured by an adjustable parameter multiplied by the residual component of the mixture viscosity model. The determination of an optimal fit parameter is a global minimization problem, ideally approached by using a set of global optimization methods. For this, we used the optimization approach described by Zuend et al. (2011). The optimal fit parameter was determined to be ~ 1.0, therefore no further adjustments were made to the mixture viscosity model aside from those adjustments made to the original Cao et al. (1993) formulation described in the main text.

S6 Determination of SOA systems

For all three SOA systems simulated in this work, each surrogate compound was assigned a fixed molar concentration in the particulate matter (PM). These fixed molar concentrations in $\mathrm{mol\,m^{-3}}$ (of air) are listed in Tables S2, S3, and S4 for α-pinene-, toluene-, and isoprene-derived SOA, respectively. To determine those molar concentration of constituents for the α-pinene and isoprene SOA systems, we begin by calculating the equilibrium gas–particle partitioning of the surrogate species in each SOA system using the MCM–EVAPORATION–AIOMFAC approach (Zuend et al., 2011) where the initial total molar concentrations (PM plus gas phase) for α-pinene and isoprene SOA were taken from Zuend and Seinfeld (2012) and Rastak et al. (2017), respectively. We extract the molar concentration of each constituent in the PM phase for a relative humidity of $40\,\%$. When relative humidity is held at $40\,\%$, the average $\mathrm{O:C}$ ratio of the SOA produced via our gas–particle partitioning prediction is representative of known $\mathrm{O:C}$ ratios from experiments. We then hold the molar concentrations of organics in the PM constant during calculations of mixture viscosity. In the case of α-pinene SOA, we have made one additional adjustment by scaling the molar amount of surrogate compound C108OOH in the PM phase by a factor of 30. This is done to better match the curvature of the experimental viscosity data at high relative humidity. In the case of toluene SOA, we have selected several constituents from the MCM-derived list of surrogate components from toluene photo-oxidation by OH radicals. To determine the molar concentrations of a given constituent (n_i) in the PM phase we use the following formula:

$$n_i = \mathrm{O:C} \times T_{\mathrm{g}} \times 10^{-10}. \tag{S5}$$

Using this scaling results in the $\mathrm{O:C}$ of the SOA produced to be similar to what is expected from laboratory chamber experiments. We note here that we have increased the concentration of compound C535OOH by a factor of 5 to increase the average mixture O:C from 0.96 to 1.12.

It is important to note that AIOMFAC-VISC predictions are relatively sensitive to adjustments made to the average $\mathrm{O:C}$ ratio, which is a reflection of the sensitivity of the model to changes in SOA composition. Figure S7 demonstrates the changes to mixture viscosity over a plausible range of average $\mathrm{O:C}$ values. However, we note that the used variations in a mixture's average $\mathrm{O:C}$ ratio are imposed here for the purpose of illustration. They are not the results of predictions by a chemical mechanism under different oxidation regimes and as such do not represent equally likely outcomes. As in Fig. 7 in the main
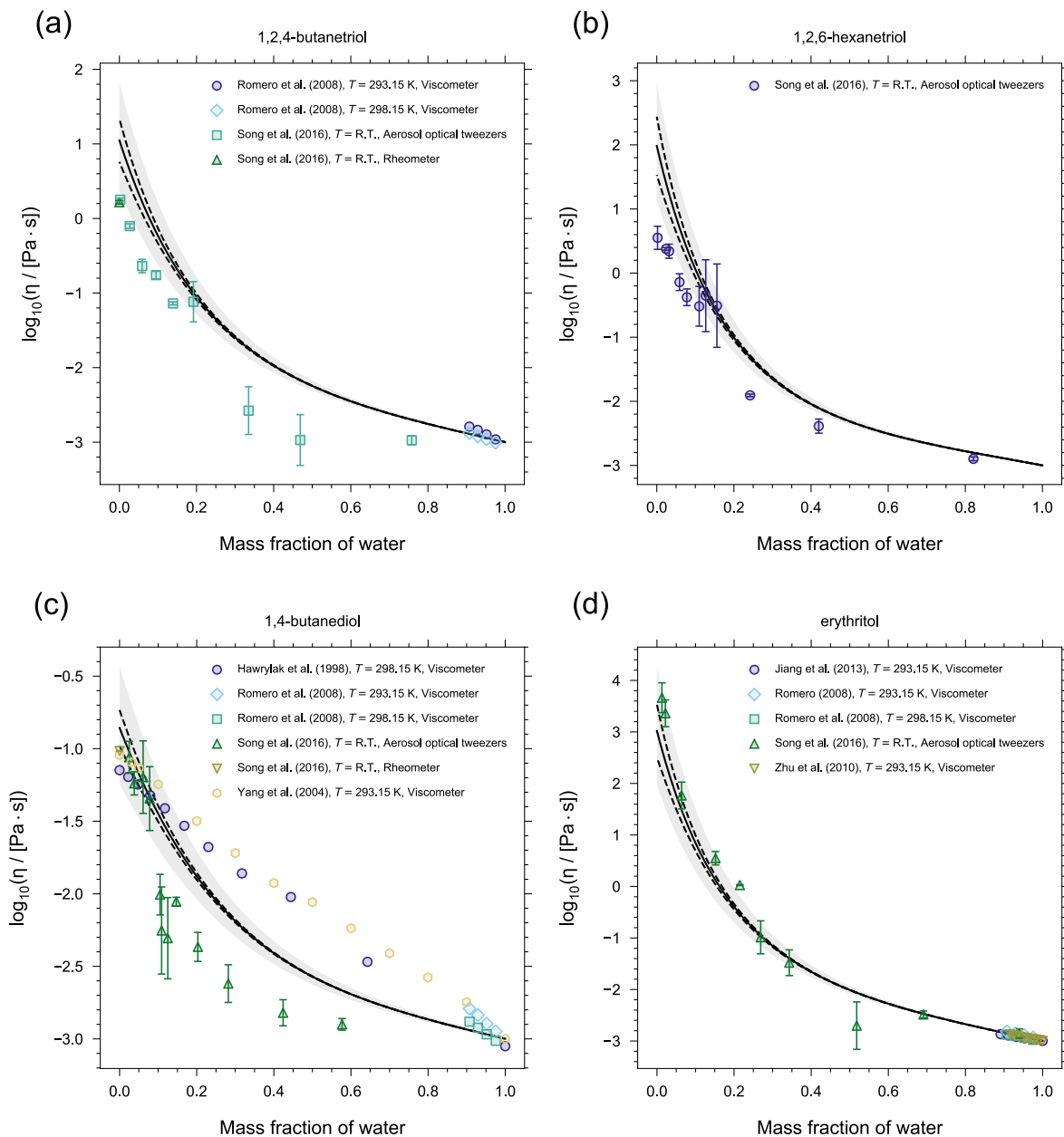
Figure S4. AIOMFAC-VISC mixture viscosity predictions as a function of mass fraction of water at 293.15 K for (**a**) 1,2,4-butanetriol, (**b**) 1,2,6-hexanetriol, (**c**) 1,4-butanetriol, and (**d**) erythritol. The solid black line is the AIOMFAC-VISC mixture viscosity prediction. The dashed black lines show the AIOMFAC-VISC sensitivity. The sensitivity is assessed by calculating the response of the model to a small change in mixture composition. The grey shaded region denotes a 5 % uncertainty in the prediction of T_g. Markers show experimental data. Error bars have been omitted when the length of the error bar does not exceed the width of the marker.
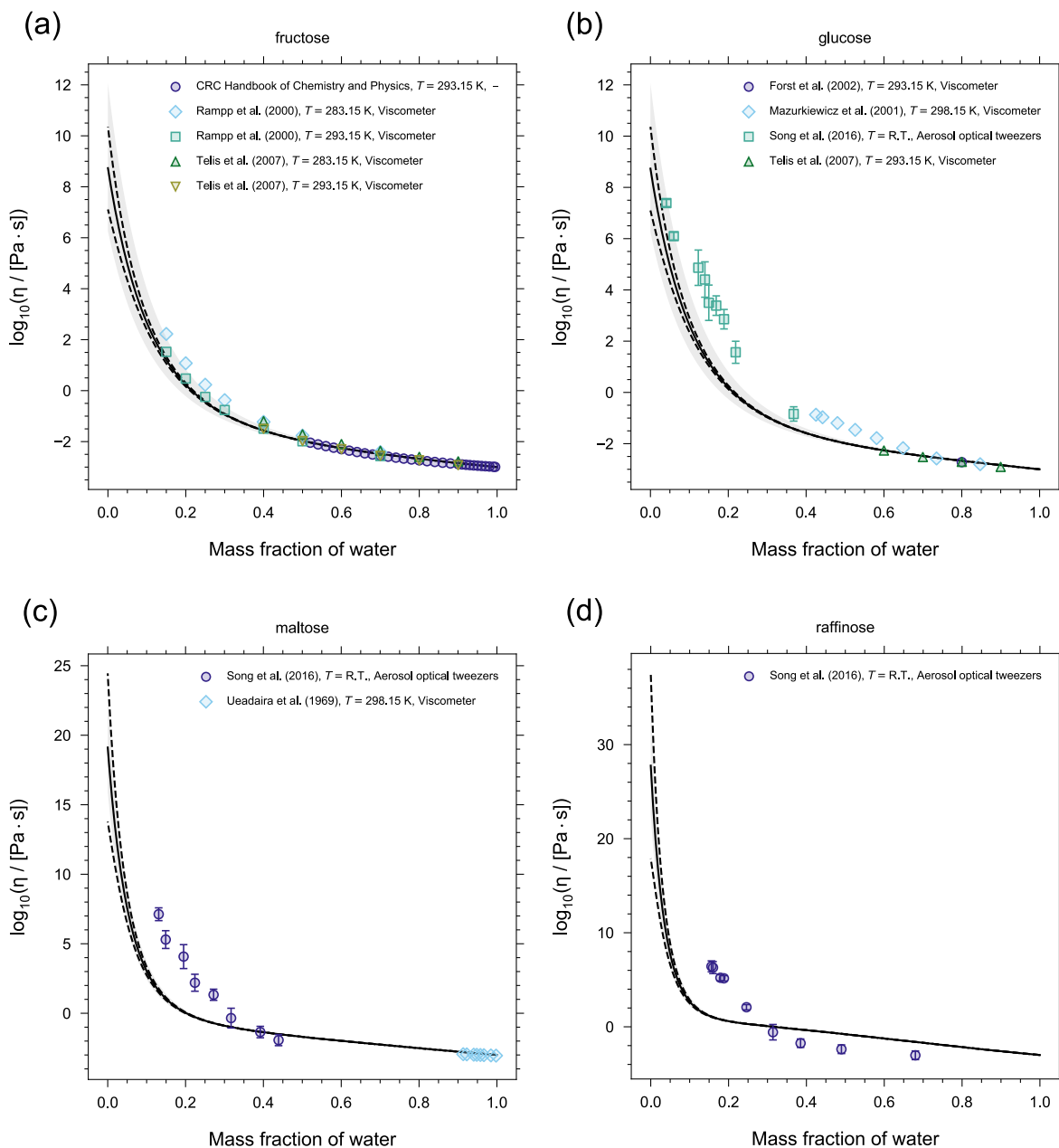
Figure S5. AIOMFAC-VISC mixture viscosity predictions as a function of mass fraction of water at 293.15 K for (**a**) fructose, (**b**) glucose, (**c**) maltose, and (**d**) raffinose. The solid black line is the AIOMFAC-VISC mixture viscosity prediction. The dashed black lines show the AIOMFAC-VISC sensitivity. The sensitivity is assessed by calculating the response of the model to a small change in mixture composition. The grey shaded region denotes a 5 % uncertainty in the prediction of T_g. Markers show experimental data. Error bars have been omitted when the length of the error bar does not exceed the width of the marker.
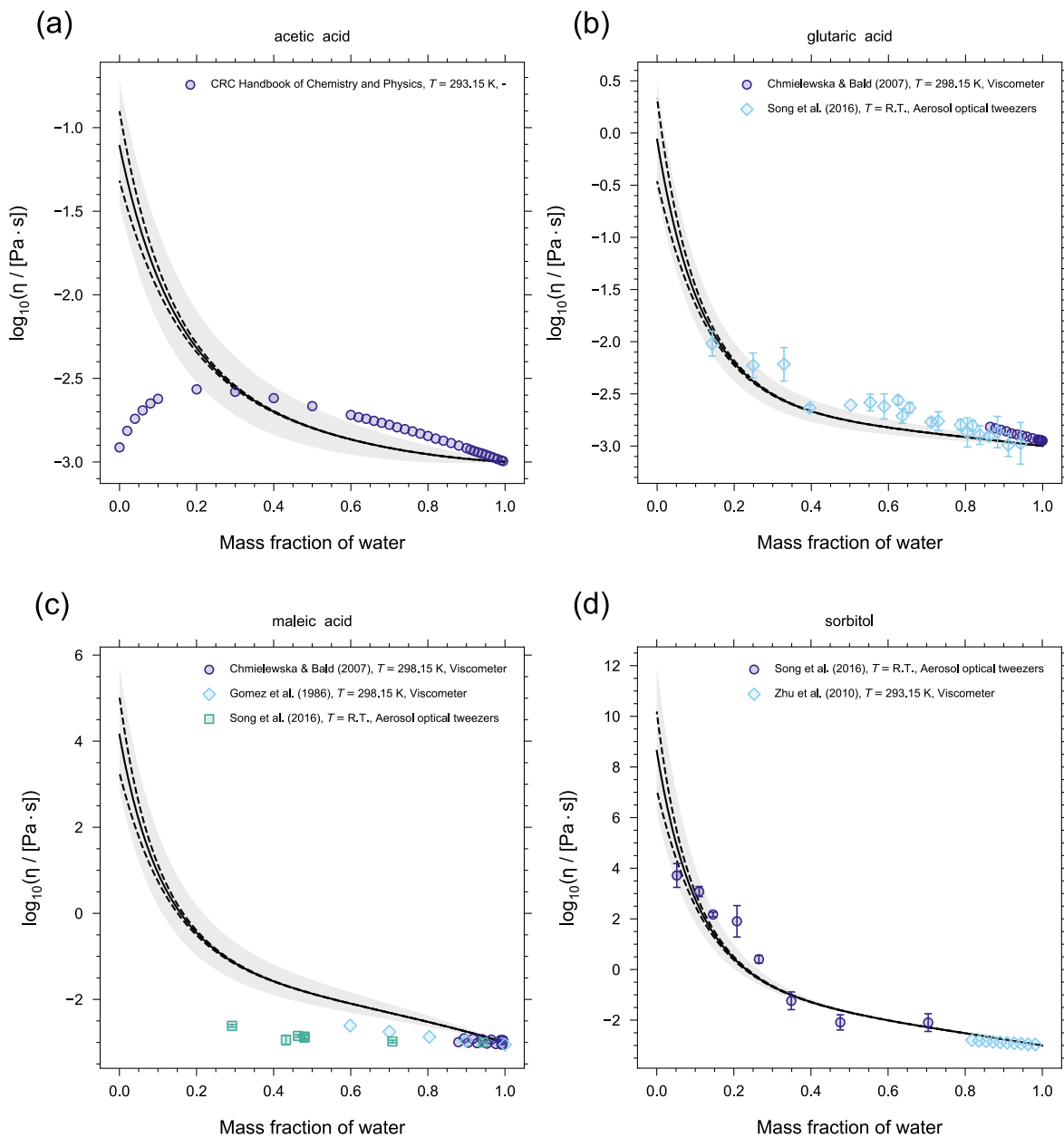
Figure S6. AIOMFAC-VISC mixture viscosity predictions as a function of mass fraction of water at 293.15 K for (**a**) acetic acid, (**b**) glutaric acid, (**c**) maleic acid, and (**d**) sorbitol. The solid black line is the AIOMFAC-VISC mixture viscosity prediction. The dashed black lines show the AIOMFAC-VISC sensitivity. The sensitivity is assessed by calculating the response of the model to a small change in mixture composition. The grey shaded region denotes a 5 % uncertainty in the prediction of T_g. Markers show experimental data. Error bars have been omitted when the length of the error bar does not exceed the width of the marker.
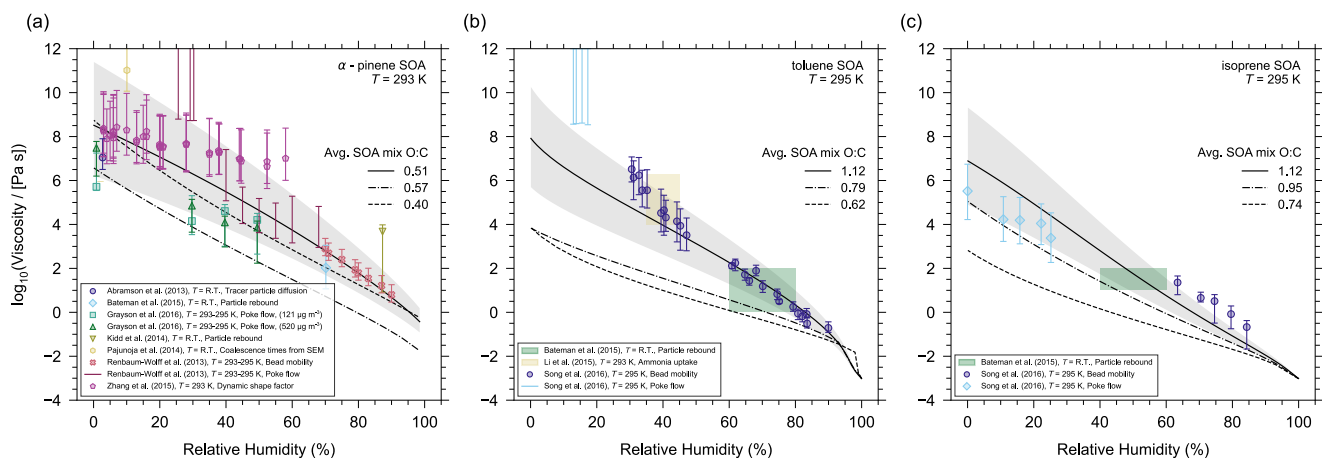
Figure S7. AIOMFAC-VISC mixture viscosity predictions for (**a**) α-pinene SOA at $T = 293$ K, (**b**) toluene SOA at $T = 295$ K, and (**c**) isoprene SOA at $T = 295$ K. The solid lines and the grey shaded regions represent the model results and their associated $5\,\%$ uncertainty in estimated T_g values from Fig. 7 of the main text. The dashed lines and dashed-dotted lines show AIOMFAC-VISC mixture viscosity for different average $O:C$ for each SOA mixture. The markers and colour shaded regions represent experimental data obtained by different methods (see legend). $T = $ R.T. indicates the measurements were taken at room temperature ($\sim 293 \pm 4$ K).

text, the relative contributions of the different organics were adjusted to change the average SOA $O:C$. The changes in mixture composition brought about from the $O:C$ adjustments are responsible for the differences in the model results. First, the mixture composition influences the curvature of the mixture viscosity prediction vs. RH. Second, the change in the relative contributions of the pure-component viscosities scales the mixture viscosity end point at $0\,\%$ RH.

5   AIOMFAC-VISC has proven to be very sensitive to mixture composition, which demonstrates that the model is flexible enough to reflect the viscosity of SOA formed under various experimental conditions. This is clear for the case of α-pinene (Fig. S7a) where the spread of experimental data is similar in magnitude to the spread in model results from varying mixture composition.

Table S2. MCM-derived surrogate components for alpha-pinene oxidation by ozone and their fixed amounts in $\mathrm{mol\,m^{-3}}$ in the particulate matter (PM) phase.

Name (MCM)	O:C	M (g mol^{-1})	mol m^{-3} in PM phase
C107OOH	0.4	200.231	2.1860×10^{-10}
PINONIC	0.3	184.232	1.2356×10^{-10}
C97OOH	0.44	188.22	2.5175×10^{-9}
C108OOH	0.5	216.231	8.4010×10^{-8}
C89CO2H	0.33	170.206	2.010×10^{-11}
PINIC	0.444	186.205	8.0263×10^{-9}
C921OOH	0.56	204.220	9.2106×10^{-9}
C109OOH	0.4	200.231	1.5748×10^{-11}
C812OOH	0.625	190.194	8.4291×10^{-9}
HOPINONIC	0.4	200.232	2.3266×10^{-9}
C811OH	0.375	158.094	8.9370×10^{-11}
C813OOH	0.75	206.193	3.2969×10^{-9}
ALDOL dimer	0.375	368.421	5.9996×10^{-10}
ESTER dimer	0.375	368.421	2.3998×10^{-9}

The ALDOL dimer and ESTER dimer are not predicted by MCM. Justification for including the dimers can be found in Zuend and Seinfeld (2012).

The average O:C ratio of the predicted α-pinene SOA mixture is 0.507 (for 27.248 µg m^{-3} of SOA formed at $T = 293.15$ K).

Table S3. MCM-derived surrogate components for toluene oxidation by OH and their fixed amounts in $\mathrm{mol\,m^{-3}}$ in the particulate matter (PM) phase.

Name (MCM)	O:C	M (g mol^{-1})	mol m^{-3} in PM phase
C5134CO2OH	0.8	130.099	1.9868×10^{-8}
C5CO234	0.6	114.099	1.3525×10^{-8}
PMALNHY2OH	0.714	174.151	1.9267×10^{-8}
C6H5CH2OOH	0.286	124.137	5.8337×10^{-9}
CRESOOH	0.857	190.151	2.4241×10^{-8}
TLEPOXMUC	0.429	140.137	1.9987×10^{-8}
MALANHY	0.75	98.057	1.6884×10^{-8}
C3DIALOOH	1.333	104.062	3.0168×10^{-8}
C33CO	1.0	86.046	2.2626×10^{-8}
C23O3CCHO	0.8	130.099	1.9868×10^{-8}
C535OOH	1.4	180.113	2.0366×10^{-7}
C534OOH	1.4	180.113	4.0863×10^{-8}

The average O:C ratio of the predicted toluene SOA mixture is 1.12 (for 301 µg m^{-3} of SOA formed at $T = 295.15$ K).

Table S4. MCM-derived surrogate components for isoprene photo-oxidation and their fixed amounts in $\mathrm{mol\,m^{-3}}$ in the particulate matter (PM) phase.

Name (MCM)	O:C	M (g mol^{-1})	mol m^{-3} in PM phase
IEB1OOH	1.0	150.1120	2.1859×10^{-9}
IEB2OOH	1.0	150.1120	3.8058×10^{-11}
C59OOH	1.0	150.0940	6.4468×10^{-9}
IEC1OOH	1.0	150.0940	2.2503×10^{-9}
C58OOH	1.0	150.1120	2.2710×10^{-10}
IEPOXA	0.6	118.1308	1.6303×10^{-31}
C57OOH	1.0	150.1120	1.8452×10^{-10}
IEPOXC	0.6	118.1308	3.7912×10^{-21}
HIEB1OOH	1.2	166.1120	2.3492×10^{-9}
INDOOH	1.4	197.1380	1.6072×10^{-9}
IEACO3H	1.0	148.0960	1.8935×10^{-19}
C525OOH	1.2	166.0940	1.7850×10^{-9}
HIEB2OOH	1.2	166.1120	1.0495×10^{-9}
IEC2OOH	1.0	148.0600	2.0814×10^{-17}
INAOOH	1.4	197.1380	7.2618×10^{-10}
C510OOH	1.4	195.1040	5.5325×10^{-13}
INB1OOH	1.4	197.1380	4.6077×10^{-10}
IECCO3H	1.0	148.1148	1.2558×10^{-17}
INCOOH	1.4	197.1380	8.7075×10^{-11}
INB2OOH	1.4	197.1380	1.8653×10^{-10}
Tetrol dimer	1.43	254.2768	3.9110×10^{-18}

The average O:C ratio of the predicted isoprene SOA mixture is 1.12 (for $3.406\,\mathrm{\mu g\,m^{-3}}$ of SOA formed at $T = 295.15$ K). See the SI of Rastak et al. (2017) for chemical formulas and justification for the tetrol dimer.

S7 AIOMFAC-VISC and the mole-fraction-based mixing rule for viscosity of binary aqueous and SOA systems

As detailed in the main text, the simple, mole-fraction-weighted mixing rule is the most competitive model that was explored for accurately capturing mixture viscosity of aqueous systems when compared to AIOMFAC-VISC. To quantitatively compare the two mixing rules, their mean absolute error (MAE) and mean bias error (MBE) as compared to binary aqueous experimental data are shown in Table S5. The MAE and the MBE are calculated as,

$$\text{MAE} = \frac{1}{N} \sum_{i=1}^{N} |\log_{10}(y_i + \delta_{x_i}) - \log_{10}(x_i + \delta_{x_i})| \quad ; \quad \text{MBE} = \frac{1}{N} \sum_{i=1}^{N} [\log_{10}(y_i + \delta_{x_i}) - \log_{10}(x_i + \delta_{x_i})]. \tag{S6}$$

Here, N is the number of data points in a given data set, y are the mixing model predictions of viscosity corresponding to the mixture composition of the experimental data and x are the experimental mixture viscosity data. The MAE and MBE are weighted by δ_{x_i}, which quantifies the measurement error or, if not available, the model sensitivity (see S3).

The MAE and MBE are shown in Table S5 for both mixing models when the pure-component viscosity is assigned as the highest confidence ("best") value. The highest confidence pure-component viscosity values are either taken from experiment, extrapolated from viscosity measurements very close to 0.0 mass fraction of water, or parameterizations of T_{g} in good agreement with experimental data (see Fig. 4 of the main text and Fig. S8). Comparing the sums of all system MAE and MBEs, when the highest confidence pure-component viscosities have been used, the mole-fraction scaled mixing rule has a slightly lower MAE and MBE. In the case of AIOMFAC-VISC, these cumulative metrics are dominated by relatively large MAE and MBE contributions from the aqueous sugar solution systems (raffinose, trehalose, maltose). These larger deviations from measurements are in part explained by the known deviations of AIOMFAC/UNIFAC water activity predictions from measurements for sugar-containing solutions. Therefore, the activity deviations impact the skill of AIOMFAC-VISC in predicting viscosity, while the mole-fraction-based mixing rule is not affected and provides the better mixture viscosity model for these systems. Notwithstanding, while the sums provide an overall comparison of the two models, they should be interpreted with caution, because large errors in case of some systems dominates the totals. An alternative and perhaps more insightful method to evaluate the two models is to compare them on a system-by-system basis. In this manner, the fraction of times AIOMFAC-VISC outperforms the mole-fraction scaled mixing rule is 61% in terms of MAE and 67% in terms of MBE when using the highest confidence pure-component viscosities. This indicates that AIOMFAC-VISC performs better particularly when uncertainties in the composition–activity relationship considered by the model do not dominate the model–measurement deviations.

Using the highest confidence pure-component viscosities offers the most direct statistical comparison of the two mixing rules; however, the MAE and MBE are also shown using the DeRieux et al. (2018) based pure-component viscosity estimation, given that this tool is used in practice in the current AIOMFAC-VISC framework. When using the DeRieux et al. (2018) method, AIOMFAC-VISC is the better performing model only in 24% of the cases in terms of MAE and 36% in terms of MBE. This is the case because the tendency of a high-bias in pure-component viscosity predictions by the DeRieux et al. (2018) (for the systems tested here) favours the mole-fraction scaled mixing rule (but not necessarily for the right reason). The discrepancy in model performance when using different pure-component viscosity estimation methods further highlights the need for an accurate pure-component viscosity prediction and supports further research to improve such models. Finally,

both AIOMFAC-VISC and the mole-fraction scaled mixing rule are clearly better than the activity-scaled mixing rule in approximately 91% of cases. Given the clear difference in performance of the activity-scaled mixing rule, compared to the other two models, the results of a detailed statistical analysis were not listed in Table S5 as it is not a recommended mixing rule.

5   For SOA systems, the AIOMFAC-VISC and the mole-fraction scaled mixing rule also give similar results (see Fig. S9). For α-pinene, the mole-fraction-weighted mixing rule overestimates the mixture viscosity at high relative humidity as compared to the AIOMFAC-VISC agreement with the data from Renbaum-Wolff et al. (2013). However, below approximately 50% RH, the model results are nearly identical. For toluene, AIOMFAC-VISC is in slightly better agreement with the experimental data, although the opposite is true for isoprene. Again, both models are very similar and the large spread in experimental

10   SOA data makes it difficult to compare the performance of the models conclusively. Both models are viable for mixture viscosity prediction and the mole-fraction-weighted mixing rule provides a robust alternative to AIOMFAC-VISC, particularly for aqueous systems exhibiting orders of magnitude change in viscosity with composition. Ultimately, we note that only a small number of binary aqueous and multicomponent SOA systems were tested here, and when more experimental data of atmospheric relevance becomes available, further model evaluations can be performed. At present, the choice to use either

15   model can be made on a system-by-system basis.
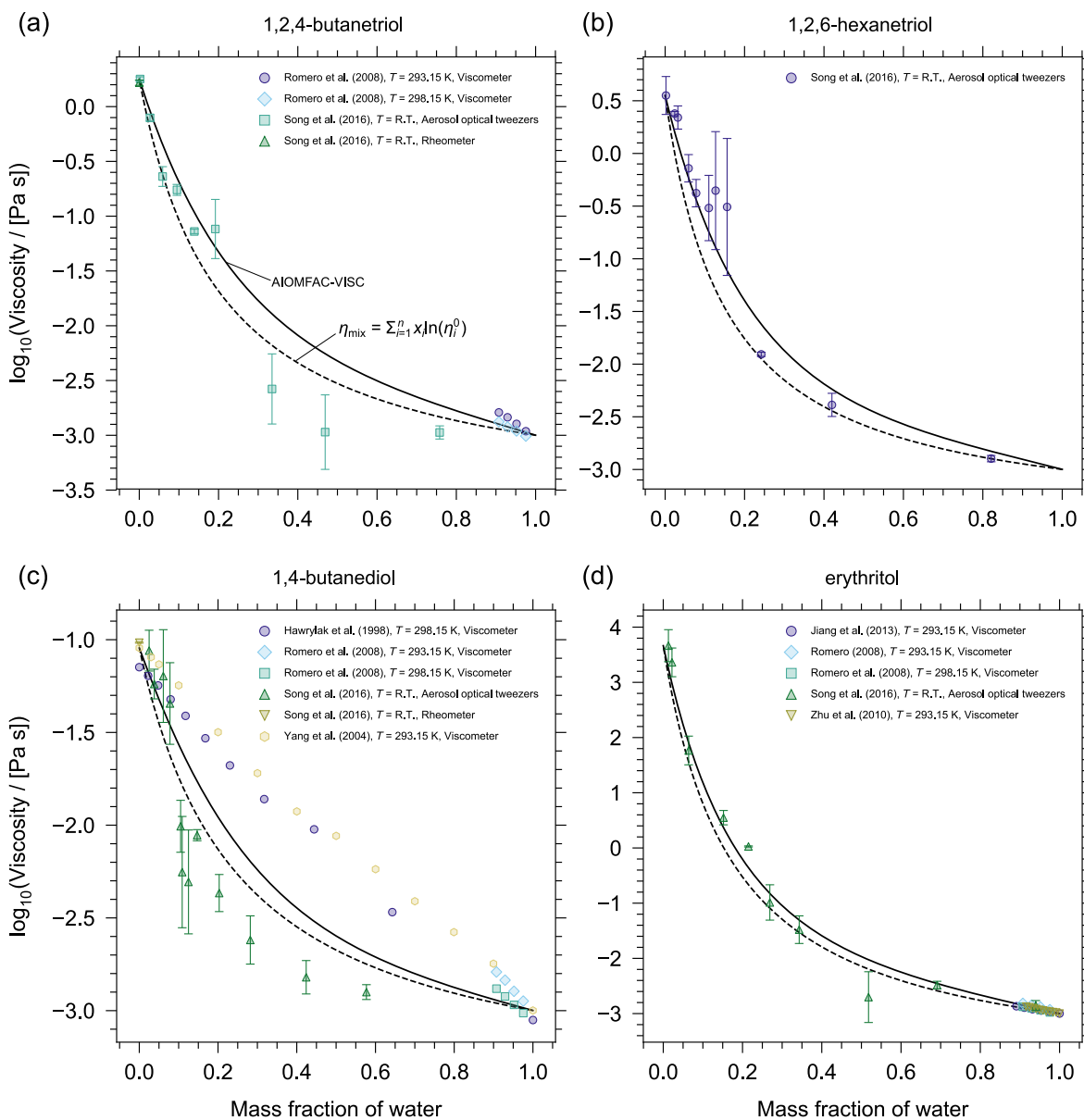
Figure S8. AIOMFAC-VISC mixture viscosity predictions as a function of mass fraction of water at 293.15 K for (**a**) 1,2,4-butanetriol, (**b**) 1,2,6-hexanetriol, (**c**) 1,4-butanetriol, and (**d**) erythritol. The solid black lines are the AIOMFAC-VISC mixture viscosity prediction. The dashed black lines are the mixture viscosity prediction from the mole-fraction-weighted mixing rule. Markers show experimental data. Error bars have been omitted when the length of the error bar does not exceed the width of the marker. The pure-component viscosities for each simulation have been assigned as the experimental data points which are measured at as close to 0 mass fraction of water.

Table S5. Mean absolute error (MAE) and mean bias error (MBE) for AIOMFAC–VISC and the mole-fraction scaled mixing rule predictions of mixture viscosity of binary aqueous organic systems as compared to experimental data at $T = 293.15$ K (or the temperature indicated in the source column).

System compound	Source	$\log_{10}\left[\dfrac{\eta^0_{\text{Best}}}{(\text{Pa s})}\right]$	AIOMFAC-VISC MAE	MBE	Mole Fraction MAE	MBE	$\log_{10}\left[\dfrac{\eta^0_{\text{DeRieux}}}{(\text{Pa s})}\right]$	AIOMFAC-VISC MAE	MBE	Mole Fraction MAE	MBE
1,2,4-butanetriol	Song et al. (2016)	0.2100	0.0152	0.0052	0.0174	-0.0171	1.0481	0.1757	0.1757	0.1300	0.1286
1,2,6-hexanetriol	Song et al. (2016)	0.5500	0.0371	-0.0363	0.0675	-0.0675	1.9845	0.3103	0.3083	0.2412	0.2286
1,4-butanediol	Song et al. (2016)	-1.0380	0.0034	0.0001	0.0040	-0.0022	-0.8571	0.0035	0.0032	0.0028	0.0002
1,4-butanediol	Yang et al. (2004)	-1.0380	0.0035	-0.0034	0.0044	-0.0043	-0.8571	0.0035	-0.0009	0.0042	-0.0023
citric acid	Haynes (2014)	7.9275	0.0000	0.0000	0.0000	0.0000	11.8101	0.0002	0.0002	0.0001	0.0001
citric acid	Song et al. (2016)	7.9275	0.4144	0.2829	0.4174	0.3460	11.8101	1.9579	1.9579	2.1932	2.1932
erythritol	Song et al. (2016)	2.9287	0.2921	-0.2915	0.3798	-0.3797	3.0174	0.2689	-0.2680	0.3574	-0.3573
fructose	Haynes (2014)	10.0678	0.0001	0.0001	0.0002	0.0002	8.7321	0.0001	0.0001	0.0001	0.0001
fructose	Rampp et al. (2000)	10.0678	0.0052	0.0021	0.0628	0.0628	8.7321	0.1001	-0.1000	0.0436	-0.0434
fructose	Telis et al. (2007)	10.0678	0.0002	0.0002	0.0011	0.0011	8.7321	0.0004	-0.0002	0.0002	0.0002
fructose	Rampp et al. (2000) (at 283 K)	12.3570	0.0212	-0.0178	0.1459	0.1459	11.0057	0.1010	-0.1010	0.0231	-0.0003
fructose	Telis et al. (2007) (at 283 K)	12.3570	0.0005	-0.0003	0.0028	0.0028	11.0057	0.0008	-0.0007	0.0011	0.0011
glucose	Gladden and Dole (1953) (at 298 K)	12.9982	0.0495	0.0495	0.1572	0.1572	7.8215	0.0397	-0.0397	0.0312	-0.0312
glucose	Song et al. (2016)	13.7472	1.1186	-0.5425	0.7435	-0.1882	8.7321	1.9370	-1.9370	1.9554	-1.9554
glutaric acid	Song et al. (2016)	0.3115	0.0003	0.0000	0.0005	0.0003	3.7869	0.0102	0.0102	0.0155	0.0155
glycerol	Haynes (2014)	0.1482	0.0011	-0.0011	0.0051	-0.0051	0.6752	0.0172	0.0172	0.0119	0.0097
glycerol	Song et al. (2016)	0.1482	0.2547	-0.2547	0.2911	-0.2911	0.6752	0.1998	-0.0305	0.1484	-0.0945
maleic acid	Song et al. (2016)	-0.8640	0.0000	0.0000	0.0003	0.0003	4.1521	0.0077	0.0077	0.0074	0.0074
maltose	Song et al. (2016)	33.9582	1.4869	-1.4851	0.3022	0.0526	19.1178	1.9059	-1.9050	1.5884	-1.5877
raffinose	Song et al. (2016)	37.3758	2.2183	-2.1854	1.3521	-1.3391	27.7649	2.2912	-2.2593	2.0317	-2.0304
sorbitol	Song et al. (2016)	8.1737	0.5003	-0.2749	0.5245	-0.4059	8.6349	0.4966	-0.2018	0.5110	-0.3179
sucrose	Gladden and Dole (1953) (at 298 K)	15.8319	0.0175	-0.0161	0.0137	-0.0137	18.1038	0.0157	-0.0141	0.0120	-0.0120
sucrose	Quintas et al. (2006)	16.7816	1.0802	-1.0802	0.8105	-0.8105	19.2312	0.9963	-0.9963	0.4997	-0.4997
sucrose	Power et al. (2013)	16.7816	1.1108	-1.0195	0.7388	-0.6270	19.2312	0.9147	-0.7647	0.4301	-0.1345
sucrose	Telis et al. (2007)	16.7816	0.0010	0.0010	0.0011	-0.0011	19.2312	0.0011	0.0011	0.0005	-0.0005
sucrose	Haynes (2014)	16.7816	0.0025	-0.0009	0.0014	-0.0014	19.2312	0.0023	-0.0007	0.0008	-0.0008
sucrose	Song et al. (2016)	16.7816	1.3781	-0.1887	1.0439	0.1545	19.2312	1.6219	0.3743	1.4092	0.9672
sucrose	Swindells et al. (1958)	16.7816	0.0159	-0.0137	0.0138	-0.0138	19.2312	0.0151	-0.0128	0.0115	-0.0115
sucrose	Först et al. (2002)	16.7816	0.0010	0.0009	0.0014	-0.0014	19.2312	0.0010	0.0010	0.0006	-0.0006
trehalose	Song et al. (2016)	33.9582	1.8832	-1.8832	0.4835	0.3433	19.1178	2.4315	-2.4315	1.9298	-1.9298
trehalose	Sampedro et al. (2002)	33.9582	0.0002	0.0002	0.0002	0.0002	19.1178	0.0002	0.0002	0.0000	0.0000
trehalose	Galmarini et al. (2011)	33.9582	0.0007	0.0007	0.0013	0.0013	19.1178	0.0006	0.0006	0.0003	-0.0003
trehalose	Miller and Corti (1997)	33.9582	0.6097	-0.6097	0.0645	0.0547	19.1178	0.6237	-0.6237	0.6304	-0.6304
	Sum =		12.523	-9.562	7.654	-2.846	Sum =	16.452	-8.830	14.223	-6.089

All values are dimensionless numbers (magnitude closer to zero is better) based on $\log_{10}\left[(\text{Pa s})/(\text{Pa s})\right]$; refer to Eq. (S6).

η^0_{DeRieux}: pure-component viscosity of organic at stated T is calculated based on the DeRieux et al. (2018) method.

η^0_{Best}: pure-component viscosity or organic at stated T is assigned as the optimal value of all methods explored to determine the pure-component viscosity.

The fraction of systems where AIOMFAC-VISC outperforms the mole-fraction scaled mixing rule is 61 % in terms of MAE and 67 % in terms of MBE when using η^0_{Best}.

Not listed are the MAE and MBE for the activity-scaled mixing rule; however, the fraction of systems where AIOMFAC-VISC is the better model is 91% in terms of MAE and 94 % in terms of MBE when using η^0_{Best}.
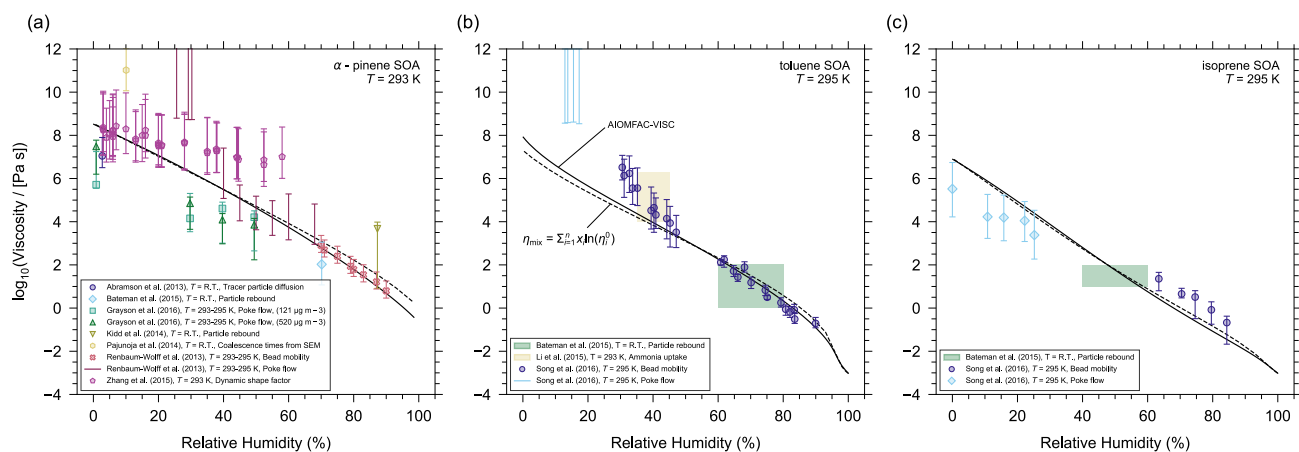
Figure S9. AIOMFAC–VISC mixture viscosity predictions for (**a**) α-pinene SOA at $T = 293$ K, (**b**) toluene SOA at $T = 295$ K, and (**c**) isoprene SOA at $T = 295$ K. The solid black lines are the AIOMFAC-VISC mixture viscosity prediction. The dashed black lines are the mixture viscosity prediction from the mole-fraction-weighted mixing rule. The markers and colour shaded regions represent experimental data obtained by different methods (see legend). $T = $ R.T. indicates the measurements were taken at room temperature ($\sim 293 \pm 4$ K). The same relative amounts of organics that are listed in Tables S2 – S4 are used for the simulations of both models.

References

Ablett, S., Izzard, M. J., Lillford, P. J., Arvanitoyannis, I., and Blanshard, J. M.: Calorimetric study of the glass transition occuring in fructose solutions, Carbohydrate Research, 246, 13–22, https://doi.org/10.1016/0008-6215(93)84020-7, 1993.

Angell, C.: Entropy and Fragility in Supercooling Liquids, vol. 102, https://doi.org/10.6028/jres.102.013, 1997.

5   Bodsworth, A., Zobrist, B., and Bertram, A. K.: Inhibition of efflorescence in mixed organic-inorganic particles at temperatures less than 250 K, Physical Chemistry Chemical Physics, 12, 12 259–12 266, https://doi.org/10.1039/c0cp00572j, 2010.

Böhmer, R., Ngai, K. L., Angell, C. A., and Plazek, D. J.: Nonexponential relaxations in strong and fragile glass formers, The Journal of Chemical Physics, 99, 4201–4209, https://doi.org/10.1063/1.466117, 1993.

Cao, W., Knudsen, K., Fredenslund, A., and Rasmussen, P.: Group-Contribution Viscosity Predictions of Liquid Mixtures Using UNIFAC-

10   VLE Parameters, Ind. Eng. Chem. Res., 32, 2088–2092, https://doi.org/10.1021/ie00021a034, 1993.

Compernolle, S., Ceulemans, K., and Muller, J. F.: EVAPORATION: a new vapour pressure estimation methodfor organic molecules including non-additivity and intramolecular interactions, Atmos. Chem. Phys., 11, 9431–9450, https://doi.org/10.5194/acp-11-9431-2011, <GotoISI>://WOS:000295368700001, 2011.

Dehaoui, A., Issenmann, B., and Caupin, F.: Viscosity of deeply supercooled water and its coupling to molecular diffusion, Proceedings of

15   the National Academy of Sciences, 112, 12 020–12 025, https://doi.org/10.1073/pnas.1508996112, 2015.

DeRieux, W. S. W., Li, Y., Lin, P., Laskin, J., Laskin, A., Bertram, A. K., Nizkorodov, S. A., and Shiraiwa, M.: Predicting the glass transition temperature and viscosity of secondary organic material using molecular composition, Atmospheric Chemistry and Physics, 18, 6331–6351, https://doi.org/10.5194/acp-18-6331-2018, 2018.

Dette, H. P., Qi, M., Schröder, D. C., Godt, A., and Koop, T.: Glass-forming properties of 3-methylbutane-1,2,3-tricarboxylic acid and its

20   mixtures with water and pinonic acid, Journal of Physical Chemistry A, 118, 7024–7033, https://doi.org/10.1021/jp505910w, 2014.

Dorfmüller, T., Dux, H., Fytas, G., and Mersch, W.: A light scattering study of the molecular motion in hexanetriol 1,2,6, The Journal of Chemical Physics, 71, 366–375, https://doi.org/10.1063/1.438079, 1979.

Först, P., Werner, F., and Delgado, A.: On the pressure dependence of the viscosity of aqueous sugar solutions, Rheologica Acta, 41, 369–374, https://doi.org/10.1007/s00397-002-0238-y, 2002.

25   Galmarini, M., Baeza, R., Sanchez, V., Zamora, M., and Chirife, J.: Comparison of the viscosity of trehalose and sucrose solutions at various temperatures: Effect of guar gum addition, LWT-Food Science and Technology, 44, 186–190, 2011.

Gladden, J. and Dole, M.: Diffusion in supersaturated solutions. II. Glucose solutions, Journal of the American Chemical Society, 75, 3900–3904, 1953.

Hancock, B. C., Shamblin, S. L., and Zografi, G.: Molecualr Mobility of Amorphous Pharmaceutical Solids Below Their Glass Transition

30   Temperatures, Pharmaceutical Research, 12, 799–806, 1995.

Haynes, W. M.: CRC handbook of chemistry and physics, CRC press, 2014.

Hoppu, P., Hietala, S., Schantz, S., and Juppo, A. M.: Rheology and molecular mobility of amorphous blends of citric acid and paracetamol, European Journal of Pharmaceutics and Biopharmaceutics, 71, 55–63, https://doi.org/10.1016/j.ejpb.2008.06.029, 2009.

Kawai, K., Hagiwara, T., Takai, R., and Suzuki, T.: Comparative investigation by two analytical approaches of enthalpy relaxation for glassy

35   glucose, sucrose, maltose, and trehalose, Pharmaceutical Research, 22, 490–495, https://doi.org/10.1007/s11095-004-1887-6, 2005.

Lienhard, D. M., Zobrist, B., Zuend, A., Krieger, U. K., and Peter, T.: Experimental evidence for excess entropy discontinuities in glass-forming solutions, Journal of Chemical Physics, 136, 74 515, https://doi.org/10.1063/1.3685902, 2012.

Lu, Q. and Zografi, G.: Properties of citric acid at the glass transition, Journal of Pharmaceutical Sciences, 86, 1374–1378, https://doi.org/10.1021/js970157y, 1997.

Marsh, A., Petters, S. S., Rothfuss, N. E., Rovelli, G., Song, Y. C., Reid, J. P., and Petters, M. D.: Amorphous phase state diagrams and viscosity of ternary aqueous organic/organic and inorganic/organic mixtures, Physical Chemistry Chemical Physics, 20, 15 086–15 097, https://doi.org/10.1039/c8cp00760h, 2018.

Miller, D.P., P. J. and Corti, H.: Thermophysical Properties of Trehalose and Its concentrated Aqueous Solutions, Pharmaceutical Research, 14, 578–590, https://doi.org/10.1023/A:1012192725996, 1997.

Murray, B. J.: Inhibition of ice crystallisation in highly viscous aqueous organic acid droplets, Atmospheric Chemistry and Physics, 8, 5423–5433, https://doi.org/10.5194/acp-8-5423-2008, 2008.

Nakanishi, M. and Nozaki, R.: Systematic study of the glass transition in polyhydric alcohols, Physical Review E - Statistical, Nonlinear, and Soft Matter Physics, 83, 51 503, https://doi.org/10.1103/PhysRevE.83.051503, 2011.

Nannoolal, Y., Rarey, J., Ramjugernath, D., and Cordes, W.: Estimation of pure component properties: Part 1. Estimation of the normal boiling point of non-electrolyte organic compounds via group contributions and group interactions, Fluid Phase Equilibria, 226, 45–63, https://doi.org/10.1016/j.fluid.2004.09.001, 2004.

Nannoolal, Y., Rarey, J., and Ramjugernath, D.: Estimation of pure component properties - Part 3. Estimation of the vapor pressure of non-electrolyte organic compounds via group contributions and group interactions, Fluid Phase Equilib., 269, http://dx.doi.org/10.1016/j.fluid.2008.04.020, 2008.

Nannoolal, Y., Rarey, J., and Ramjugernath, D.: Estimation of pure component properties. Part 4: Estimation of the saturated liquid viscosity of non-electrolyte organic compounds via group contributions and group interactions, Fluid Phase Equilibria, 281, 97–119, https://doi.org/10.1016/j.fluid.2009.02.016, 2009.

Ollet, A. L. and Parker, R.: The Viscosity of Supercooled Fructose and Its Glass Transition Temperature, Journal of Texture Studies, 21, 355–362, https://doi.org/10.1111/j.1745-4603.1990.tb00484.x, 1990.

Power, R. M., Simpson, S. H., Reid, J. P., and Hudson, A. J.: The transition from liquid to solid-like behaviour in ultrahigh viscosity aerosol particles, Chemical Science, 4, 2597–2604, https://doi.org/10.1039/c3sc50682g, 2013.

Quintas, M., Brandão, T. R., Silva, C. L., and Cunha, R. L.: Rheology of supersaturated sucrose solutions, Journal of Food Engineering, 77, 844–852, https://doi.org/10.1016/j.jfoodeng.2005.08.011, 2006.

Rampp, M., Buttersack, C., and Lüdemann, H.-D.: c,T-Dependence of the viscosity and the self-diffusion coefficients in some aqueous carbohydrate solutions, Carbohydrate Research, 328, 561–572, https://doi.org/10.1016/S0008-6215(00)00141-5, 2000.

Rastak, N., Pajunoja, A., Acosta Navarro, J. C., Ma, J., Song, M., Partridge, D. G., Kirkevåg, A., Leong, Y., Hu, W. W., Taylor, N. F., Lambe, A., Cerully, K., Bougiatioti, A., Liu, P., Krejci, R., Petäjä, T., Percival, C., Davidovits, P., Worsnop, D. R., Ekman, A. M. L., Nenes, A., Martin, S., Jimenez, J. L., Collins, D. R., Topping, D. O., Bertram, A. K., Zuend, A., Virtanen, A., and Riipinen, I.: Microphysical explanation of the RH-dependent water affinity of biogenic organic aerosol and its importance for climate, Geophys. Res. Lett., 44, 5167–5177, https://doi.org/10.1002/2017GL073056, https://doi.org/10.1002/2017GL073056, 2017.

Renbaum-Wolff, L., Grayson, J. W., Bateman, A. P., Kuwata, M., Sellier, M., Murray, B. J., Shilling, J. E., Martin, S. T., and Bertram, A. K.: Viscosity of -pinene secondary organic material and implications for particle growth and reactivity, Proceedings of the National Academy of Sciences, 110, 8014–8019, https://doi.org/10.1073/pnas.1219548110, 2013.

Rothfuss, N. E. and Petters, M. D.: Influence of Functional Groups on the Viscosity of Organic Aerosol, Environmental Science and Technology, 51, 271–279, https://doi.org/10.1021/acs.est.6b04478, 2017.

Sampedro, J. G., Munoz-Clares, R. A., and Uribe, S.: Trehalose-mediated inhibition of the plasma membrane H+-ATPase from Kluyveromyces lactis: dependence on viscosity and temperature, Journal of bacteriology, 184, 4384–4391, 2002.

Seidl, M., Loerting, T., Bohmer, R., Gainaru, C., Nelson, H., Amann-Winkel, K., and Handle, P. H.: Water's second glass transition, Proceedings of the National Academy of Sciences, 110, 17 720–17 725, https://doi.org/10.1073/pnas.1311718110, 2013.

Simatos, D., Blond, G., Roudaut, G., Champion, D., Perez, J., and Faivre, A. L.: Influence of heating and cooling rates on the glass transition temperature and the fragility parameter of sorbitol and fructose as measured by DSC, Journal of Thermal Analysis, 47, 1419–1436, https://doi.org/10.1007/BF01992837, 1996.

Simperler, A., Kornherr, A., Chopra, R., Bonnet, P. A., Jones, W., Motherwell, W. D., and Zifferer, G.: Glass transition temperature of glucose, sucrose, and trehalose: An experimental and in silico study, Journal of Physical Chemistry B, 110, 19 678–19 684, https://doi.org/10.1021/jp063134t, 2006.

Song, M., Liu, P. F., Hanna, S. J., Zaveri, R. A., Potter, K., You, Y., Martin, S. T., and Bertram, A. K.: Relative humidity-dependent viscosity of secondary organic material from toluene photo-oxidation and possible implications for organic particulate matter over megacities, Atmospheric Chemistry and Physics, 16, 8817–8830, https://doi.org/10.5194/acp-16-8817-2016, 2016.

Swindells, J., Snyder, C., Hardy, R., and Golden, P.: Viscosities of sucrose solutions at various temperatures: Tables of recalculated values, https://doi.org/10.1016/S0016-7037(03)00105-4, 1958.

Telis, V. R., Telis-Romero, J., Mazzotti, H. B., and Gabas, A. L.: Viscosity of aqueous carbohydrate solutions at different temperatures and concentrations, International Journal of Food Properties, 10, 185–195, https://doi.org/10.1080/10942910600673636, 2007.

Timko, R. J. and Lordi, N. G.: Thermal characterization of citric acid solid dispersions with benzoic acid and phenobarbital, in: Journal of Pharmaceutical Sciences, vol. 68, pp. 601–605, Elsevier, https://doi.org/10.1002/jps.2600680523, https://www.sciencedirect.com/science/article/pii/S0022354915426504, 1979.

Viswanath, D. S., Ghosh, T. K., Prasad, D. H. L., Dutt, N. V., and Rani, K. Y.: Viscosity of Liquids, Springer, 2007.

Yang, C., Ma, P., and Zhou, Q.: Excess Molar Volume, Viscosity, and Heat Capacity for the Mixtures of 1,4-Butanediol + Water at Different Temperatures, Journal of Chemical and Engineering Data, 49, 582–587, https://doi.org/10.1021/je0341918, 2004.

Zhang, Y., Katira, S., Lee, A., Lambe, A. T., Onasch, T. B., Xu, W., Brooks, W. A., Canagaratna, M. R., Freedman, A., Jayne, J. T., Worsnop, D. R., Davidovits, P., Chandler, D., and Kolb, C. E.: Kinetically controlled glass transition measurement of organic aerosol thin films using broadband dielectric spectroscopy, Atmospheric Measurement Techniques, 11, 3479–3490, https://doi.org/10.5194/amt-11-3479-2018, 2018.

Zobrist, B., Marcolli, C., Pedernera, D. A., and Koop, T.: Do atmospheric aerosols form glasses?, Atmospheric Chemistry and Physics, 8, 5221–5244, https://doi.org/10.5194/acp-8-5221-2008, 2008.

Zuend, A. and Seinfeld, J. H.: Modeling the gas-particle partitioning of secondary organic aerosol: The importance of liquid-liquid phase separation, Atmospheric Chemistry and Physics, 12, 3857–3882, https://doi.org/10.5194/acp-12-3857-2012, 2012.

Zuend, A., Marcolli, C., Booth, A. M., Lienhard, D. M., Soonsin, V., Krieger, U. K., Topping, D. O., McFiggans, G., Peter, T., and Seinfeld, J. H.: New and extended parameterization of the thermodynamic model AIOMFAC: Calculation of activity coefficients for organic-inorganic mixtures containing carboxyl, hydroxyl, carbonyl, ether, ester, alkenyl, alkyl, and aromatic functional groups, Atmospheric Chemistry and Physics, 11, 9155–9206, https://doi.org/10.5194/acp-11-9155-2011, 2011.